ANALOG AND DIGITAL ADIABATIC QUANTUM ANNEALING WITH OSCILLATING TRANSVERSE FIELDS

by

Zhijie Tang

A thesis submitted to the Faculty and the Board of Trustees of the Colorado School of Mines in partial fulfillment of the requirements for the degree of Doctor of Philosophy (Applied Physics).

Golden, Colorado

Date _____

Signed: _____

Zhijie Tang

Signed: _____

Dr. Eliot Kapit
Thesis Advisor

Golden, Colorado

Date _____

Signed: _____

Dr. Uwe Greife
Professor and Department Head
Department of Physics

ABSTRACT

This thesis investigates both analog Quantum Annealing and digital Quantum Annealing with oscillating transverse field in solving hard optimization problems.

In the first part, we consider a range of unconventional modifications to Quantum Annealing (QA), applied to an artificial trial problem with continuously tunable difficulty. In this problem, inspired by "transverse field chaos" in larger systems, classical and quantum methods are steered toward a false local minimum. To go from this local minimum to the global minimum, all N spins must flip, making this problem exponentially difficult to solve. We numerically study this problem by using a variety of new methods from the literature: inhomogeneous driving, adding transverse couplers, and other types of coherent oscillations in the transverse field terms (collectively known as RFQA). We show that all these methods improve the scaling of the time to solution (relative to the standard uniform sweep evolution) in at least some regimes. Comparison of these methods could help identify promising paths towards a demonstrable quantum speedup over classical algorithms in solving some realistic problems with near-term quantum annealing hardware.

In the second part of the thesis, we explore a digitized version of RFQA inspired by the performance of RFQA in analog quantum computing. The digitization of Quantum Annealing is a combination of analog Quantum Annealing(QA) and Quantum Approximate Optimization Algorithm (QAOA). Digitized-QA can be applied to full-scale, fault-tolerant quantum algorithms. We apply the digitized version of RFQA and QA to various trial problems using classical numerical simulation and show that digitized-RFQA is a potentially promising tool in solving hard optimization problems and can be a new tool to complement QAOA and traditional digitized-QA.

In the third part of the thesis, for the preparation of an experiment, we investigate the 1D TFIM(transverse field ising model) and show that RFQA-D is able to accelerating the N-spin tunneling, the acceleration suggests that RFQA has the potential of mitigating the cost of minor embedding overhead.

TABLE OF CONTENTS

LIST OF FIGURES

LIST OF TABLES

ACKNOWLEDGMENTS

Throughout the writing of this dissertation I have received a great deal of support and assistance.

I would first like to thank my supervisor, Professor Eliot Kapit. Your insightful feedback helped me to sharpen my thinking and brought my work to a higher level.

I would also like to acknowledge my colleagues David Rodriguez Perez and Nick Materise for their fruitful discussion and patient support.

Finally, I must express my profound gratitude to my family for providing me with support and encouragement throughout my years of study and through the process of researching and writing this thesis. This accomplishment would not have been possible without them.

CHAPTER 1
INTRODUCTION

Optimization problems are ubiquitous in many fields, for example, image recognition problems in industry settings [1], problems involving decision-making in engineering [2], protein folding configurations in biology [3], SAT problems in computer science [4], minimizing energy consumption in process plants in chemistry [5], and solving for the ground state of quantum systems in physics [6].

Some problems belonging to the complexity class P can be solved in polynomial time. For problems in class P [7](P refer to polynomial scaling in resources), a classical computer can solve them in polynomial time and memory. However, many of the most interesting and important optimization problems are intractable with classical computers given their exponential complexity. In fact, most of these problems belong to the NP-hard or NP-complete classes (say NPC in short), i.e. it is unlikely to find polynomial-time algorithms to solve them. The exponential complexity for hard problems generally comes from the search space scaling exponentially with system size. Finding efficient algorithms to tackle hard optimization problems is critical solve the pressing issues of today. The nontrivial problems, especially those that are challenging for classical computers, stand to benefit most from quantum computation.

The interest in studying optimization problems with quantum computing is motivated by its potential to provide a quantum speedup with respect to the best known classical algorithms. A quantum computer takes advantage of quantum properties, such as superposition and entanglement, allowing it to simulate problems that are intractable on classical computer. Several quantum algorithms, such as Grover's algorithm, achieve polynomial speedups over their classical counterparts in finding a marked item in an unstructured data set. Shor's algorithm can factor integers into their primes superpolynomially faster than the best classical algorithm. Simulating quantum systems on quantum computers can also provide advantages over classical algorithms.

Both the quantum gate model and Quantum Annealing are promising for solving hard optimization problems. Quantum gate model computers use quantum parallelism to achieve considerable quantum speedup, but is very sensitive to decoherence. Quantum decoherence comes from the interaction of the quantum systems with the external environment. Information loss occurs as an irreversible process in the evolution of the system. Addressing quantum decoherence is a great challenge in producing scalable quantum computers. Error correction is then required to ensure the performance of quantum gate model in the presence of decoherence. Unlike the strong dependence on error correction in the quantum gate model, Quantum Annealing(QA) is an "analog" method which is less sensitive to decoherence, and does not

perform operations based on quantum circuits. QA takes advantage of quantum tunneling to tunnel through energy barriers between two minima, beating analogous classical algorithms that use thermal fluctuations to overcome barriers in some specific problems. The advantage is most pronounced when the barriers are thin and high. QA is somewhat resilient in flux qubits, where all the energy scales are large compared to the environmental temperature. However, to date, there is no rigorous mathematical proof guaranteeing quantum speedup in QA.

We consider analog Quantum Annealing as a promising method for solving optimization problems. Conventional QA introduces quantum fluctuation with a uniform transverse field $-\sum_i \sigma_i^x$. A total time dependent Hamiltonian is composed of the transverse field Hamiltonian and the problem Hamiltonian. The ground state of the problem Hamiltonian encodes the solution to the target optimization problem. The system is prepared in the ground state of the transverse field Hamiltonian initially, which is a uniform superposition of all possible states. Then, we evolve the system sufficiently slow. According to the adiabatic theorem, if the system starts in the instantaneous ground state, it will stay in the instantaneous ground state at the end of the anneal. By slowing ramping down the transverse field, we interpolate between the initial Hamiltonian and the problem Hamiltonian, ending in the ground state of the problem Hamiltonian, following the adiabatic theorem. Usually the performance of a quantum algorithm is compared with their classical counterpart, but in our case, we compare with standard uniform-transverse field QA.

In the analog quantum annealing simulations, we ask the question: can we find some variations of the traditional transverse field quantum annealing algorithm that provide polynomial or even exponential quantum speedup? We address this question in Chapter 3. We will show in Chapter 3 that some variations of QA can provide performance improvement, such as adding an inhomogeneous transverse field, adding transverse couplers, and adding an oscillating transverse field. We compare the performance of these variations of QA in solving a specifically designed hard optimization problem The artificial toy problem has a local minimum and a global minimum separated by an energy barrier. The Hamming distance [8] from the local minimum to the global minimum is N, which is the system size. To solve such a problem, a classical algorithm, such as simulated annealing, applies a local search, starting at an initial random state over the solution space and iterating to next state, tending towards lower energy. Since the random initial state is mostly distributed around the local minimum, simulated annealing has a tendency to get stuck in the local minimum. In quantum computing, the hardness of the problem lies in flipping all the N spins to go through the first order transition to reach the global minimum. For algorithms that can solve this toy problem efficiently, we believe they can solve such generic problems efficiently as well.

Within these promising candidates, one method, random field or radio frequency quantum annealing (RFQA), is the most promising among the ones we vetted. Since RFQA relies on real time dynamics,

quantum Monte Carlo methods will suffer from the so called "sign problem," [9], thus the Hamiltonian used in RFQA cannot be simulated efficiently on classical computers. Furthermore, implementing RFQA only requires minor changes in the quantum annealer. We expect RFQA to preserve its superiority either under moderate noise in an annealer, or in an error-free digital quantum computer. Also, the exponential proliferation of weak resonances in RFQA mixes states more rapidly, which leads to a polynomial speedup over a uniform transverse field sweep. We then want to expand the RFQA method from the analog QA regime to the quantum gate based circuit model. We study the behavior of the digitized RFQA and QA algorithms with similar generic problems that have exponential difficulty in reaching the global minimum, and we show the Trotterized implementation of RFQA in digital quantum computing also outperforms the digitized uniform field QA. Based on our simulations, we expect future RFQA experiments to demonstrate a quantum speedup over classical algorithms. In the third part of our work, to prepare for an experiment on RFQA, we explore the behavior of RFQA in 1D TFIM(transverse field ising model). The state is initially prepared as the false ferromagnetic ground state and we measure the success probability of reaching the true ferromagnetic ground state. We show that RFQA is able to accelerate the N-spin tunneling in reaching the true ground state, and the acceleration is promising to mitigate the heavy minor embedding overhead in experiment.

1.1 Analog QA

One promising way of solving combinatorial optimization problems is by Quantum Annealing, which takes advantage of quantum tunneling to tunnel through barriers between two minimum. Some classical algorithms use thermal fluctuations to climb over the barrier as shown in Figure 1.1. In the cost-configuration landscape of most optimization problems, there are high energy barriers at a phase transition or many local minima in a glassy system that makes the problem hard to solve. For classical algorithms such as Gradient Descent Algorithm (GDA), it's very likely to get stuck in a local minimum without overcoming energy barriers between the local and global minimum. In GDA, where one starts with a random configuration and moves a small step to a new configuration, a lower-energy configuration is always preferred while a higher-energy configuration is always forbidden. So the system will mostly end in a local minimum. The only chance of finding the global minimum is when the initial random configuration is fortuitously generated nearby the global minimum instead of a local minimum. To provide the chance of overcoming an energy barrier, a thermal fluctuation assisted algorithm, Simulated Annealing (SA)[10], assigns a probability to tunnel through the barrier based on temperature. In SA, a new timestep toward lower-energy configuration is also always preferred but a higher-energy configuration can be adopted with a temperature dependent probability $P = e^{-\Delta/KT}$ that decreases with the annealing temperature T. If the

temperature decreases with time sufficiently slow, the system will end in a global minimum at $t \to \infty$. By introducing thermal fluctuation in the annealing process, SA assigns a finite probability of reaching higher-energy configurations, so that one can avoid the situation of always moving towards lower-energy configurations.

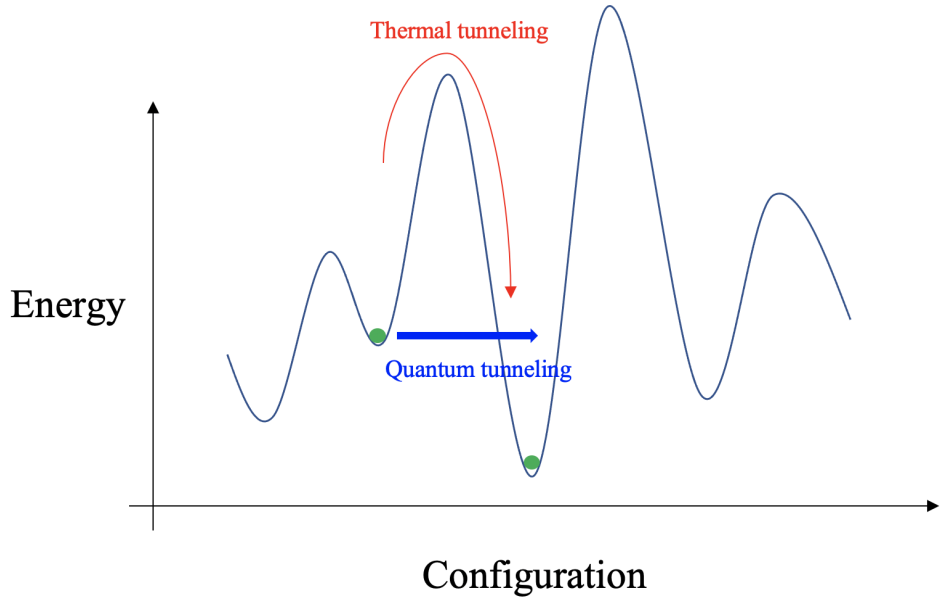

Figure 1.1 An example of the complex energy landscape in an optimization problem. Quantum Annealing uses quantum fluctuations to tunnel through barriers while Simulated Annealing climb the barrier with the help of thermal fluctuations. The latter method can get stuck in a local minimum.

SA updates the system to a new random configuration with a probability associated with the decreasing temperature, the non-ergodic local search in SA is not able to explore all the configurations of the system. A superior version of SA was developed to overcome the non-ergodicity of SA, called Parallel Tempering (PT)[11–15]. PT prepares several replicas of the system that are run in parallel at different temperatures, and swaps two different configurations with probability

$$p = min\left(1, e^{(E_i - E_j)(\frac{1}{kT_i} - \frac{1}{kT_j})}\right). \tag{1.1}$$

The exchange of high temperature configurations with low temperature ones allows a more efficient exploration of the configuration space.

The quantum version of annealing, Quantum Annealing, is distinguished from SA and PT by employing quantum fluctuations. The idea of QA is solving a hard problem H_p with the help of an easy one H_0, with the two Hamiltonians not commuting with one another. By starting from the ground state of the easy Hamiltonian, and evolving a Hamiltonian that interpolates between the easy Hamiltonian and the hard Hamiltonian sufficiently slow, the system will end up in the ground state of the hard Hamiltonian with

high probability. The ground state of the hard Hamiltonian encodes the solution to the hard problem. The form of the QA Hamiltonian is as follows

$$H(t) = A(t)H_0 + B(t)H_p, \tag{1.2}$$

where $t \in [0, t_f]$ and t_f is the total annealing time. The interpolation of the easy Hamiltonian H_0 and the hard problem Hamiltonian H_p is controlled by the annealing schedules $A(t)$ and $B(t)$. The annealing schedules usually satisfy $A(0) = 1, A(t_f) = 0$ and $B(0) = 0, B(t_f) = 1$, so that the initial total Hamiltonian is the easy problem and the final Hamiltonian is the hard one. The quantum fluctuation modifies the probabilities of finding all the possible states, reduced slowly to zero. By using the quantum tunneling to escape the classically localized states, QA can explore the landscape ergodically and find the ground state with high probability after the quantum fluctuation stops. There is numerical and theoretical evidence show that QA can outperform SA in most cases[16–19].

QA is the analog version of quantum computation, with the implementation being problem specific. There are many ways to evaluate the performance of QA, such as comparing the residual energy or the Hamming distance between the target state and the final state. To provide a straightforward illustration of scaling advantage, we consider the scaling of time to solution (TTS). TTS makes a trade off between the success probability and runtime. The success probability $P(t_f)$ is defined as the square of the overlap of the instantaneous state and the true ground state $|GS\rangle$ as

$$P(t_f) = |\langle\psi(t)|GS\rangle|^2. \tag{1.3}$$

1.1.1 Variations of Quantum Annealing

Conventional quantum annealing is implemented with a uniform transverse field to induce spin flips. Methods that assist or control the conventional quantum annealing are of broad interest now; in this section we list some outstanding ones.

To improve the performance of conventional quantum annealing, some modifications can be made on the uniform transverse field in the conventional quantum annealing. For example inhomogeneous driving field method can avoid the first order phase transition; or adding transverse couplers to enlarge the minimum gap energy gap; or oscillating field approaches can provide more opportunities in mixing states.

In inhomogeneous driving field method, the driving field applies different strengths to each spin, i.e. the transverse field on each spin will not be turned off simultaneously with the annealing time. A widely used choice is to turn off the field on each spin sequentially, a form of quantum annealing with inhomogeneous

driving field can be expressed as [20]

$$
\begin{aligned}
H(t) &= -\sum_{i=1}^{N} g_i(s)\sigma_i^x + sH_p, \\
g_i(s) &= \begin{cases} 1 & \text{if } n - vt > \frac{1}{2\alpha} \\ 0 & \text{if } n - vt < -\frac{1}{2\alpha} \\ \frac{1}{2} + \alpha(n - vt) & \text{otherwise} \end{cases}
\end{aligned}
\tag{1.4}
$$

The field on each spin attenuates with time at different rates. Of course, inhomogeneous field is not restricted to this form. Theoretical, numerical and experimental works show that the inhomogneous field method can outperform the homogeneous field in conventional quantum annealing [20–24]. It can remove or mitigate the first order transition, and thus provide performance improvements, such as minimizing the residual energy of the final state, promoting ground state success probability, or elevating escape rates from metastable clusters.

Adding transverse couplers is another modification made to conventional quantum annealing [25–29], a general form can be

$$
H(t) = s(t)H_p + (1 - s(t))H_0 + \lambda s(t)(1 - s(t))H_I \tag{1.5}
$$

where H_I can be a ferromagnetic coupler (H_I^F), an antiferromagnetic coupler (H_I^A) or a mixture coupler (H_I^M) as follows

$$
\begin{aligned}
H_I^F &= -\sum_{<i,j>}^{N} \sigma_i^x \sigma_j^x \\
H_I^A &= +\sum_{<i,j>}^{N} \sigma_i^x \sigma_j^x \\
H_I^M &= \sum_{<i,j>}^{N} r_{ij} \sigma_i^x \sigma_j^x
\end{aligned}
\tag{1.6}
$$

where r_{ij} is randomly chosen from $\{-1, 1\}$ to include both ferromagnetic and antiferromagnetic cases. Adding the ferromagnetic coupler H_I^F leads to a stoquastic Hamiltonian, while adding the antiferromagnetic or mixture coupler leads to a non-stoquastic Hamiltonian. The off-diagonal matrix elements in a stoquastic Hamiltonian are real and non-positive, whereas the path-integral configurations for such a Hamiltonian have real and non-negative contributions to the partition function and thus can be efficiently simulated by classical algorithms such as Quantum Monte Carlo algorithm (QMC)[9, 30]. However, a non-stoquastic Hamiltonian contains positive off-diagonal matrix elements, resulting in an oscillating probability distribution and will suffer from the so called "sign problem." Usually the sign problem is NP-hard and reveals the limitations of QMC. Since universal adiabatic quantum computing can

solve for the ground state of a non-stoquastic Hamiltonian, quantum speedup in quantum annealing is more likely to occur in problems with non-stoquastic Hamiltonians. In an long-range ising spin glass model[29], the ferromagnetic coupler that leads to a stoquastic Hamiltonian increases the energy gap and improves the success probability. The antiferromagnetic and mixture couplers that lead to a non-stoquastic Hamiltonian improve the success probability by increasing the number of anticrossings in the energy landscape. The improvement achieved in non-stoquastic Hamiltonians is large compared with the stoquastic Hamiltonian.

RFQA, as another modification of conventional quantum annealing, replaces the uniform transverse field with an oscillating one. The driving Hamiltonian in RFQA is either a magnitude-dependent oscillating field (referred to as $RFQA-M$) or a field with an oscillating direction in the x-y plane (referred to as $RFQA-D$). RFQA not only results in a non-stoquastic Hamiltonian, it requires minor changes to existing hardware.

The above methods are promising in solving hard optimization problems, so we investigate their behavior in solving generic hard problems in chapter 3.

Besides modifying the form of the Hamiltonian itself, many efforts have been made on the annealing schedule. The form of the annealing schedule can significantly change the efficiency of QA. Instead of using the conventional linear annealing schedule, $A(t) = 1 - s(t), B(t) = s(t)$, with $s(t) = \frac{t}{T}$, various annealing schedules can enhance the success probability. Here we list some important ones: the first one is a non-linear annealing schedule, where the $A(t)$ and $B(t)$ can be defined as a quadratic or higher order polynomial function of $s(t)$, but still follows the same boundary conditions that $A(0) = 1, A(T) = 0$ and $B(0) = 0, B(T) = 1$. A hybrid of quantum simulation and classical optimization can help find the optimal non-linear annealing schedule. Nonmonotonic annealing schedules show performance enhancement in many works [31–34] and are available on D-Wave processors [35, 36]. In the conventional forward annealing schedule, a pause during the anneal can also increase the chance of finding the ground state [37, 38], especially when pausing the system right after the minimum gap. The above adaptions are all classified as forward annealing that $A(t)$ decreases while $B(t)$ increases in the annealing process. In contrast with forward annealing, reverse annealing [31, 38–42] prepares the system in a local minimum of the problem Hamiltonian at $s(t) = 1$, then evolves backward to a point s_p, and evolving forward to $s(t) = 1$; the quantum fluctuations will increase then decrease to 0. Reverse annealing can circumvent the difficulty associated with traversing a first-order phase transition in some cases [39] and has demonstrated enhanced success probability. Figure 1.2 shows an example of a non-linear annealing schedule and Figure 1.3 a reverse annealing schedule.

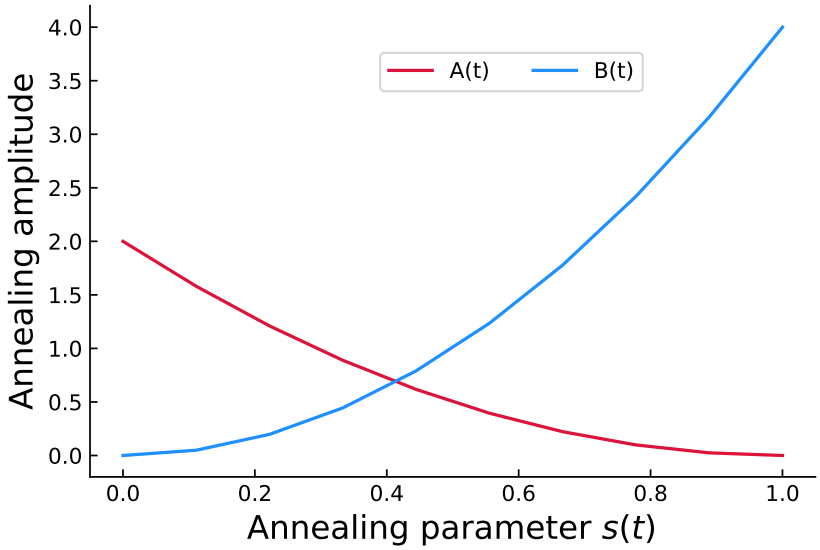

Figure 1.2 An example of non-linear annealing schedule, similar to the schedules applied in the D-Wave quantum annealer. A non-linear annealing schedule can sometimes improve the success probability in QA.

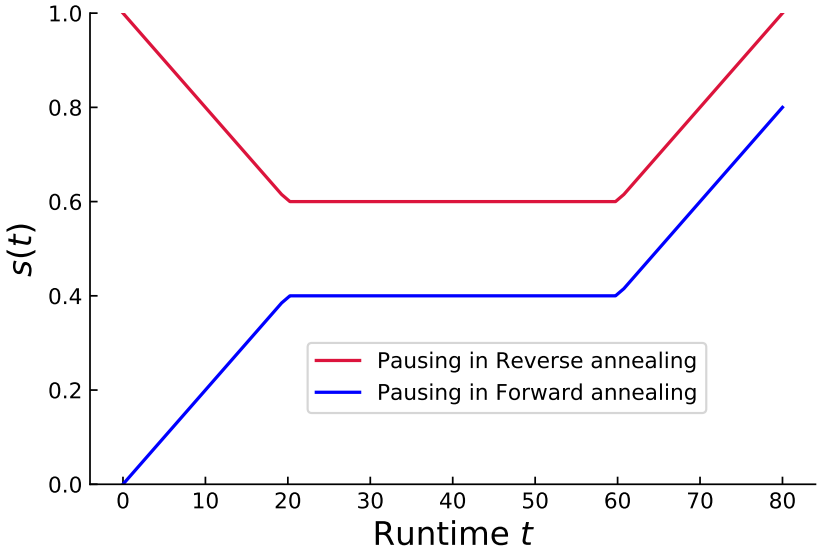

Figure 1.3 Example annealing schedules for pausing in forward and reverse annealing.

Intermediate pausing can also help in an annealing schedule[43]. Figure 1.3 shows a pausing in forward annealing and reverse annealing.

Except for the intermediate pausing, pauses during the annealing process starting before the transverse field strength reaches 0 can help minimize the Hamming distance between the desired ground state and the final state in spin glasses [44]. Moreover, starting with excited states instead of the ground state can be helpful as well [45, 46]. However, these adaptions are beyond the scope of this work.

1.1.2 Artificial hard problem instance in the analog quantum annealing

In chapter 3, we study an artificial toy problem that exhibits exponential hardness in finding a global minimum. Conventionally, the problem Hamiltonian is encoded into the Ising model and solve it with a uniform transverse field. We use this artificial problem as the problem model, since it is easier to study analytically. The problem model is defined on the magnetization $m = \frac{1}{2N}\sum_{i=1}^{N}(1+\sigma_i^z)$. The formulation of the problem Hamiltonian H_p is given by Eq.(3.6), in which the parameters A and x_p control the energy gap of H_p and the position of the energy barrier between local and global minimum. We make the problem tunable via the two parameters. In the definition of H_p, the local minimum locates in the position where the energy is 0 and magnetization equals 0. Here, every qubit spin is set in the down state so that $\frac{1}{2N}\sum_{i=1}^{N}(1+\sigma_i^z) = 0$. The global minimum, on the contrary, is an all spins up state and locates at $m = 1$ where the energy is $-A$. The two competing ground states are separated by the largest Hamming distance in this problem and both states are unique in their energy levels. However, the states in other energy levels are degenerate. For example, if half qubits are in the spin down state at $m = 0.5$, there are a total of $\binom{N}{N/2}$ degenerate states within this energy level. This results in a bell curve energy density distribution as shown in Figure 3.1.

To approach this problem classically, the random initial state is selected according to the energy density distribution as shown in Figure 3.1. This state will be centered near $m = 0.5$, and the iterations in classical algorithm will have a large tendency to stay in the all spin down configuration, a local minimum. Thermal fluctuations provide some probability to overcome the global maximum, but this problem is still difficult to solve with classical algorithms. Problem models with similar energy landscapes have been studied in [47, 48], where classical algorithms such as simulated annealing have been proven to be inefficient in finding the global minimum.

Quantum approaches to this problem will also be frustrated by the small energy gap. We choose a set of $\{A, x_p\}$ that leads to problems with exponentially decreasing minimum energy gaps (between the ground state and first excited state of $H(t)$). The corresponding runtime of the problem sets will increase exponentially with system size.

At the beginning of the evolution, the transverse field is turned on, and the system is prepared in the ground state of the driving Hamiltonian, which is a uniform superposition of states corresponding to all

possible assignments of bit values, i.e. the probability of finding the system in any one of the states is the same at the beginning. As the system evolves, the problem Hamiltonian is introduced, the magnitude of transverse field decreases, and the quantum fluctuation decreases. The instantaneous state is the ground state of this mixed Hamiltonian, with the probability of finding each state changing with time. At the end of the anneal cycle, the transverse field is turned off, and the quantum fluctuation stops, the system will end with the true ground state of H_p. However, the system may transit into the first excited state at some critical point, especially near the minimum gap. The minimum gap is a bottleneck in our problem model, as small perturbations may excite the system in the vicinity of minimum gap. When the system stays in the instantaneous first excited state, the probability of finding the true ground state will be suppressed while the probability of finding the false ground state dominates as shown in Fig.4(b).

1.2 Quantum computing

Classical computers encounter problems when simulating large quantum systems, where the Hilbert space scales exponentially with the system size N. The cost of simulating a many-particle quantum system is therefore exponentially large. Generally speaking, classical systems cannot efficiently simulate many-particle quantum systems. In the 1980s, Richard Feynman proposed the idea of quantum simulation, which uses particles that preserve quantum behavior instead of the classical bits, to simulate quantum mechanical processes [49]. This inspired interest in building a quantum computer. Such particles preserve quantum mechanical behavior are known as qubits in quantum computers. Unlike classical bits that are either 0 or 1, qubits are in a quantum superposition states of 0 and 1. A general expression of a quantum state is

$$|\psi\rangle = \cos\frac{\theta}{2}|0\rangle + e^{i\phi}\sin\frac{\theta}{2}|1\rangle, \tag{1.7}$$

which is represented by a point on the Bloch sphere. $|0\rangle$ and $|1\rangle$ are computational basis states, pointing along the z-axis of Bloch sphere, and θ, ϕ are the azimuthal and polar angles in spherical coordinates. The measurement outcome will be $|0\rangle$ with probability $\left|cos\frac{\theta}{2}\right|^2$, and $|1\rangle$ with probability $\left|sin\frac{\theta}{2}\right|^2$. For a spin 1/2 particle, the $|0\rangle$ and $|1\rangle$ represent the spin up and spin down states, defined by

$$|0\rangle = \begin{pmatrix}1\\0\end{pmatrix}, |1\rangle = \begin{pmatrix}0\\1\end{pmatrix}. \tag{1.8}$$

At any time t, a quantum computer is in a probabilistic state instead of a deterministic state. The quantum superposition is a big difference between quantum world and classical world. In a classical world, a bit in either $|0\rangle$ or $|1\rangle$ is enough to simulate the classical dynamics, but in the quantum world, a superposition state is needed to describe the fact that a quantum system can be in many states at the same time. In a pair of qubits, the state can be expressed as a superposition of $|00\rangle, |01\rangle, |10\rangle, |11\rangle$,

generally speaking, n qubits quantum system can be in 2^n states. For hundreds qubits, this number is impossible to be stored on classical computers especially because an n bits classical computer can only be one of the 2^n states. In contrast with classical computers, a quantum computer can be in the 2^n states simultaneously and only requires $\mathcal{O}(n)$ qubits to simulate the quantum system. Quantum computers utilize quantum mechanical properties such as quantum superposition, quantum tunneling, and quantum entanglement, which provide improvements in computational efficiency over their classical counterparts. Quantum computers promise to efficiently solve problems that are almost impossible in classical digital computers. Although superposition provides the possibility to simulate 2^n states simultaneously, measurement of the system will collapse it to a unique state if all the qubits are measured.

Following Feynman's idea of simulating a large physical system with special particles that show quantum mechanical effects, Shor found an efficient algorithm to compute discrete logarithms and factoring large numbers in their prime factors [50]. Shor then came up with the quantum error-correcting code and fault-tolerant methods to help quanutm computers resist decoherence [51, 52], which makes the idea of "quantum computer" no longer a "theorist's dream." In the integer factorization task, Shor's algorithm reduces the superpolynomial runtime $\mathcal{O}(e^{c(\log n)^{1/3}(\log\log n)^{2/3}})$ of the best-known classical algorithm to polynomial time $\mathcal{O}(n^3)$ in quantum computation. The significance of Shor's algorithm is that public key cryptography might be easily broken by a quantum computer, since Shor's algorithm can break RSA[53] in polynomial time. The speedup from Shor's algorithm thus sparks many efforts in developing quantum computers. Besides Shor's algorithm, Grover's algorithm also exhibits quadratic quantum speedup in searching for an item from an unsorted database [54]. The classical searching time $\mathcal{O}(n)$ is reduced to $\mathcal{O}(\sqrt{n})$. Grover's algorithm can be applied to speeding up algorithms that search for a solution. These quantum algorithms have generated interest in studying quantum computing algorithms and building quantum computing hardware.

Nowadays, quantum computing is a new tool for many fields[55–58]. Quantum Annealing is one type of quantum computing and an alternative to the quantum circuit model.

1.2.1 NISQ

We don't expect quantum computers to have practical commercial usage right away, since decoherence and errors are fatal issues when performing quantum circuits on larger systems. Existing quantum error correction proposals require a large number of additional qubits and logic gates to perform such corrections [59, 60]. Consider the smallest error rate per gate that can be achieved in today's quantum devices; it may still require one hundred thousand or even millions of additional qubits to run a practical algorithm. But it's still possible to take advantage of existing quantum computers of relatively small qubit

numbers in the *Noisy Intermediate-Scale Quantum Computing* (NISQ) regime [61, 62]. *Noisy* means the devices are not protected by error correction, leading to imperfect gates limiting the size and scope of problems that can be solved. *Intermediate-Scale* refers to a quantum device with 50 to 100 qubits, which at the upper end becomes infeasible to simulate on classical computers. Proof-of-principle demonstrations of quantum speedup from quantum computers is possible in such a regime even without comprehensive error correction. Although the performance of quantum algorithms may not have any practical purpose or are not implementable in larger systems, they can still motivate us to develop more advanced quantum devices to overcome the limitations of decoherence and investigate the future of quantum computing.

With the development of quantum error correction, we can expect to extend the computational power of useful algorithms in the NISQ regime to larger systems or even fully fault-tolerant quantum computing.

1.2.2 Quantum circuit model

After Feynman's quantum simulator proposal, Deutsch developed the quantum circuit model [63]. A universal quantum circuit model can simulate any Turing machine computation with at most polynomial cost. Whether a classical Turing machine can efficiently simulate a quantum circuit model is not known yet [64].

Quantum circuit model is different from analog QA, where an analog quantum simulator is very problem-specific and the dynamics of qubits resembles the target problem system. A quantum circuit model, composed of a sequence of reversible unitary quantum gates, is a universal gate-based quantum computation that can be designed to simulate any physical system of interest. Quantum logic gates will make a transformation of the qubit state, fundamental operators are the identity I and three Pauli matrices $\sigma_x, \sigma_y, \sigma_z$. Their matrix representations in the z-basis are given by

$$I = \begin{pmatrix} 1 & 0 \\ 0 & 1 \end{pmatrix}, \sigma_x = \begin{pmatrix} 0 & 1 \\ 1 & 0 \end{pmatrix}, \sigma_y = \begin{pmatrix} 0 & -i \\ i & 0 \end{pmatrix}, \sigma_z = \begin{pmatrix} 1 & 0 \\ 0 & -1 \end{pmatrix}, \tag{1.9}$$

in which σ_x gate introduces an bit flip, σ_z gate introduces a phase flip, and σ_y gate introduces both bit and phase flips. Besides the four fundamental single qubit gates, a set of universal gates is necessary in quantum computation. A finite set of quantum gates that can simulate any arbitrary quantum computation is called a universal gate set. This is analogous to the NAND and NOR gates that form a universal gate set in classical computation. Given the fact that the CNOT gate and single qubit gates can simulate any multi-qubit logic gates, a frequently used universal quantum gate set is $\{CNOT, H, T\}$, CNOT gate (short for "controlled-NOT" gate, also known as CX gate) flips the target qubit state if and only if the control qubit is $|1\rangle$, H gate (or Hadamard gate) maps state $|0\rangle$ to $\frac{|0\rangle+|1\rangle}{\sqrt{2}}$ and $|1\rangle$ to $\frac{|0\rangle-|1\rangle}{\sqrt{2}}$, T gate(or $\pi/8$ gate) is a phase shift gate that maps $|0\rangle$ to $|0\rangle$ and $|1\rangle$ to $e^{i\varphi}|1\rangle$, where the angle φ in the T

gate is $\pi/4$. The matrix representations of CNOT, Hadamard and T gate are

$$CNOT = \begin{pmatrix} 1 & 0 & 0 & 0 \\ 0 & 1 & 0 & 0 \\ 0 & 0 & 0 & 1 \\ 0 & 0 & 1 & 0 \end{pmatrix}, H = \frac{1}{\sqrt{2}} \begin{pmatrix} 1 & 1 \\ 1 & -1 \end{pmatrix}, T = \begin{pmatrix} 1 & 0 \\ 0 & e^{i\pi/4} \end{pmatrix}. \tag{1.10}$$

This set of universal quantum gate is not unique, there are other universal gate sets, but they can be approximated by each other with only a small overhead [65].

One of the distinct properties of quantum gates is the reversibility of a quantum logic operator. The input information can be determined from the output results, while gates in classical computation maybe be reversible or irreversible. Another difference between quantum computers and classical computers is the entanglement of qubits. Take the Bell states as examples,

$$\begin{aligned} |\beta_{00}\rangle &= \frac{1}{\sqrt{2}}(|00\rangle + |11\rangle); \\ |\beta_{01}\rangle &= \frac{1}{\sqrt{2}}(|01\rangle + |10\rangle); \\ |\beta_{10}\rangle &= \frac{1}{\sqrt{2}}(|00\rangle - |11\rangle); \\ |\beta_{11}\rangle &= \frac{1}{\sqrt{2}}(|01\rangle - |10\rangle). \end{aligned} \tag{1.11}$$

In any one of these entangled states, as long as we know the state of the first qubit, the state of second qubit is immediately specified. The state of each qubit cannot be considered independently in these states; this is called entanglement between the two qubits. The entanglement will not disappear even when the two qubits are physically separated. This is a unique property of quantum computation. Moreover, superposition and entanglement of quantum states enable quantum parallellism that can provide enormous quantum speedup over classical computers.

A fundamental rule in digital quantum computation is that for an operator A that squares to the identity, its matrix exponential has the property [66],

$$e^{iAt} = \cos(t)I + i\sin tA, \tag{1.12}$$

where t can be any real number. For general cases, the exponentiation of an operator(not necessarily squares to identity) can be decomposed as a Taylor series

$$e^{iH} = 1 + iH + \frac{1}{2!}(iH)^2 + \frac{1}{3!}(iH)^3 + ... = \sum_{n=0}^{\infty} \frac{1}{n!}(iH)^n, \tag{1.13}$$

The decomposition of the exponentiated operator can be expressed in a matrix representation. To implement a quantum circuit, we first need to prepare an initial state, which by convention is chosen as all $|0\rangle$ states: $|0\rangle^{\otimes n}$. It is easy to prepare all qubits in $|0\rangle$ state and make modifications based on the simple

product states to obtain any other desired initial state. Then, we apply quantum gates sequentially to induce state transformation. Finally, we make a measurement at the end of the circuits. After a measurement, the state will collapse to a classical state. A simplified illustration of gate model is shown in Figure 1.4. Take a 2-qubit computation as an example, the input state $|\Psi_0\rangle$ is usually prepared as $|00\rangle$, after n steps of unitary transformations, the final state will be $|\Psi_n\rangle$. The unitary operator U_i represents the discrete transformation of the state in one timestep of the evolution. The circuit depth in this simple case is n, which is the longest path of the circuit.

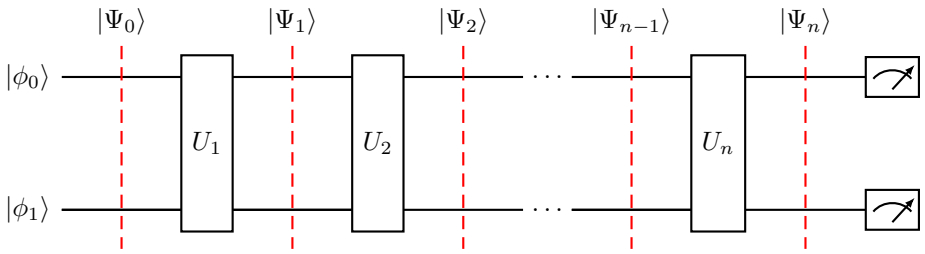

Figure 1.4 An algorithm in quantum gate model, the state of the two qubits are represented by $|\phi_0\rangle$ and $|\phi_1\rangle$ respectively, each boxes U_i represents a unitary transformation of the state of the system, the final meters in the end of the circuits represents classical measurements.

Since quantum computation is probabilistic, we assess a given algorithm in a quantum computer by analyzing both the runtime and the success probability, rather than only analyzing the computation time.

1.2.3 Error correction

To make a large-scale quantum computer, errors are not ignorable. The errors in a classical computer come from the unpredictable changes of the bit value, which is not very hard to detect and correct. Introducing redundant information is the basis of error-correction in classical computers [67]. Simply making copies of the bit and applying majority votes to the final results can eliminate errors.

In quantum computing, the same technique doesn't apply, since the quantum non-cloning theorem states that we cannot make a copy of an unknown quantum state [68–70]. This makes it nontrivial to apply error correction in quantum computing. However, the quantum threshold theorem [71, 72] states that a quantum computer with the help of quantum error correction, can be made fault tolerant if the physical error rate is below a certain threshold.

A quantum computer not only has bit errors (bit value flips) but it also experiences phase errors. A phase error, for example, changes the state $|\psi\rangle = \alpha|0\rangle + \beta|1\rangle$ to $|\psi\rangle = \alpha|0\rangle + e^{i\theta}\beta|1\rangle$ with an unwanted phase factor. These errors mostly come from the imperfection of gates or interactions between the quantum system and the external environment. Fortunately, both bit flips and phase flips are detectable

and correctable. The 3-qubit bit flip code [73], which uses 3 physical qubits to encode one logical qubit, is capable of detecting bit flips. The phase flips can be detected by the 3-qubit phase flip code. The 3-qubit bit flip code and phase flip code can detect errors, although they cannot correct bit and phase errors simultaneously [74], and they cannot detect more than one error.

The combination of the 3-qubit bit flip code and phase flip code makes the first quantum error correcting code, Shor's 9-qubit code [51]. In Shor's 9-qubit code, a single logical qubit is represented by 9 highly entangled physical qubits. The code can detect and correct arbitrary single qubit errors (bit error, or phase error, or both). Besides Shor's 9-qubit code, there are many other error correction codes [59, 75–78]. With the development of superior error correction codes, quantum computers can be expanded to larger sizes and provide more significant computing power.

1.2.4 Superconducting qubits

To perform a quantum computation, we need to initialize the qubits into desired states and measure the output in the end. There are several qubit representations that can satisfy the above conditions such as photon, charge and spin.

Some widely used physical realizations of qubits are (especially the first two):

1. superconducting qubits [79–81]
2. trapped ions [82–84]
3. quantum dots [85]
4. nuclear magnetic resonance (NMR) [86, 87]

Superconducting qubits include flux qubits [88, 89], charge qubits [90–92], and phase qubits [93, 94]. Current QA hardware utilizes superconducting flux qubits.

In the construction of flux qubits, the Josephson junction is an essential element due to its non-linearity and low dissipation at millikelvin temperatures. The Josephson junction consists of two superconducting thin aluminium films that are separated by a thin, insulating aluminium oxide layer. The following figure Figure 1.5 depicts the construction of a Josephson junction, The thin layer between the two superconducting layers not only can be an insulator [95], but also can consist of a normal metal [96, 97] or a kink of the superconductor [98] that weakens the superconductivity.

Below a critical temperature, T_c, the aluminum layers become superconducting, where electrical current flows without resistance. The superconductivity is due to the formation of Cooper pairs, or two electrons of opposite spin and momenta are weakly bound. The energy cost to break a Cooper pair is large under the critical temperature, such that the thermal energy is not enough to break a Cooper pair. In a Josephson Junction, the Cooper pairs in one of the superconducting layers are able to tunnel through the insulator,

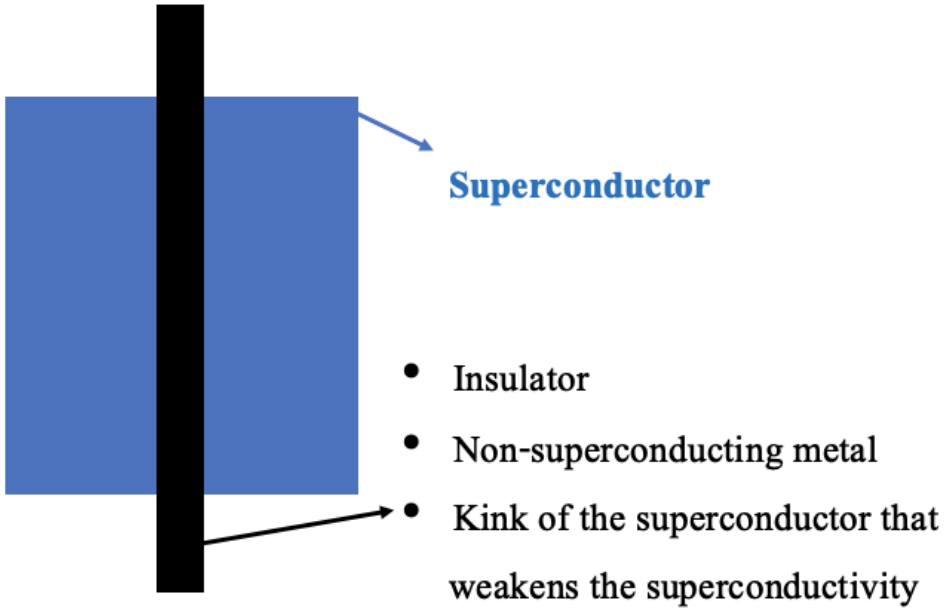

Figure 1.5 A Josephson Junction consists of a thin layer of insulator, sandwiched between two superconducting layers.

generating a supercurrent between the superconductors. Supercurrent that flows infinitely long without any voltage applied across a Josephson Junction is known as the dc Josephson effect [99, 100].

The Josephson inductance includes a non-linear term that restricts the dynamics of the system to the two qubit computational space, higher energy states are separated from the two lowest energy states. The separation creates a two level system that serves as the computational basis.

The coupling energy, or Josephson energy, that measures the strength of the coupling in the junction is denoted as E_J. The Coulomb charging energy is defined as E_C. When $E_J > E_C$, the circuit is a flux qubit, allowing the supercurrent to flow continuously with applied external magnetic flux. A flux qubit is composed of several superconducting loops interrupted by Josephson junctions. A typical three-junction flux qubit is made of three Josephson junctions connected by a superconducting loop. The superconducting loops are subjected to an external flux bias that tunes the frequency of qubit.

1.2.5 Digitized-QA

Analog Quantum Annealing is restricted by limited connectivity and interactions between qubits. As an alternative approach, digital quantum computation can provide more flexible interactions and is compatible with error correction. In the digital quantum computation, the Trotterization of the unitary

time evolution operator is divided into r Trotter steps

$$U(t) = \left(e^{-iHT/r}\right)^r, \tag{1.14}$$

in which we assume H is time independent. The Trotter steps r are defined in terms of the runtime T and time step dt as $r = T/dt$. A combination of the AQC and digital quantum computation was proposed by Barends *et al.* [101] and implemented on a superconducting quantum circuit with 5 Trotter steps. This digital adiabatic quantum computing is referred to as digitized-QA or digitized-AQC [102–104]. We use digitized-QA throughout our work.

The digitization of continuous time evolution in quantum annealing is constructed with the time-evolution operator

$$U(t_{n+1}, t_n) = e^{-iH(t_{n+1})dt}, \tag{1.15}$$

in which $dt = t_{n+1} - t_n$. By applying the first order Trotterization approximation [66, 105], these unitary operators can be represented by single or multi-qubit gates. A digitized-QA is a promising approach to realizing scalable quantum computation, albeit the overall error can be a combination of non-adiabatic error, Trotterization error, gate error and measurement error [101, 104].

The basic quantum circuit can be built from single qubit rotations and some two qubit gates, such as CZ, iSWAP or CNOT. Some complicated operations in a quantum circuit may need additional ancilla qubits. Gate errors from the single qubit and two qubit gates will accumulate, increasing linearly with the circuit depth. The Trotterization error is associated with the $\mathcal{O}(dt^2)$ term of the first order Trotterization approximation, even though there are higher order Trotterization approximations that give more precise approximation such as Eq.2.31, they inevitably introduce more gates and thus increase the gate errors. Since the gate error is usually large compared with the Trotter error, we can stay with the first order Trotterization approximation. Although an infinitely small time step dt approaches the continuous evolution of QA and can reduce the non-adiabatic errors, more Trotter steps introduce cumulative gate errors. In near term digital quantum computers, it's important to find a balance between the Trotterization error and gate error. The restriction on the number of gates will be removed if a fully fault-tolerant quantum computer can be realized.

1.3 Approximation algorithms

Finding the exact solution to optimization problems is usually intractable. An approximate algorithm does not guarantee an exact solution, but the bound on the deviation between the returned answer and the exact solution is predictable. Such as the two well-known quantum-classical hybrid algorithms Quantum Approximate Optimization Algorithm (QAOA), and Variational Quantum Eigensolver (VQE). The two

algorithms are essentially the same idea with the difference being that the problem Hamiltonian in QAOA is diagonal along Z, and the problem Hamiltonian in VQE is not constrained to be diagonal in the Z basis.

1.3.1 VQE

Variational methods are in quantum mechanics that provide approximations to the exact wave function and energy. These methods start with a trial wavefunction that is defined with variational parameters. The parameters are updated until the energy of the trial wavefunction is minimized. The Variational Theorem states that the energy of the trial wavefunction will always be larger than or equal to the ground state energy E_0

$$E_0 \leq \langle \psi | H | \psi \rangle \,. \tag{1.16}$$

The Variational Quantum Eigensolver (VQE) [106], a quantum-classical hybrid algorithm, has wide applications in quantum chemistry and optimization problems [107, 108]. VQE implements a variational method on a quantum computer to find the eigenvalues of a Hamiltonian H.

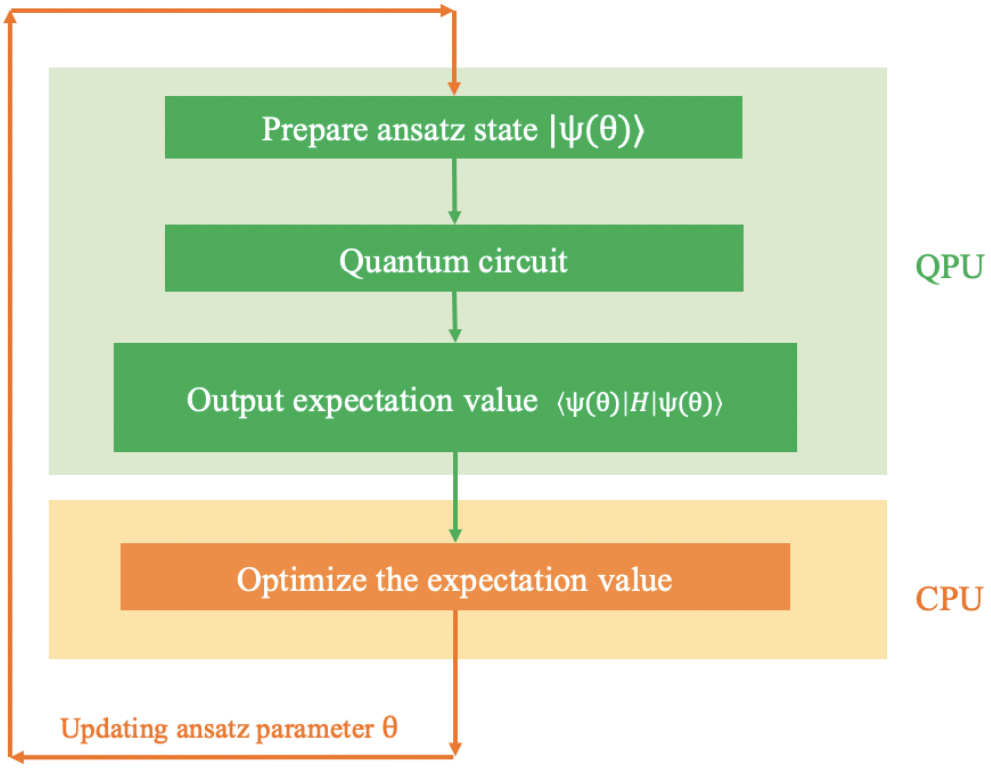

Figure 1.6 The computation of VQE is implemented on both the QPU (quantum processing unit) and CPU (central processing unit). The QPU prepares a parameterized ansatz state and returns the expectation value of the Hamiltonian H on the ansatz state. The CPU will optimize the expectation value and update the ansatz parameter to generate a new ansatz state on the QPU. The optimization process will stop if the minimum value satisfies the convergence criteria.

VQE prepares an *ansatz* state $|\psi(\theta)\rangle$ and measures the expectation value of the Hamiltonian $\langle\psi(\theta)|H|\psi(\theta)\rangle$. A classical optimizer then updates the ansatz parameter θ by minimizing the expectation value until it satisfies its convergence condition (s). The *ansatz* state here is an initial guess to the solution; it is ideally an ansatz state that covers the most possible states and with fewest number of parameters.

An illustration of how VQE works shown in Figure 1.6, the VQE is implemented with a quantum computer and a classical optimizer, by updating the ansatz parameter with the classical optimizer, VQE returns an approximation of the ground state energy. In some realistic problems, VQE doesn't require many qubits and is resistant to noise to some extent, and the circuit depth of VQE can be reduced if we properly choose an easier ansatz. Thus, VQE is compatible with NISQ-era devices.

1.3.2 QAOA

Quantum Approximate Optimization Algorithm(QAOA) is proposed by Farhi *et al.* [109] to produces approximate solutions for combinatorial optimization problems [109–112]. It has been shown that QAOA is able to generate output distributions [113] that are intractable on a classical computer and provide polynomial quantum advantages over classical algorithms to some specific problems [114–117]. An optimal solution approximation of the problem Hamiltonian can be generated with an optimized time sequence for each evolution stage, so the success of the QAOA highly depends on finding a good time sequence. An algorithm for Grover's search problem inspired by QAOA shows a quantum advantage over the original Grover's algorithm [114], although the rigorous proof of the quantum speedup from QAOA is not applicable to practical problems when noise is considered, QAOA is still a promising application of noisy quantum computers to realistic problems.

The implementation of QAOA takes advantage of the main idea in AQC, providing an approximation to the exact solution. The Hamiltonian in QAOA interpolates between a cost Hamiltonian H_C and a mixer Hamiltonian H_M, where the H_C encodes the optimization function, H_M is usually chosen as a homogeneous transverse field and serves as the driving Hamiltonian which has an easily prepared ground state. For example, when aiming at finding the minimum value of a optimization function, $H_M = -\sum_i \sigma_i^x$ is chosen by convention, whose ground state is $|\psi_0\rangle = |+\rangle^{\otimes N}$. A level-p QAOA circuit consists of $2p$ unitary gates that alternate between the exponentiation of H_M and H_C, and the variational wave function is

$$\begin{aligned} |\psi_p(\vec{\gamma},\vec{\beta})\rangle &= U(H_M,\beta_p)U(H_C,\gamma_p)U(H_M,\beta_{p-1})U(H_C,\gamma_{p-1})\cdots U(H_M,\beta_1)U(H_C,\gamma_1)\,|\psi_0\rangle \\ &= e^{-i\beta_p H_M}e^{-i\gamma_p H_C}\cdots e^{-i\beta_1 H_M}e^{-i\gamma_1 H_C}\,|\psi_0\rangle\,. \end{aligned} \tag{1.17}$$

The unitary operators $U(H_M,\beta)$ and $U(H_C,\gamma)$ are the exponentiation of parameterized Hamiltonians $e^{-i\beta H_M}$ and $e^{-i\gamma H_C}$ respectively. The approximation quality improves in QAOA as circuit depth p

increases.

The combination of H_M and H_C resembles the formulation of AQC, and the $2p$ parameters $\vec{\beta}$ and $\vec{\gamma}$ can be viewed as the annealing parameters. QAOA differs from AQC in that the parameters of QAOA will be optimized through a classical optimizer to help minimize the expectation value of H_C in this state:

$$E_p(\vec{\gamma},\vec{\beta}) = \left\langle \psi_p(\vec{\gamma},\vec{\beta}) \middle| H_C \middle| \psi_p(\vec{\gamma},\vec{\beta}) \right\rangle . \tag{1.18}$$

The approximate solution can be found by repeating the above measurement and minimizing $E_p(\vec{\gamma},\vec{\beta})$ with optimal parameters $(\vec{\gamma},\vec{\beta}) = (\gamma_1,\cdots,\gamma_p,\beta_1,\cdots,\beta_p)$ updated through a classical optimizer. The angles are allowed to arbitrarily vary during the evolution in QAOA. Besides that, AQC aims to find the optimal solution with a long enough runtime. The time step dt in the Trotterization of AQC in each step is the same and usually has to be very small to promise a success in AQC. While QAOA focuses on finding a good approximation, the circuit depth can be shallow to meet the requirements. For now, the lowest depth $p = 1$ QAOA has been extensively studied, its performance in the intermediate region $1 < p < \infty$ is also studied in some works[109, 118]. Moreover, since the parameters are appropriately optimized by the classical algorithm, QAOA is relatively robust to the small energy gaps which thwart the continuous time evolution in QA. Although QAOA includes digital errors, gate errors as well as non-adiabatic errors, the gate based algorithm is compatible with error correction, so it's in principle can be made fault tolerant.

CHAPTER 2

BACKGROUND

We introduce some background and preliminaries to readers in this chapter.

2.1 Computational complexity class

To have a better understanding of how powerful quantum computers are and what kind of problems are mostly investigated by Quantum Annealing, we introduce the computational complexity class in complexity theory which classifies the difficulty of problems and quantifies the resources and time required to perform an set of operations. A complexity class includes a collection of problems that requires similar computational resources to solve. Two fundamental classes are P and NP, problems in "P" class can be solved by a deterministic classical computer in polynomial time. Problems that are computable in polynomial time are relatively feasible, but for some problems that require more computational resources, they can be intractable to find an exact solution, such as some problems in "NP" class. The solutions of "NP" problems can be verified by a deterministic classical computer in polynomial time, but a polynomial time to solution is not known. One thing to note is that it's not always true that P problems are easy and NP problems are hard. Many problems (or subclasses of problem) in NP for example are fairly tractable for smart classical algorithms, even if the hardest problems remain exponentially hard

Some problems that cannot be solved efficiently, such as "NP-complete" (NPC) and "NP-hard" problems, are encompass a large swath of realistic problems. Any NPC problem is at least as hard as all other problems in NP, and every problem in NP is reducible to NPC in polynomial time. An efficient solution to even a single NPC problem can be used to efficiently solve all NP problems at the cost of extra overhead in time that depends polynomially on the system size. The famous 3-SAT problem can be classified as NPC. An NP-hard problem is at least as hard (in the worst case) as the hardest problem classes in the NP classes, but does not have to be in NP. A problem is NP-hard if NP problems can be reduced to it with polynomial overhead, or an NPC problem can be reduced to it in polynomial time. The traveling salesman problem is NP-hard. Whether NP problems can be quickly solved is not determined, this is also known as the famous question of whether P=NP. It's widely expected that P != NP, which indicates that there is no polynomial-time, exact algorithms for any NP-hard problems .

The above computational complexity classes are for classical computations, there are complexity classes defined for quantum computers such as BQP, QMA (Quantum Merlin Arthur) that resemble the P and NP defined for classical computers. The BQP problems can be solved by a quantum computer in polynomial

time. In QMA problems, the answer "YES" can be verified by a quantum computer in polynomial time. The relationship between NP and BQP is likewise unknown, and it is suspected to be disjoint from NPC class, which means many of the truly hard problems are still not solvable in polynomial time, even by a quantum computer. So the focus in quantum computation is mostly on how a quantum computer performs on NPC or NP-hard problems, e.g. optimization problems.

And exact algorithms to solving hard problems are very rare, so in most cases we have to build algorithms based intuition, which are called heuristic algorithms. Although the accuracy or the runtime for the worst case instance in heuristic algorithms are not guaranteed, these algorithms can provide effective solutions to the intended problems. Figure 2.1 is a diagram showing the relationship between the above mentioned computational complexity classes, in which P!= NP (but this has not been proven so far).

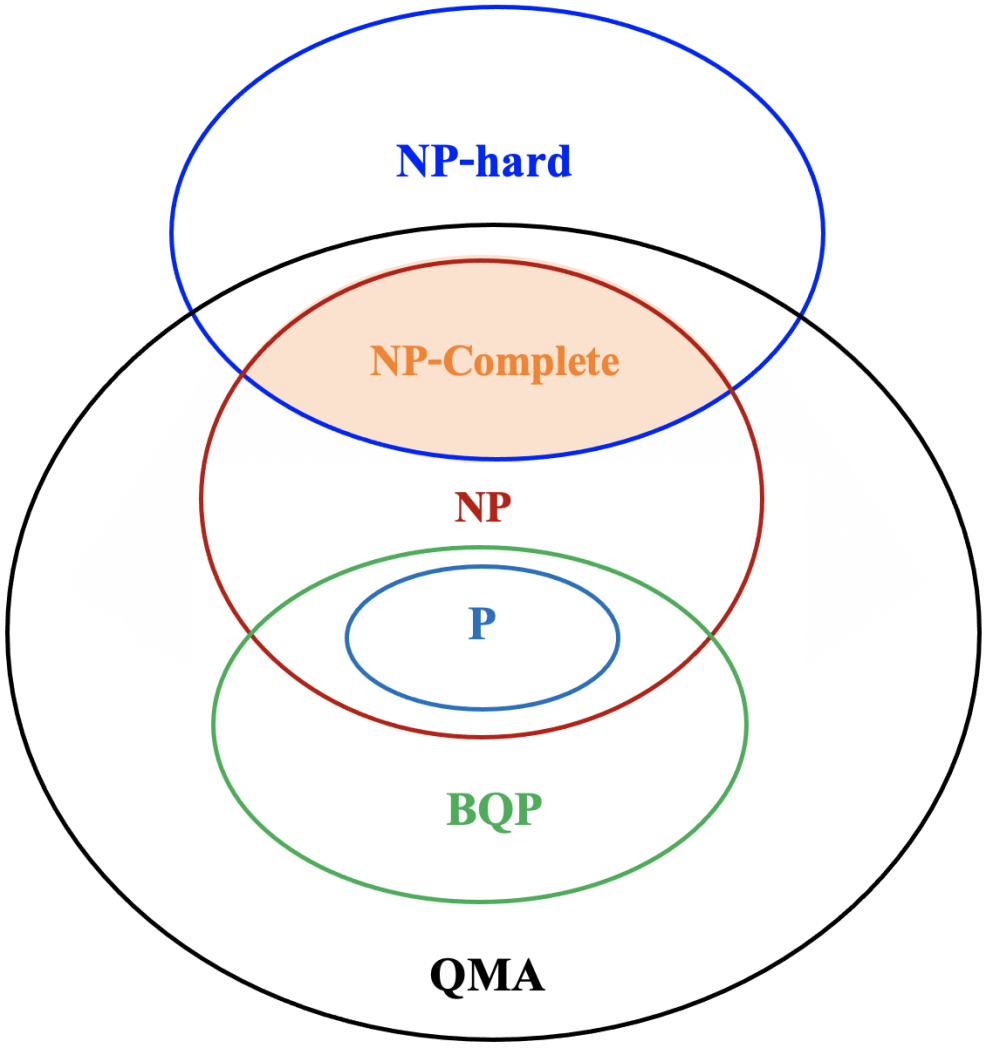

Figure 2.1 Conjectured lationships between classical and quantum complexity classes(not proven).

2.2 Combinatorial optimization problems

The task of an optimization problem is to find the best solution (maximum or minimum) among all options that depend on many independent factors, which can be cast as minimizing (or maximizing) a given cost function $H(s_1, s_2, ..., s_N)$. We need to find a variable set of $\{s_1, s_2, ..., s_N\}$ that gives the minimum value of $H(s_i)$. In many cases, problems with continuous variables $\{s_i\}$ can be transformed to problems with discrete variables [119], where s_i takes a finite and discrete number of values, being called combinatorial optimization problems.

All combinatorial optimization problems involve searching for the best variable set of some set of discrete variables. There are some famous combinatorial optimization problems such as the Travelling Salesman Problem (TSP), minimum spanning tree problem, exact cover, maximum cut, and satisfiability problems. Most of the interesting problems belong to NP class, especially NP-hard and NP-complete class, so to find an exact solution will take exponentially many steps or even is impossible as the system size grows. Therefore, approximate algorithms that can efficiently find an approximate, but accurate solution will be more practical. Generic algorithms, such Simulated Annealing and Quantum Annealing, are alternative approaches to solve combinatorial optimization problems, as they can reach an exact solution after an infinitely long runtime. Simulated and quantum annealing can also provide an approximate solution within a finite runtime.

2.3 Preliminaries of analog QA

In this part, we introduce adiabatic theorem and Landau-Zener transition and discuss the relationship between AQC and QA, as well as quantum combinatorial optimization in quantum spin glasses system, then we discuss the experimental realization of analog QA in the D-WAVE quantum annealer.

2.3.1 Adiabatic theorem

Adiabatic processes are traditionally used in thermodynamics, which means there is no heat transfer between the system and its environment. Such processes occur most often at equilibrium. However, in a quantum mechanics, an adiabatic process is used to describe a slow process where conditions change gradually and the system can adapt its configuration, i.e. if the system starts in an instantaneous eigenstate of its Hamiltonian, it will end in the corresponding instantaneous eigenstate of the Hamiltonian. A diabatic process, in contrast with an adiabatic process, describes a process where the system cannot adapt its configuration due to rapidly changing conditions. The state from time t_a to time t_b will look the same at runtime $T \to 0$: $|\psi(x, t_a)|^2 = |\psi(x, t_b)|^2$. Although the spatial probability density will not change, diabatic process will lead to an eigenstate that resembles the form of the initial state composed of a

superposition of different eigenstates of $H(t)$.

The Hamiltonian in a quantum annealing process is time dependent, denoted as $H(t)$. The state evolves under this time-dependent Hamiltonian according to the time-dependent Schrödinger equation

$$i\hbar\frac{\partial}{\partial t}\Psi(t) = \hat{H}(t)\Psi(t) \tag{2.1}$$

The adiabatic theorem describes properties of a quantum system evolving according to the schrödinger equation: A physical system remains in its instantaneous eigenstate if a given perturbation is acting on it slowly enough and if there is a gap between the eigenvalue and the rest of the Hamiltonian's spectrum[120].

A usual expression of the adiabaticity condition can be derived from the adiabatic theorem:

$$\frac{1}{\Delta_{10}^2(t)}\left|\langle 1(t)|\frac{\mathrm{d}H(t)}{\mathrm{d}t}|0(t)\rangle\right| \ll 1, \tag{2.2}$$

where the $|1(t)\rangle$ and $|0(t)\rangle$ are instantaneous first excited state and ground state, and $\Delta_{10}(t)$ is the energy gap between the ground state and first excited state. Choosing an appropriate runtime T is crucial in quantum annealing. With a linear annealing schedule $s(t) = t/T$, we can deduce from the adiabaticity condition that the required evolution time T to finding the ground state is

$$T \gg \frac{1}{\Delta_{min}^2}\left|\langle 1(s)|\frac{\mathrm{d}H(s)}{\mathrm{d}s}|0(s)\rangle\right|, \tag{2.3}$$

where the Δ_{min} is defined as

$$\Delta_{min} = \min_{0\leq s\leq 1}\left(E_1(s) - E_0(s)\right), \tag{2.4}$$

it denotes the minimum gap between the ground state and first excited state. From this more common adiabatic condition, we see that the efficiency of quantum annealing is limited by the small gap between two competing ground states. The total annealing time required to end up with the ground state of the final Hamiltonian has a inverse dependence on the minimum gap. For systems that go through a second order phase transition, the minimum gap is usually polynomially decreasing with system size, correspondingly, the runtime will increase polynomially with system size. The computational complexity in passing through a second order phase transition can be classified as "easy," but a first order phase transition [121, 122] is usually accompanied by an exponentially decreasing minimum gap and thus the required runtime to find the ground state accurately will increase exponentially with system size. We see the first order transition is the bottleneck in quantum annealing, in many NPC problems, the exponentially closing gap always appears near the end of the annealing, leading the system to be trapped by many local minima [123]. Figure 2.2 shows an example of an avoided crossing between the ground state and first excited state. The minimum gap between the two competing states is extremely small and the corresponding runtime will be very long. For a level crossing case, which corresponds to $\Delta_{min} = 0$, the adiabatic theorem doesn't apply.

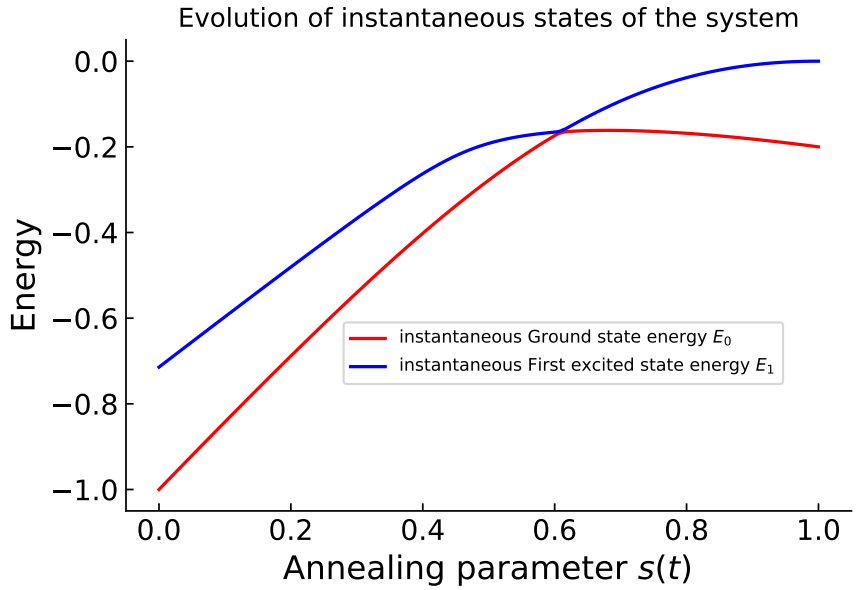

Figure 2.2 An example of the evolution of a system during quantum annealing. The instantaneous ground state and first excited state has an avoided crossing at a critical point. An exponentially closing gap of this kind can be a fatal issue in a conventional quantum annealing process.

To avoid the level crossing, the initial Hamiltonian H_0 and problem Hamiltonian H_p are always chosen as operating in orthogonal bases so that a level crossing is unlikely to happen.

For an annealing parameter s that changes uniformly with time, we can denote the evolution as global evolution. The criteria in Eq.2.3, specifically for the linear annealing schedule, reveals that the runtime T in the global evolution scheme is proportional to the inverse of minimum gap squared: $T \propto \Delta_{min}^{-2}$. In contrast with the global evolution, a non-linear annealing schedule represents a local evolution that can provide a quadratic enhancement of the computation time. Local evolution can decrease the runtime T to $T \propto \Delta_{min}^{-1}$ if we can slow down the annealing in the vicinity of the avoided crossing. By applying the chain rule $\frac{\mathrm{d}H(t)}{\mathrm{d}t} = \frac{\mathrm{d}H(s)}{\mathrm{d}s}\frac{\mathrm{d}s}{\mathrm{d}t}$ in Eq.2.2, we find the rate of change of the annealing parameter s has to satisfy

$$\left|\frac{\mathrm{d}s}{\mathrm{d}t}\right| \gg \frac{1}{\Delta_{10}^2(t)}\left|\langle 1(s)|\frac{\mathrm{d}H(s)}{\mathrm{d}s}|0(s)\rangle\right|. \tag{2.5}$$

However, properties (location and magnitude) of an avoided crossing is generically unknown and there is no straightforward way to predict them. To discuss general cases, we apply the global evolution to QA.

2.3.2 Landau-Zener transition

In an ideal case where the system is isolated from the environment, we assume the system is a two-level system and transitions only happen between the ground state (the ground state is not degenerate) and first

excited state. The transition dynamics of a two-level system is governed by the Landau-Zener formula, where the time-dependent Hamiltonian of the system can be written as

$$H(t) = \frac{\alpha t}{2}\sigma_z + \Omega\sigma_x, \tag{2.6}$$

the matrix representation is

$$H(t) = \begin{pmatrix} \frac{\alpha t}{2} & \Omega \\ \Omega & -\frac{\alpha t}{2} \end{pmatrix}, \tag{2.7}$$

where $\alpha > 0$. The total Hamiltonian is the sum of an unperturbed Hamiltonian $H_0 = \frac{\alpha t}{2}\sigma_z$ and a perturbation term $H' = \Omega\sigma_x$. The matrix representation of the unperturbed Hamiltonian is

$$H_0 = \begin{pmatrix} \frac{\alpha t}{2} & 0 \\ 0 & -\frac{\alpha t}{2} \end{pmatrix}, \tag{2.8}$$

the ground state energy is $E_0^{(0)}(t) = -\frac{\alpha t}{2}$ and the first excited state energy is $E_1^{(0)}(t) = \frac{\alpha t}{2}$. At an initial time $t < 0$, the instantaneous ground state is $|0\rangle = \binom{1}{0}$ and the first excited state is $|1\rangle = \binom{0}{1}$. As time evolves to $t > 0$, the two states reverse. We regard the energy difference between them as $\Delta_{01} = \alpha t$, which is a linear function of time and will disappear at a critical time (level crossing). After introducing the perturbation term, a constant transverse field, the energy separation between the two states will be lifted and contribute to an avoided crossing as shown in Figure 2.3.

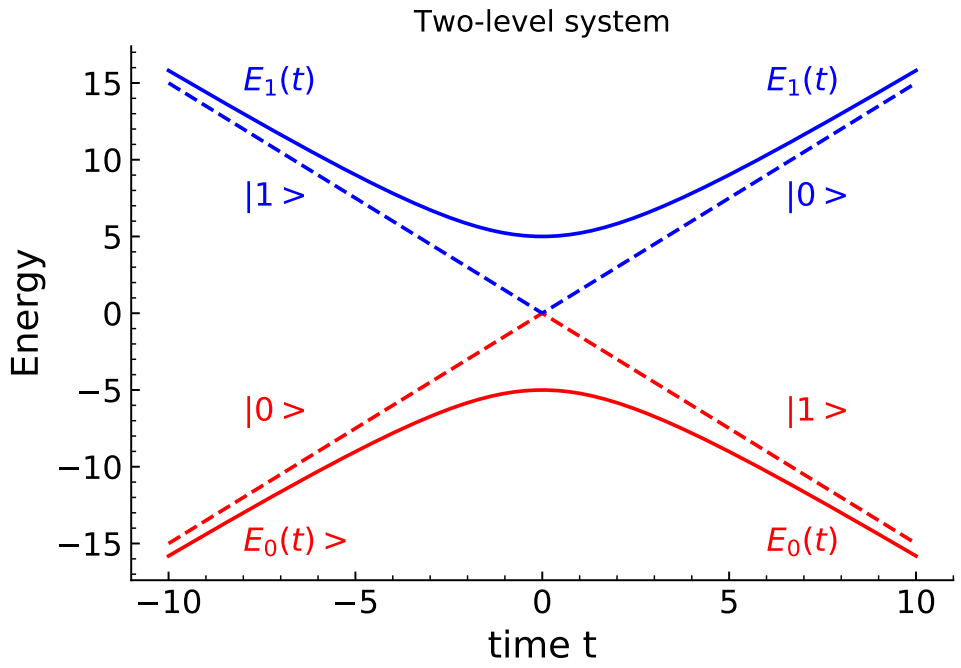

Figure 2.3 The energy landscape of $H(t)$ in a two-level system, the red and blue dashed lines are the instantaneous ground state and first excited state without a perturbation, which is $\Omega = 0$. The states with a perturbation are represented by red and blue solid lines.

The lifted ground state and first excited state energy in the perturbed Hamiltonian are given by

$$\begin{aligned} E_0(t) &= -\sqrt{|\Omega|^2 + \frac{\alpha^2 t^2}{r}}, \\ E_1(t) &= \sqrt{|\Omega|^2 + \frac{\alpha^2 t^2}{r}}. \end{aligned} \tag{2.9}$$

The minimum gap between the two states is $\Delta_{min} = 2\Omega$ at the critical time. In a infinitely slow quantum annealing process, the adiabatic theorem promises that the system will stay in the instantaneous eigenstate of the Hamiltonian. However, in realistic quantum annealing evolution, a non-adiabatic transition is possible due to the finite runtime. If the system starts in the ground state, the Landau-Zener formula gives the diabatic transition probability as [124]

$$P_{0\to 1} = e^{-2\pi \frac{|\Omega|^2}{\hbar\alpha}}. \tag{2.10}$$

The transition probability decreases exponentially with the minimum gap 2Ω. For a large system size, a second order transition results in a polynomially small minimum gap, while a first order transition comes with an exponentially small minimum gap. Thus, the excitation probability of a system undergoing a first order transition will be a bottleneck of QA.

From Figure 2.3, we define τ_{01} as the timescale for the system to change into a new state, which is proportional to $\frac{\Omega}{\alpha}$. In the neighborhood of $t \to 0$, the Hamiltonian can be approximated by

$$H(t=0) = \begin{pmatrix} 0 & \Omega \\ \Omega & 0 \end{pmatrix}. \tag{2.11}$$

If the system starts with the state $|0\rangle$, the transition probability from $|0\rangle$ to $|1\rangle$ is

$$P_1 = \sin^2(\frac{\Omega t}{\hbar}). \tag{2.12}$$

This transition probability is dominated by the Rabi frequency[125] $\omega_{01} = \frac{\Omega}{\hbar}$, with the timescale of the Rabi oscillation in the small region given by $T_{01} = \frac{2\pi\hbar}{\Omega}$. The evolution is an adiabatic process if the system state change timescale τ_{01} is much larger than the Rabi oscillation timescale T_{01}. We can derive the adiabaticity condition in the Landau-Zener transition process as

$$\frac{\Omega^2}{\hbar\alpha} \gg 1. \tag{2.13}$$

The above results for the Landau-Zener transition is valid under the assumption that there are only two ground states in competition with the transverse field controlling the minimum gap between them, and the ground state is not degenerate. When states are degenerated, the crossing structure can be more complicated, so we do not expect the same results apply in the case of many competing ground states.

2.3.3 AQC and QA

Adiabatic Quantum Computing(AQC), as an alternative to the quantum gate model, is an analog quantum computation which shares essentially the same idea with Quantum Annealing (QA). AQC is equivalent to the quantum circuit model up to a polynomial overhead in resource, and that such constructions require more comlicated terms than a transverse field and problem Hamiltonian along Z. QA was originally invented by Hidetoshi Nishimori in the late 90s [126], and then Edward Farhi in the early 2000s proposed Adiabatic Quantum Computing [127, 128]. They are very similar in concept and the basic technical difference is that AQC is formally a closed system idea and QA is an open system one. AQC requires adiabaticity in the evolution process while QA is not restricted to adiabaticity. In AQC, the algorithm runs adiabatically on closed system such that there is no interference from the external environment. Thus, the adiabatic theorem can be applied to make a good prediction of the annealing process and provide a reasonable bound on the computation time, which makes AQC an exact algorithm. In QA, however, the algorithm is implemented on a realistic quantum platform where noise can interfere with the system since real quantum hardware cannot be perfectly isolated from its environment. Adiabaticity is not guaranteed in an open system. As a result, the strong theoretical guarantees on runtime and success probability in AQC does not promise the success in QA. The lack of a precise bound on computational resources makes QA a heuristic algorithm. Generally speaking, QA is a heuristic algorithm that incorporates the basic concepts of AQC with realistic quantum hardware and allows non-adiabatic transitions to happen during the annealing process.

AQC is a universal quantum computation that can run any quantum algorithm, not only applied on optimization problems. The computational power of AQC has been proved to be equivalent to the quantum circuit model up to a polynomial prefactor [127, 129]. AQC differs from the quantum gate model in that the evolution in AQC is not discrete time, and there are no gates applied during the evolution. The Hamiltonian will be transformed gradually from an initial Hamiltonian H_0 to final Hamiltonian H_p. The qubit states are measured when the anneal ends. What makes AQC sometimes more useful than quantum circuit model is that it is more robust against decoherence. The interaction between qubits and external environment will result in the loss of information and a decrease in the success probability in quantum gate model. In AQC, the state is always kept in the ground state, as long as the environmental temperature is not comparable to the energy gap between the ground state and first excited state, the excitations from external environment can be ignored. The system can stay coherent for a relatively long time, thus decoherence is no longer threat to AQC, although other challenges remain.

The total time-dependent Hamiltonian used in AQC is

$$H(t) = A(t)H_0 + B(t)H_p, \tag{2.14}$$

where $A(t)$ and $B(t)$ ensure that $H(0) = H_0, H(T) = H_p$. T is the total annealing time (or runtime). The ground state of a problem Hamiltonian is guaranteed by the adiabatic theorem after a sufficiently long annealing time. A state is initialised in a trivial state, such as the equal superposition of all possible states, in AQC and evolves adiabatically to the solution. In QA, the driving Hamiltonian H_0 is usually chosen to be orthogonal to the problem Hamiltonian H_p, so that the heuristic search is able to escape local minima. The state in QA can start in an arbitrary initial state and eventually converge to the ground state or find a state with a high overlap with the ground state under diabatic evolution. The general form of QA is a bit different from AQC,

$$H(t) = \Gamma(t)H_0 + H_p, \tag{2.15}$$

where $\Gamma(t)$ is the strength of transverse field, and starts with a large value and reduces to 0 at $t = T$. The two forms are essentially the same, and have been used interchangeably, we will use the formulation of AQC throughout our work. The D-Wave quantum annealer also implements QA using the "AQC" formulation of the Hamiltonian. The speedup mechanisms we simulate are claimed to be resilient to noise in the open system setting. In addition, we will discuss the use of a cold bath to decrease the time to solution. From hereon, we will refer to these algorithms as quantum annealing.

2.3.4 Spin glasses and ising model

Quantum Annealing is promising in solving optimization problems. An important task in physics is searching for the ground state of a spin system, especially a system with frustration and disorder such as spin glasses. Many practically intractable problems can be reformulated as the task of finding the ground state of a spin glass system, which has been extensively studied with Quantum Annealing [130–134]. Spin glasses are amenable to simulating on a quantum computer.

Let's first take a ferromagnetically coupled spin chain(original ferromagnetic Ising model) as an example. The ground states for such a system will be either the all spin up state or the all spin down state, and the rest of the states are excited states, the energy landscape of which will be a double well. But in spin glasses, the coupling between pairwise spins are randomly ferromagnetic or antiferromagnetic. In this picture, the general model is

$$H = -\sum_{<i,j>} J_{ij} S_i S_j - \sum_i h_i S_i, \tag{2.16}$$

where S_i are Ising spins and J_{ij} are frustrated interactions, random in sign and magnitude. h_i are random longitudinal fields. The difficulty of reaching the ground state of spin glasses lies in the first order phase transition at zero temperature. In the absence of an external field, the spin glass can be described by the Edwards-Anderson model[135], the Hamiltonian can be expressed as:

$$H = -\sum_{<i,j>} J_{ij} S_i S_j. \tag{2.17}$$

The couplings are between all nearest neighbors, the distribution of strength J_{ij} subjects to some probability distribution $P(J_{ij})$. Another model that is usually used to model spin glass is Sherrington–Kirkpatrick model[136], this model is an infinite-range spin glasses model, the Hamiltonian is

$$H = -\sum_{i<j} J_{ij} S_i S_j. \tag{2.18}$$

The couplings are between all distinct pairs of spins. Both Edwards-Anderson (EA) model and Sherrington-Kirkpatrick (SK) model are well studied.

The energy landscape in a spin glass includes many local minima and global minima with entropic barriers between them. This differs from the energy landscape of the easy model we mentioned above. The frustration and disorder in the spin glass will lead to a complex energy landscape and can be encoded as a hard combinatorial optimization problem. The model of spin glasses can also be used to model some NP-Complete problems and other hard problems, such as the SAT problems. To study spin glass with quantum annealing, the uniform transverse field is always introduced, which leads to the famous transverse field Ising model (TFIM).

Another widely studied problem similar to spin glasses is the Ising model, which is designed as the problem Hamiltonian H_p in the D-Wave quantum annealer. The D-Wave chip is a type of quantum computer implementing the quantum annealing algorithm to solve NP-hard optimization problems. The Ising model in statistical mechanics is given by

$$H(s) = -\sum_{<i,j>} J_{ij} s_i s_j - \sum_i h_i s_i, \tag{2.19}$$

where s_i is the spin of each particle and can take the value -1 or +1, h_i is the external field applied to each particle, and J_{ij} is the interaction between two particles. By convention, there is a negative sign before J_{ij} and h_i. $J_{ij} > 0$ represents a ferromagnetic coupling, $J_{ij} < 0$ represents an antiferromagnetic coupling. The optimization problem built on the Ising model is to find a spin configuration $s = \{s_1 s_2 ... s_n\}$ that minimizes $H(s)$. To encode this model in quantum annealing, we use the Pauli-z operator σ_i^z of each qubit to represent s_i of each particle. The problem model H_p in QA is defined by

$$H_{ising} = -\sum_{<i,j>} J_{ij} \sigma_i^z \sigma_j^z - \sum_i h_i \sigma_i^z. \tag{2.20}$$

The Ising model is closely related to Quadratic Unconstrained Binary Optimization (QUBO) problems that are a central problem class for AQC and QA. In QUBO problems, variables $x_i \in 0, 1$, which are more convenient to work with since heuristic algorithms deal with binary-valued inputs and outputs. The spin variables σ_i^z in the Ising model can take discrete values from $-1, 1$. The Ising model can be easily modified to a QUBO problem by the transformation $\sigma \to 2x - 1$.

2.3.5 D-Wave quantum annealer

A Canadian quantum computing company, D-Wave, produced the first commercially available analog quantum annealing device. However, the quantum computers made by D-Wave are not universal ones, they are designed to implement the quantum annealing algorithm to solve problems mapped to a specific objective function, such as The Ising model or QUBO functions. Any higher order problem can be reduced to a QUBO with polynomial overhead, but the overhead can be costly for many body interactions. In an Ising model, given a set of J_{ij} and h_i, the task in this optimization problem is to find a spin configuration that minimizes the objective function (2.19). The electronic signals that control the weights h_i and J_{ij} are called "biases" applied to the qubit and to the couplings between qubits. These biases correspond to applied currents on the flux bias lines of the tunable couplers between connected qubits and biases applied to the flux qubits representing the spins.

To solve an optimization problem with the D-Wave quantum chip, first we have to map the problem to the quantum Ising model as in Equation (2.20) and embed the Ising model on the hardware to start the annealing process. Transforming a realistic NP-hard or NP-Complete optimization problem to the Ising formulation is usually not difficult to realize. The D-wave machine now has a wide range of usage in material science, chemical engineering, machine learning, financial modeling, risk management, and so on.

The driving field Hamiltonian H_0 in the quantum annealing of the D-Wave QPU is

$$H_0 = -\sum_i \sigma_i^x, \tag{2.21}$$

and the total Hamiltonian implemented in the D-Wave quantum annealer is

$$H(t) = A(t)H_0 + B(t)H_{ising}, \tag{2.22}$$

There the annealing schedule is similar to the schedule in Figure 1.2. The problem Hamiltonian H_p is a 2-local Hamiltonian, with the k-local Hamiltonian as the sum of independent Hamiltonians each involving at most k qubits. The operators in H_p act on at most 2 qubits. The limited connectivity structure in local Hamiltonians makes them more applicable to a real quantum computer. The initial state of the system is prepared as the ground state of H_0, which is equal superposition of all possible states. A sufficiently long runtime can return the solution with high success probability. However, after we translate a realistic

problem to an operable Ising model on the QPU, we have to follow some hardware restrictions to map the Ising model to the hardware working graph. For example, some qubits and couplers are actually nonfunctional in the QPU, the J_{ij} and h_i on these null qubits should be set to 0, which leads to a sparse connectivity in the QPU. Besides that limitation, the weights of J_{ij} and h_i have to match the hardware design and have limited precision and range. There are errors introduced when mapping h_i and J_{ij} onto the qubit and coupler biases.

The processor chip in D-Wave is based on superconducting qubits, a qubit is composed of a niobium ring and the interrupted by two Josephson junctions. External biases Φ_i on each qubit controls the weight h_i and the annealing schedule. The qubit state is represented by the direction of current in the loop of niobium. A clockwise superconducting current to the spin up state $|0\rangle$, while an anti-clockwise current encodes the spin down state $|1\rangle$. Current in the loop that flows in both directions represents a superposition state at millikelvin temperatures. This reveals a drawback of the D-Wave chip, the QPU has to be operated in a dilution refrigerator that is supercooled to below 15mK (near absolute zero) to maintain the quantum effects and isolation from the environment. But the D-Wave QPU has a high level of tunability and is robust against certain types of crosstalk and decoherence. A small amount of thermal noise from the external environment can sometimes help improve the success probability in the annealing process [137].

The QPU in D-Wave such as the *D-Wave 2000Q* and earlier versions are embedded into the Chimera structure denoted as C_k in Figure 2.4. A Chimera graph consists of a $k \times k$ grid of unit cells. In this structure, each cell is composed of 8 interconnected qubits, and cells are connected in a way that four horizontal qubits are coupled to their adjacent horizontal qubits in external cells, and four vertical qubits are coupled to their adjacent vertical qubits in external cells. Most qubits are connected to 6 other qubits in the Chimera structure. The new D-Wave QPU available in mid-2020, *Advantage*, claims to be the first and only quantum computer for business purposes. Advantage chips use the Pegasus topology instead of the Chimera graph. Qubits also oriented horizontally or vertically, but the couplings between qubits are different from the Chimera structure. Each qubit in the Pegasus topology has 15 connections and the chip has more than 5000 qubits and 35000 couplers. The potential of quantum annealing will be extensively explored by more powerful QPUs.

Although we don't use the D-Wave machine in this thesis, it inspires a lot of the work we did.

2.4 Preliminaries of RFQA

As one of the important variations of conventional QA and the focus of our work, RFQA modifies the uniform transverse field in conventional QA in two ways:

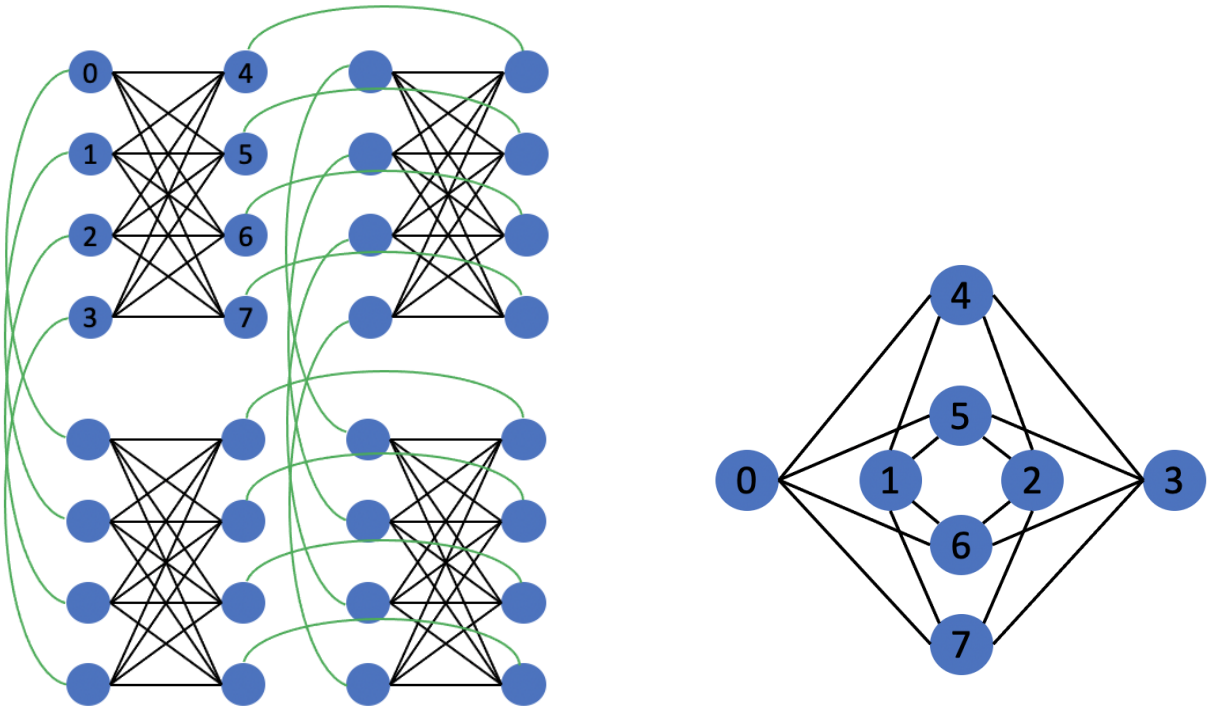

(a) A 2×2 Chimera graph

(b) One unit cell in the form of a bipartite graph $K_{4,4}$

Figure 2.4 There are a total of 4 unit cells in the above 2×2 Chimera graph. Each blue dot represents a qubit, and each unit cell is composed of 8 interconnected qubits. The internal couplings are represented by black lines, and the external couplings are represented by green lines. In the Chimera structure, four horizontal qubits (such as dots 0, 1, 2, 3) are connected to their vertical neighbors in other unit cells. Four vertical qubits (such as dots 4, 5, 6, 7) in a unit cell will be connected to their vertical neighbors in other unit cells. The layout of the top left unit cell is a $K_{4,4}$ bipartite graph shown in (b). The qubits 0, 1, 2, 3 are labeled as horizontal qubits, and qubits 4, 5, 6, 7 are vertical ones.

1. RFQA-M: $H_0 = -\sum_{i=1}^{N} \sigma_i^x \rightarrow H_M = -\sum_{i=1}^{N}(1 + \bar{\alpha}_i \sin(2\pi f_i t))\sigma_i^x$, which modifies the uniform field to a transverse field with oscillating magnitude.

2. RFQA-D: $H_0 = -\sum_{i=1}^{N} \sigma_i^x \rightarrow H_D = -\sum_{i=1}^{N}[\cos(\bar{\alpha}_i \sin(2\pi f_i t))\sigma_i^x + \sin(\bar{\alpha}_i \sin(2\pi f_i t))\sigma_i^y]$, which modifies the uniform field into a field with oscillating direction in the x-y plane, with the magnitude of the oscillating field unchanged. This oscillating field can be transformed back to the uniform transverse field with a basis rotation, so the instantaneous energy spectrum will be preserved in the evolution.

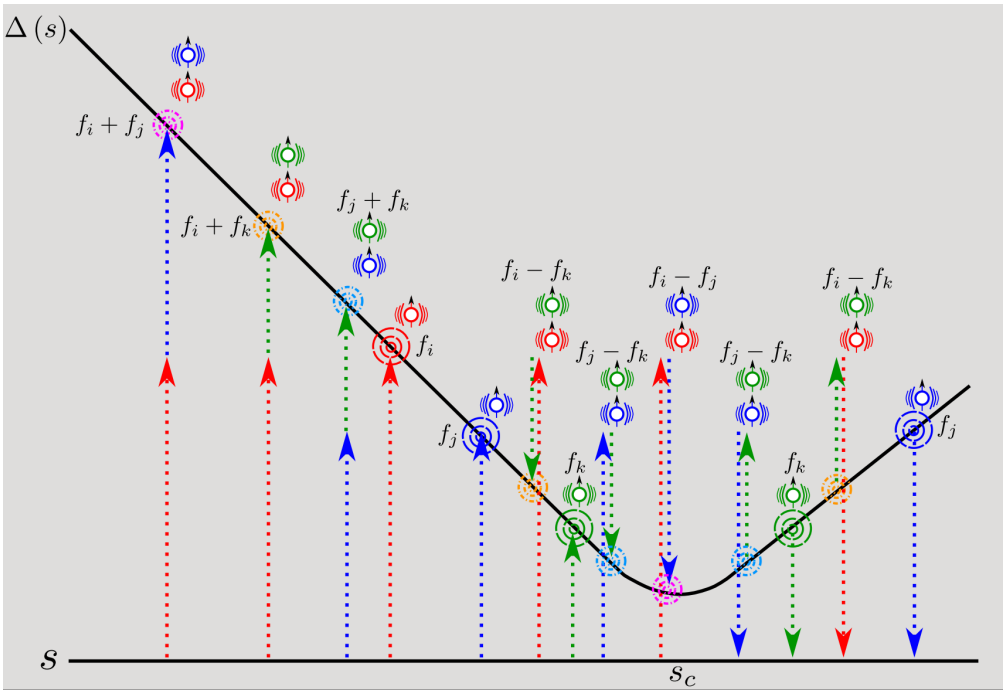

Figure 2.5 Multi-spin tunneling in RFQA from the original work [138]. The is a sketch of the energy gap between ground state and first excited state, the avoided crossing happens at some critical s_c. Each colored dashed arrow represents the energy provided by oscillating fields on each site. For example, the rightmost $f_i + f_j$ blue plus red arrows, depicts a resonance process that the system absorbs two photons(from site i and j) and creates an excitation. A reverse process can happen if the sign of f_i and f_j flips. Extensive number of multi-tone tunneling mixes the two competing ground states rapidly, which can provide a quantum speedup.

We drive each spin with oscillating fields in different random frequencies f_i chosen in the range $\{f_{min}, f_{max}\}$, and the sign of f_i is also randomly chosen. The oscillating fields provide each site different external random energies. These random energies can give more opportunities to mix the ground state and first excited state of the total Hamiltonian in the neighborhood of the minimum gap. In an N spin system, many m-tone transitions can occur. Now we consider the case where we drive the magnitude or direction of two spins. Near the minimum gap, between the two competing ground states, when the driven frequencies f_i and f_j on spin i and spin j meet the requirement that $f_i + f_j$ equals the energy difference of the two

competing ground states of the total Hamiltonian, the system reaches a resonance condition. In the resonant process, the true ground state absorbs two photons from these two spins to mix with the false ground states. There are total $2^2\binom{N}{2}$ two spin driven terms for any pair of two spins that are driven by different random frequencies. Besides the 2-tone transitions, there are $2^l\binom{N}{l}$ distinct terms for the $l-th$ order resonance. All the multi-spin driven terms contribute to the solution rate Γ_T in the Laudau-Zener transition. For large N, the contribution from the $2^l\binom{N}{l}$ terms will dominate, we then have an exponential number of driven transitions between the ground state and first excited state. The exponential proliferation of weak multi photon resonances in RFQA is shown in Figure 2.5.

The energy-averaged tunneling rate for a N-spin tunneling event scales as

$$\begin{aligned}\Gamma_T &= \frac{\sum_{i=1}^{N}|\Omega_i|^2}{W} \simeq \frac{\Omega_0^2}{W}\sum_{l=1}^{N}\Lambda^{2l}\binom{N}{l}2^l \\ &\simeq \frac{\Omega_0^2}{W}\left(1+2\Lambda^2\right)^N.\end{aligned} \tag{2.23}$$

Predicting Λ is a subtle challenge and something we will leave for future work; we restrict our study of RFQA to purely numerical simulations here.

The basic form of oscillating field quantum annealing is $H(t) = A(t)H_{M/D} + B(t)H_p$. In the implementation of digitized-RFQA, RFQA-M evolves under the unitary

$$\hat{U}(t)\left|\psi\right\rangle \approx \prod_{j=1}^{N} e^{i[A(t)dt(1+\bar{\alpha_i}\sin(2\pi f_i t))]\sigma_j^x}\prod_{j=1}^{N} e^{-iB(t)dtH_p}. \tag{2.24}$$

In RFQA-D, one can just split the oscillating field in the x-y plane into separate rotation X and rotation Y gates, but to provide a more implementable version of RFQA-D, we need to make a transformation here. Considering the following equation

$$\cos\theta\sigma_i^x + \sin\theta\sigma_i^y = e^{-i\frac{\theta}{2}\sigma^z}\sigma_x e^{i\frac{\theta}{2}\sigma^z}, \tag{2.25}$$

we denote $\bar{\alpha_i}\sin(2\pi f_i t)$ as $\theta_i(t)$, and the Hamiltonian $A(t)H_D + B(t)H_p$ can be reformulated as

$$\begin{aligned}H(t) &= A(t)H_D + B(t)H_p \\ &= -A(t)\sum_{i=1}^{N}[\cos(\theta_i(t))\sigma_i^x + \sin(\theta_i(t))\sigma_i^y] + B(t)H_p \\ &= e^{-\frac{i}{2}\sum_i\theta_i(t)\sigma_i^z}(A(t)H_0 + B(t)H_p)e^{\frac{i}{2}\sum_i\theta_i(t)\sigma_i^z},\end{aligned} \tag{2.26}$$

where $H_0 = -\sum_i\sigma_i^x$. The equation (F4) in the original paper of RFQA [138] indicates that the driving term in RFQA-D involved in the evolution can have another implementation. That is it can be treated as adding a time dependent oscillating z-bias field to a uniform transverse field. It is functionally equivalent

to writing H_D as

$$H_D = -\sum_i \sigma_i^x + -\sum_i \pi f_i \bar{\alpha}_i \cos(2\pi f_i t)\sigma_i^z, \tag{2.27}$$

which is adding an oscillating Z field to the original uniform transverse field. By using this formulation of RFQA-D, we see that the implementation of both RFQA methods is straightforward.

2.5 Preliminaries of QA in quantum gate model

In this section, we discuss the Trotterization approximation, the basic transformation from analog QA to digitized QA, and compare QAOA with digitized-QA. Finally, we introduce the focus of our work, the RFQA method. The basic form of the oscillating transverse field in RFQA, and the accelerating mechanism in RFQA , as well as the physical implementation of RFQA, will be mentioned in the last part of this section.

2.5.1 Trotterization approximation

In the implementation of quantum gates, an exponentiation of the form e^{A+B} presents itself in the definition of the time evolution operator. If A and B commute with each other, we have

$$e^{A+B} = e^A e^B. \tag{2.28}$$

For two Hermitian operators that do not commute with each other, the Trotter formula provides the following decomposition

$$\lim_{n\to\infty} (e^{iAt/n} e^{iBt/n})^n = e^{i(A+B)t}. \tag{2.29}$$

From this formula, we can derive the Trotter approximation of $e^{i(A+B)dt}$ by omitting the $\mathcal{O}(dt^2)$ terms

$$e^{i(A+B)dt} = e^{iAdt} e^{iBdt}, \tag{2.30}$$

More precise higher order Trotter approximations can be constructed by further expanding the matrix exponential, such as in [66, 105, 139]

$$\begin{aligned} e^{i(A+B)dt} &= e^{iAdt/2} e^{iBdt} e^{iAdt/2} + \mathcal{O}(dt^3) \\ e^{i(A+B)dt} &= e^{\frac{7}{24}iAdt} e^{\frac{2}{3}iBdt} e^{\frac{3}{4}iAdt} e^{-\frac{2}{3}iBdt} e^{-\frac{1}{24}iAdt} e^{iBdt} + \mathcal{O}(dt^4). \end{aligned} \tag{2.31}$$

However, the higher order approximations introduce lots of commutators and can be messed up quickly in the evolution. Thus, the first order trotter approximations is mostly used in near-term quantum algorithms performed without error correction.

Take the Hamiltonian in D-Wave quantum annealer as an example; the time dependent Hamiltonian is expressed as

$$H(t) = -A(t)\sum_{j=1}^{N}\sigma_j^x - B(t)\left(\sum_{<i,j>} J_{ij}\sigma_i^z\sigma_j^z + \sum_{i=1}^{N} h_i\sigma_i^z\right). \tag{2.32}$$

quantum annealing leads to a final state $|\psi(t_f)\rangle = U(t_f,t_i)\,|\psi(t_i)\rangle$, where $|\psi(t_i)\rangle$ is the initial state. In the digitization of quantum annealing, we define a small time step dt and decompose the annealing process into many discrete steps by applying the decomposition property to the time-evolution operator $U(t_f,t_i)$

$$\begin{aligned}|\psi(t)\rangle &= e^{-iH(t)t}\,|\psi(0)\rangle \\ &= e^{-iH(t)dt}e^{-iH(t-dt)dt}\cdots e^{-iH(dt)dt}\,|\psi(0)\rangle\,.\end{aligned} \tag{2.33}$$

In each time step, we apply the Trotterization approximation to $e^{-iH(t)dt}$

$$\begin{aligned}e^{-iH(t)dt} &= e^{idtA(t)\sum_{j=1}^{N}\sigma_j^x + idtB(t)\sum_{<j,k>}J_{jk}\sigma_j^z\sigma_k^z + idtB(t)\sum_{j=1}^{N}h_j\sigma_j^z} \\ &= \prod_{j=1}^{N} e^{idtA(t)\sigma_j^x}\prod_{<j,k>} e^{idtB(t)J_{jk}\sigma_j^z\sigma_k^z}\prod_{j=1}^{N} e^{idtB(t)h_j\sigma_j^z}.\end{aligned} \tag{2.34}$$

From the above decomposition, we see that each time-evolution operator can be implemented by single and multiple qubit gates sequentially. By applying the Trotterization approximation in each small time step, we arrive at the final state $|\psi(t)\rangle$, after performing a measurement on the system.

2.6 Hard trial problems in digital quantum annealing

In chapter 4, we investigate a series of benchmark problems to show that digitizing RFQA could be a good basis for a digital quantum optimization algorithm either for noisy machines, or ultimately, error corrected ones, as a new tool to complement QAOA and traditional digitized QA. We modify the shamrock model to a hard problem with one avoided crossing and combine the modified shamrock model with square-grid embedding to make a problem that is easier to implement in a near term quantum computer. We also investigate tunneling between two ferromagnetic states in TFIM.

2.6.1 Shamrock model

Evgeny *et al.* proposed a shamrock model to compare the quantum scaling of QA and QMC[140], the shamrock model simulates an N-spin tunneling bottleneck and is hard for both QA and classical QMC simulation. They state that the QMC escape rate is suppressed by the number of homotopy-inequivalent tunneling paths compared with the incoherent tunneling rate in QA,

$$\Gamma_{QMC} \propto \frac{\Gamma_{tunl}}{N_{paths}} \tag{2.35}$$

Γ_{tunl} represents the incoherent tunneling rate, Γ_{QMC} is the QMC escape rate, and N_{paths} denotes the number of homotopy-inequivalent tunneling paths. In a simple uniform ferromagnet model, the problem

Hamiltonian is encoded as

$$H_p = -J \sum_{i,j=1}^{N} \sigma_i^z \sigma_j^z. \tag{2.36}$$

The $N!$ tunneling paths between two ferromagnetic states are homotopy equivalent, the N_{paths} in this case is just 1, thus the QMC would behave similarly to QA. But in a frustrated ring model as shown in Figure 2.6(a), there are two dominant tunneling paths between two ferromagnetic minima, the incoherent tunneling in QA has a factor of 2 quantum advantage over QMC. To enlarge the quantum advantage in QA, they further designed the shamrock model as shown in Figure 2.6(b), where there is one central spin ferromagnetically coupled to K frustrated petals, and petal spins are anti-ferromagnetically coupled. There are 2^K homotopy-inequivalent tunneling paths in this structure and will lead to an exponential advantage of incoherent tunneling in QA over QMC escape rate.

The topological frustration leads to a proliferation of homotopy-inequivalent tunneling paths between two ground states and therefore the quantum advantage of the incoherent tunneling in QA over QMC. The frustration is common in many hard trial problems and is a promising route to demonstrate a quantum advantage.

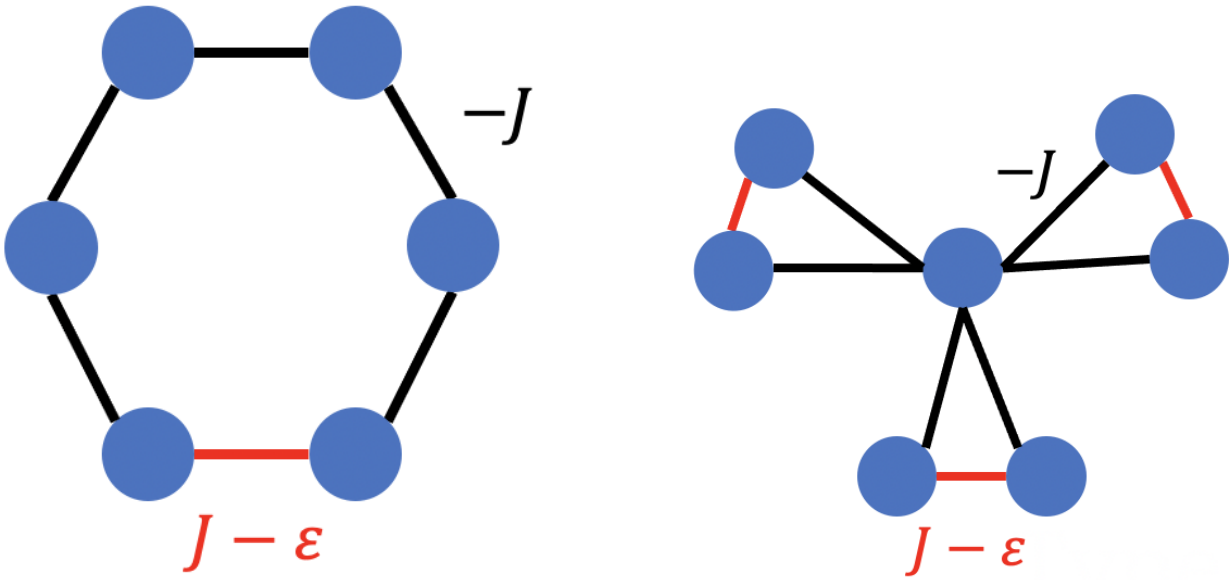

(a) Frustrated ring model. The ferromagnetic couplings are represented by black lines, only one of the coupling is antiferromagnetic, which is represented by red line.

(b) Shamrock model. One central spin is ferromagnetically(black line) connected with K frustrated petals, the petal spins are antiferromagnetically(red line) coupled.

Figure 2.6 The frustrated ring model only has two tunneling paths that contribute to the incoherent tunneling, while the shamrock model has 2^K homotopy-inequivalent tunneling path. Therefore, in the shamrock model, the incoherent tunneling in QA gives an exponential advantage over QMC.

In the original formulation of the shamrock model,

$$H_p = J_{FM} \sum_j \sigma_C^z \sigma_j^z + J_{AFM} \sum_{<j,k>} \sigma_j^z \sigma_k^z - h_0 \sum_j \sigma_j^z + h_0(1-A)(N-1)\sigma_C^z, \tag{2.37}$$

there are two competing ground states, they are the all spins up state and the all spins down state. The σ_C represents the single central spin in the shamrock model. Based on this original formulation, we add a local z bias field to the central spin, and opposite local fields h_0 to all of the petal spins. For A between 0 and 1, the z local field on the central spin is much stronger than the field on the petal spins. With the external local fields, the all spins up state will be the global minimum, and the all spins down state will be the local minimum. Since the global minimum aligns along the direction of the local fields in the petals, the much stronger local field on the central spin steers the system toward the local minimum easily. This can make the problem exponentially difficult to solve. For a fixed h_0, we can control the difficulty level of the problem model by adjusting the value of A. The tunable shamrock model is relatively hard compared with the random constraint problem in a small system size. However, in the shamrock model with only one central spin, a single error in the central qubit can have extensive energy cost. This issue disappears for a chain of copies of that problem, where the number of petals per central qubit does not increase with N, the modified shamrock model is shown in Figure 4.4.

2.6.2 Square-grid tile planting

Besides the modified shamrock problem, we also investigated a square grid model, that naturally maps to near term quantum computing hardware. Nowadays, there is no analytical evidence of quantum advantage in solving generic optimization problems. The demand of benchmarking the performance of quantum algorithms has been rapidly increasing with the development of quantum hardware. Problems with planted solutions, where the ground state is known *a priori*, are suitable for benchmarking. Some proposed planted solution schemes, however, fail to generate real, hard benchmark problems that can be extended to larger system sizes [141–144]. An ideal benchmarking problem should have tunable hardness and have scalability. To meet these requirements, the tile planting model has been proposed [145]. The square lattice tile planting is of great interest because the sparse connectivity of a square lattice can be adapted to current quantum annealing hardware.

The graph structure of square lattice is shown in Figure 2.7(a), where the square grid is decomposed into vertex-sharing subproblems. Each subproblem has frustration that leads to many degenerate ground states, but the ferromagnetic states are always the ground state in each subproblem. The ground state of the square-grid has a known ferromagnetic ground states, which is the tile planted solution in this model.

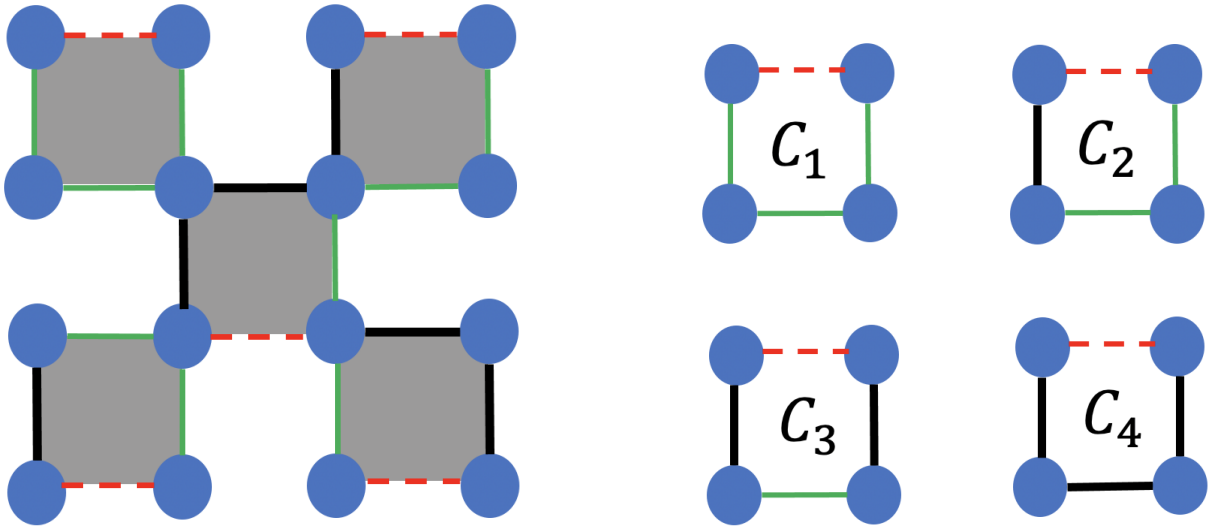

(a) square grid model with tile planting

(b) Four subproblem types

Figure 2.7 (a) is an example of a square grid model with tile planting, a square grid problem is partitioned into many subproblems, which are represented by the grey cells. Subproblems are connected by one vertex qubit, and they share a ground state configuration. The resultant global ground state of the square grid is known *a priori*. Each subproblem is a frustrated square chosen from four types of frustration as shown in (b). The couplings between nearest neighbors are either ferromagnetic coupling or antiferromagnetic. Red dashed lines represent antiferromagnetic coupling, green lines represent ferromangetic coupling with the same magnitude as the antiferromagnetic coupling, and black lines represent stronger ferromagnetic coupling.

The graph of the overall problem is denoted as $G = (V, E)$, with the unit cell subproblem graph represented by $G_m = (V_m, E_m)$. Each subproblem is defined as an Ising Hamiltonian

$$H_m = \sum_{(i,j)\in E_m} J_{ij} s_i s_j, \tag{2.38}$$

the overall problem Hamiltonian is the summation of the subproblem Hamiltonians

$$H = \sum_{m\in M} H_m, \tag{2.39}$$

where M is the set of all subproblems. From this formulation, it is clear that if the subproblem Hamiltonians share a common ground state configuration $s^* = \{s_1, s_2, ..., s_N\}$, this configuration $s^*$is also a ground state of the total Hamiltonian H.

The subproblems can be classified as four different types. In each unit cell, the couplings are randomly chosen from antiferromagnetic, ferromagnetic, and weak ferromagnetic couplings. For a C_i type subproblem, it is constructed with one edge being antiferromagnetic coupling, and randomly assigning ferromagnetic coupling to $i-1$ edges, the remaining edges are stronger ferromagnetic couplings. A C_i type subproblem has i ground states, and ferromagnetic states are always one of them. To generate a tile

planting square grid hard instance, simply pick a subproblem type and assign it to a unit cell. The frustration in each subproblem results in a degeneracy of the ground state in the energy landscape of the Hamiltonian of the square grid, and the ferromagnetic states are always one of the ground states. By specifying four types of subproblem and assigning them to the square grid unit cells, we are able to generate numerous benchmark problems with tunable hardness.

2.6.3 TFIM model

The quantum version of Ising model is referred to as the Transverse Field Ising Model(TFIM), which is formulated as

$$H = -J\left(\sum_i \sigma_i^z \sigma_{i+1}^z + \kappa \sum_i \sigma_i^x\right) \tag{2.40}$$

In this model, the transverse field magnitude κ plays a crucial role in controlling the phase of the 1D TFIM.

For strong transverse field $|\kappa| > 1$, in the limit where $|\kappa| \gg 1$, the Hamiltonian is dominated by the transverse field term

$$H \approx -J\kappa \sum_i \sigma_i^x, \tag{2.41}$$

the ground state of which is the superposition state of all possible states $|+++\cdots+\rangle$, where $|+\rangle = \frac{1}{\sqrt{2}}(|0\rangle + |1\rangle)$ represents each spin pointing along the $+x$ direction. The excited state is the state that with one of the spins flipped, pointing in $-x$ direction as $|++\cdots+-+\cdots+\rangle$. The system with a strong transverse field is in the disordered phase. For any g such that $|\kappa| > 1$, the energy gap between the two competing ground states will be lifted by the perturbation $-J\sum_i \sigma_i^z \sigma_{i+1}^z$, The minimum energy gap between them is $\Delta_{min} = 2|J|(|\kappa| - 1)$.

In weak transverse field $|\kappa| < 1$, we consider in the limit of $|\kappa| \to 0$,

$$H \approx -J \sum_i \sigma_i^z \sigma_{i+1}^z, \tag{2.42}$$

the ground states of which are ferromagnetic states $|000\cdots0\rangle$ and $|111\cdots1\rangle$ where all spins point toward the z axis. The excitation states are states with domain walls. The system with a weak transverse field exhibits an ordered phase. The transverse field is considered as a perturbation term in this case, and the minimum energy gap is lifted by the perturbation $\Delta_{min} = 2|J|(1 - |\kappa|)$.

In the strong and weak transverse case, we see the behavior of the Hamiltonian is qualitatively different, the quantum phase transition happens in the TFIM can be shown to occur at $\kappa_c = 1$ by making use of duality.

2.7 Outline

In this thesis, we first give a brief introduction on the important quantum circuit model and its alternative method Quantum Annealing in chapter 1, then we give preliminaries and background of our work in chapter 2, the main results are presented in the subsequent chapters.

In chapter 3, we investigate analog quantum annealing and its variations on solving an artificial hard combinatorial optimization problem. The problem is designed to have a local minimum and a global minimum separated by an energy barrier. The energy cost to flip from the local minimum to the global minimum is extensive (scales as the system size) and the complexity of this artificial problem can be designed to be scale exponentially with the system size. We argue that all of the modified quantum annealing methods can provide a quantum speedup over the standard uniform sweep routine of QA. We see RFQA as the most promising one in near-term quantum annealing, given that RFQA can introduce a non-stoquastic Hamiltonian that cannot be efficiently simulated by classical computers, and it only requires circuit control in future experimental implementations.

In chapter 4, motivated by the performance of RFQA and its potential to be a practical be a near-term quantum computation method, we digitized RFQA methods for solving hard optimization problems. By Trotterizing the quantum annealing process into many quantum gates, and assuming we apply digitized-QA and digitized-RFQA in an error-free quantum gate model, we show that the gate-based version of RFQA can still provide quantum speedup over the digitized standard uniform sweep QA. We hope that the results can give guidance on implementing RFQA in a real quantum annealer.

In chapter 5, we investigate the behavior of digitized RFQA on the TFIM model and show the performance improvement of RFQA over the linear sweep QA approach. The stark scaling advantage of RFQA indicates RFQA can overcome the overhead of minor embedding required for the problems under investigation.

We make a conclusion of our work in chapter 6.

CHAPTER 3

UNCONVENTIONAL QUANTUM ANNEALING METHODS FOR DIFFICULT TRIAL PROBLEMS

Modified from a paper published in PHYSICAL REVIEW A[1].

Zhijie Tang[2], Eliot Kapit[3]

3.1 Abstract

We consider a range of unconventional modifications to Quantum Annealing (QA), applied to an artificial trial problem with continuously tunable difficulty. In this problem, inspired by "transverse field chaos" in larger systems, classical and quantum methods are steered toward a false local minimum. To go from this local minimum to the global minimum, all N spins must flip, making this problem exponentially difficult to solve. We numerically study this problem by using a variety of new methods from the literature: inhomogeneous driving, adding transverse couplers, and other types of coherent oscillations in the transverse field terms (collectively known as RFQA). We show that all of these methods improve the scaling of the time to solution (relative to the standard uniform sweep evolution) in at least some regimes. Comparison of these methods could help identify promising paths towards a demonstrable quantum speedup over classical algorithms in solving some realistic problems with near-term quantum annealing hardware.

3.2 Introduction

Quantum Annealing (QA) [18, 126, 146–149] is a promising method to solve optimization problems with noisy quantum hardware, with applications in machine learning, artificial intelligence [150–155], and many other topics. The time-dependent Hamiltonian of QA is engineered to encode the solutions of classical optimization problems in its ground state. By initializing the system in the ground state of a trivial driver Hamiltonian and evolving the system sufficiently slowly, QA can find the ground state of the target (classical) problem Hamiltonian. However, it is notoriously difficult to predict the performance of QA for realistic problems. Conclusive proof of a quantum speedup over classical methods for real problems remains elusive, with the possible exception of a frustrated magnet systems [156], where an empirical scaling advantage over classical path-integral Quantum Monte Carlo (QMC) algorithms was shown. To

[2]First author; Colorado School of Mines
[3]Corresponding author; Colorado School of Mines

help address this challenge, in this paper we theoretically survey a range of promising extensions to QA applied to a difficult trial problem, and identify a number of potential routes to a quantum speedup.

In the setup for QA, the total Hamiltonian in the standard uniform sweep evolution is a combination of a driving Hamiltonian H_0 and problem Hamiltonian H_p,

$$H(t) = (1 - s(t))H_0 + s(t)H_p \tag{3.1}$$

with the ground state of H_0 being easy to prepare. H_0 and H_p do not commute and the time-dependent annealing parameter $s(t)$ controls the time evolution of the system. The standard uniform sweep starts from $s(0) = 0$ and ends with $s(t_f) = 1$. Different functional choices for $s(t)$ may vary the efficiency of finding the ground state, such as a 'reverse annealing schedule' [157]. It's intuitive to see that slowing down the annealing process in the vicinity of minimum gap can help increase the success probability, and this tuning is required to recover the quantum speedup in the QA formulation of Grover's search problem [158]. However, the instantaneous minimum gap value and location is not knowable in most realistic problems, and such fine tuning is often frustrated by noise, so we will study the simplest form, a linear schedule, $s(t)$: $s(t) = \frac{t}{t_f}$ throughout this paper.

In QA, the ground state of a problem Hamiltonian, H_p, encodes the optimization problem solution. Experimentally realistic formulations of quantum annealing are typically arranged to solve quadratic unconstrained binary optimization (QUBO) problems, where the problem Hamiltonian is given by the Ising model,

$$H_{\text{ising}} = \sum_{<i,j>} J_{ij}\sigma_i^z\sigma_j^z + \sum_{i=1}^{N} h_i\sigma_i^z \tag{3.2}$$

the ground state of which can be encoded as the solution space of some NP-hard problems [159], and given enough additional qubits, any NP complete problem can be expressed in this form. To find the ground state of the problem Hamiltonian, we first prepare the system in the ground state of H_0, which is chosen as a uniform transverse field Hamiltonian,

$$H_0 = -\sum_{i=1}^{N} \sigma_i^x. \tag{3.3}$$

The initial state is

$$|\psi(0)\rangle = |+\rangle^{\bigotimes N}, \tag{3.4}$$

where $|+\rangle = \frac{1}{\sqrt{2}}(|0\rangle + |1\rangle)$, $|\psi(0)\rangle$ is a uniform superposition state in the computational basis. The quantum adiabatic theorem states that as long as the annealing evolution is slow enough, the system remains in the instantaneous eigenstate of the time-dependent Hamiltonian at all times. This theorem also provides a widely used criterion that, with the linear annealing schedule, the total adiabatic evolution time

t_f to find the ground state with high probability has an inverse minimum gap squared dependence,

$$t_f \propto \frac{W}{\Delta_{min}^2}. \tag{3.5}$$

Here, Δ_{min} is the minimum energy gap, W scales as the total energy change of the final ground state $|0\rangle$ over the entire evolution: $W \sim \langle 0| H_0 |0\rangle - \langle 0| H_p |0\rangle$. Note that this result is a *worst case* scaling estimate of the time to solution, and a variety of diabatic effects can substantially increase performance–we will encounter a number of examples of this later in this work.

In cases where the system undergoes a first order transition [121], Δ_{min} typically decreases exponentially with the system size N, and the corresponding evolution time t_f (and thus, time to solution) grows exponentially. For hard optimization problems which suffer from such phase transitions, many new schemes have been proposed to accelerate QA, such as the use of non-stoquastic Hamiltonians [26, 27, 47, 134, 160, 161], inhomogeneous driving of the transverse field [23, 162], and oscillatory transverse fields (RFQA) [138]. We study a range of examples drawn from these works.

To investigate a number of new methods from the literature, we make our own artificially difficult problem Hamiltonian, partially inspired by previous studies of "spike problems" [47, 163], rather than studying QUBO problems directly as was done in [160]. In this problem, which we call the Asymmetric Magnetization Problem (AMP), local searches and QA steer the system toward a false minimum. This 'wrong way steering' makes finding the true ground state exponentially difficult. The difficulty exponent associated with the AMP can be continuously tuned for further investigation of the performance of these alternative QA methods with problem hardness. Further, the energy landscape depends only on total magnetization m, making it easier to study analytically. We do not consider noise in this paper, as none of the methods we consider require fine tuning. We expect these methods to be resilient to noise described by the empirical noise model for superconducting flux qubits. There is strong theoretical evidence for this resiliency in the case of RFQA [138], and both theoretical and experimental evidence for inhomogeneous driving [23, 162, 164, 165].

In the work of analog QA, we first introduce our trial problem, and provide an analytical prediction of its minimum gap. Secondly, we discuss the performance of the standard uniform sweep applied to this problem, against which we benchmark all other methods. Then we introduce inhomogenous driving, transverse couplers and RFQA, comparing their behavior with the standard uniform sweep routine. Finally, we summarize our results and provides comments on the performance of these methods.

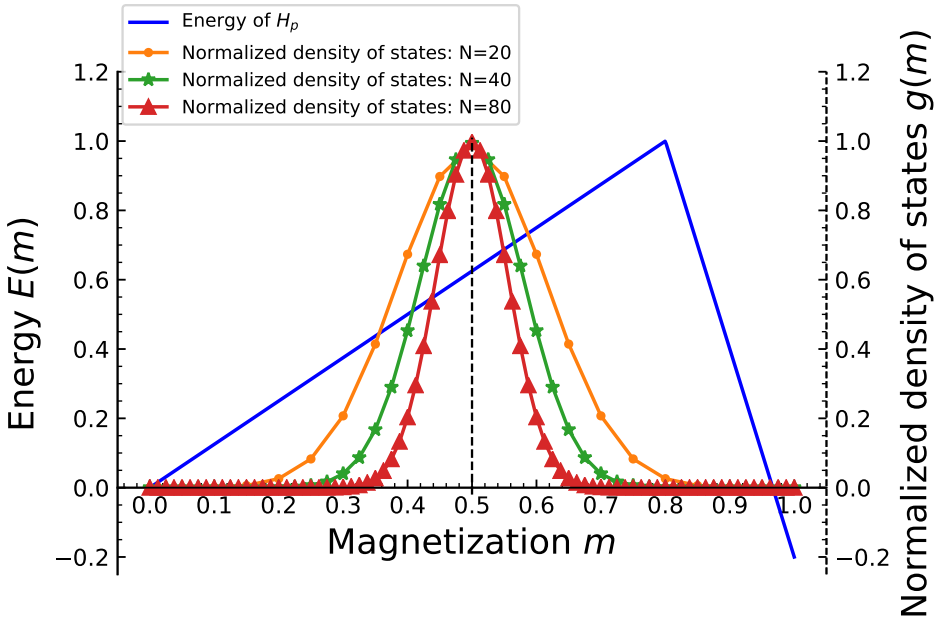

Figure 3.1 Density of states distribution and energy of the problem Hamiltonian in the AMP model. The x axis is the total magnetization m, the y axis represents both the energy spectrum of the problem Hamiltonian(left) and the density of states distribution(right). The lines with markers are the density of states for system sizes of N=10, 11, 12. The distributions become narrower with increasing system size. The solid blue line is the energy landscape of H_p. In our model, the distribution follows a Gaussian distribution, centered at $m = 0.5$. Comparing the distribution of density of states with the energy spectrum of the problem Hamiltonian, we see the peaks of the density of states are distributed behind the global maximum. The asymmetry of the H_p results in an exponentially difficult problem.

3.3 Asymmetric Magnetization Problem

While conventional Ising Hamiltonians can encode nearly any combinatorial optimization problem, we choose an artificial toy problem model to better study a variety of new methods to find its solution. This is in part because extracting exponential difficulty scaling is notoriously difficult and unreliable in random structured problems, at least when N is small enough for exact classical simulation. Our artificial problem, the "AMP", has the problem Hamiltonian defined as function of total magnetization m,

$$H_p = f(m); \quad m = \frac{1}{2N}\sum_{i=1}^{N}(1+\sigma_i^z) \tag{3.6}$$

where N is the system size, σ_i^z is the Pauli matrix with discrete eigenvalues ± 1, $f(m)$ is designed to have two competing minima at $m = 0$ and $m = 1$ with all spins down and all spins up. The form of $f(m)$ is controlled by two free parameters, A and x_p:

$$f(x) = \begin{cases} \frac{x}{x_p} & \text{if } x < x_p \\ 1-(1+A)\frac{x-x_p}{1-x_p} & \text{if } x \geq x_p \end{cases} \tag{3.7}$$

Here, $f(1)$ is the true ground state, and $f(0)$ is the false minimum. x_p defines the location of the global maximum, and A defines the energy difference of the two competing states: $f(0) - f(1) = A$. By adjusting these two parameters, we can continuously tune the difficulty of the problem.

The difficulty of finding the global minimum in our model is strongly related to the distribution of the density of states. The density of states follows a Gaussian distribution as shown in Figure 3.1, with the most probable initial state centered at $m = 0.5$ where half of the spins are flipped from the true ground state, and a global maximum is distributed at $m = x_p > 0.5$. We see the system has a large tendency to get stuck in the local minimum, since the possible initial state is settled behind the global maximum. The wrong way guidance is the generic failure mechanism for classical and quantum optimization algorithms [166], as if local guidance from a random initial state tends to point toward the true solution of a problem it can be solved trivially. But if local guidance points toward false minima, then the problem can quickly become hard, and in more realistic problems at large N there are often exponentially many local minima. Multiqubit tunneling between well-separated minima–exactly the process we simulate here–has been identified as a critical bottleneck in many realistic problems [167].

In the AMP problem, we set the global maximum at $m = x_p$ where $x_p > 0.5$, with two competing minima at each end. From the density of states distribution in Figure 3.1, we can tell the system has a large tendency to be steered toward the false minimum. In classical algorithms such as simulated annealing, the system will easily get stuck in the false minimum since the possible initial state is mostly distributed around $m = 0.5$. The possibility of finding the global minimum is large if the initial instantaneous state of H_p happens to be guessed beyond the global maximum at a position that $m > x_p$, but if the initial state is located at any $m < x_p$, the possibility of climbing the hill is exponentially small. Cost functions similar to the AMP model have been studied in [47, 163], and classical simulated annealing was shown to be inefficient for solving such problems. We will show that the AMP problem is also exponentially difficult to solve with quantum annealing, and we focus on how various modifications to QA compare with a homogeneous transverse field and uniform sweep (the "default" quantum annealing method) in solving the AMP problem.

When applying QA to the AMP problem, performance is bottlenecked by an exponentially small gap at a first-order transition [121, 168, 169]. As shown in Figure 3.2, the magnetization is entropically steered toward 0 as the system evolves, and all N spins must simultaneously flip to reach the true ground state.

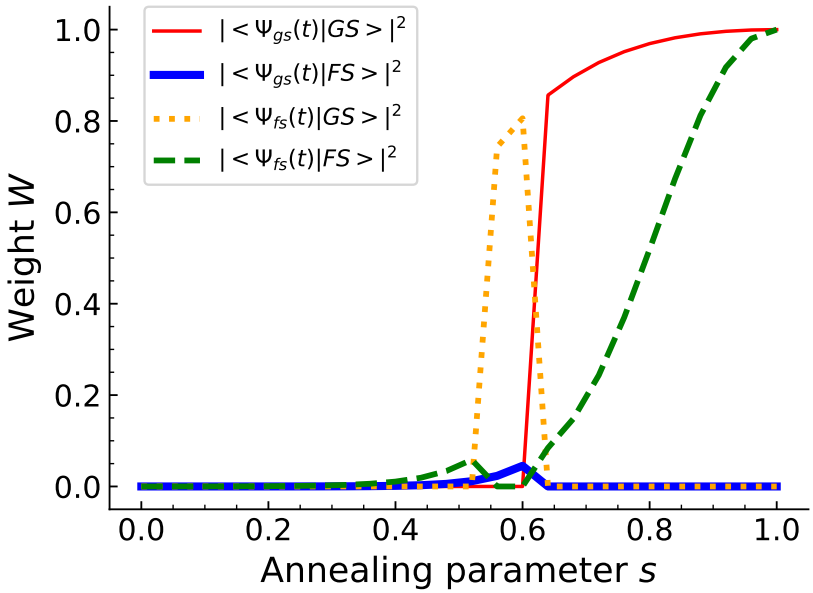

Figure 3.2 The instantaneous overlap of the ground and first excited states with the true and false ground states of the classical problem as a function of the annealing parameter s, with system size $N = 18$, and the problem Hamiltonian is defined with parameters: $A = 0.2, x_p = 0.8$. The x axis is the annealing parameter s, the y axis denotes the probability of getting a specific state. The red(thin line) and blue(thick line) solid lines are the overlap of the instantaneous ground state with the true and false ground state of H_p, the orange(dotted line) and green(dashed line) dashed lines are the overlap of the instantaneous first excited state with the true and false ground state of H_p. The comparison shows that the system is steered toward the false minimum first and all N spins have to flip to reach the true ground state.

The difficulty scaling of the problem model can be tuned by A and x_p; smaller A corresponds to a smaller energy gap between the two competing minima, which intuitively increases the difficulty level of the problem. Similarly, larger x_p moves the peak further away from the center of the density of states, and the system then has larger tendency to be steered to the false local minimum, which also increases problem difficulty. We make an ensemble of problem models with different A and x_p so that we can investigate the relationship between the performance of different methods with the difficulty of the problem models. We make modifications to the traditional QA method and evaluate their performance by numerically calculating the time to solution, and show that the AMP problem is exponentially difficult to solve with quantum algorithms, but modifications to the traditional QA method can lead to substantial improvements in the scaling of the time to solution. The exponential scaling coefficients for each method are listed in Table I.

Although this toy model is just a simplified artificial problem without a realistic implementation, as described above, it captures the basic bottleneck of most classical and quantum optimization problems. So

any method which accelerates finding a solution in the AMP is likely broadly applicable to more realistic cases.

3.4 Standard uniform sweep routine

We first investigate the performance of the standard uniform sweep method, for system sizes N ranging from 5 to 18 spins. In this method, the driving Hamiltonian is a homogeneous transverse field: $H_0 = -\sum_{i=1}^{N} \sigma_i^x$. The total Hamiltonian is a combination of the drive Hamiltonian and problem Hamiltonian H_p

$$H(s) = -(1-s)\frac{1}{N}\sum_{i=1}^{N}\sigma_i^x + sH_p. \tag{3.8}$$

The initial ground state of the system is the ground state of H_0, which is a uniform superposition of states corresponding to all possible assignments of bit values with equal weights. As the system evolves, the Hamiltonian linearly interpolates between the transverse field Hamiltonian and the problem Hamiltonian, i.e. starting as H_0 and ending in H_p. As long as the system stays in the instantaneous ground state, the system will be steered toward the false minimum first, but at some critical s_c the true and false ground states cross and all N spins must flip, as shown in Figure 3.2 with red and blue solid lines. For this problem, there is only one avoided crossing in the standard uniform sweep method (though we find multiple crossings when inhomogenous driving is employed). Since the gap at the phase transition point is exponentially small in N, unless the evolution is performed extremely slowly, the avoided crossing will be diabatically missed and the probability of finding the true ground state will be suppressed, while the probability of finding the false ground state dominates, as shown in Figure 3.2 with orange and green dashed lines.

We evaluate the performance of the standard uniform sweep algorithm by computing the time to solution(TTS) over a range of system sizes. The TTS measures the time needed to find the ground state with 99% success probability [166]

$$TTS \propto t_f \frac{\ln(1-0.99)}{\ln(1-p(t_f))}, \tag{3.9}$$

where $p(t_f)$ is the success probability in a single-trial with runtime t_f; for small $p(t_f)$, $TTS \propto t_f/p(t_f)$. A short t_f taking advantage of diabaticity might not show how different methods change the scaling of multi-qubit tunneling at large N, so we assume polynomially increasing t_f with N in our work, as one would likely want to use in a real annealer at much larger N, the t_f is empirically chosen as $20(\frac{N}{7})^2$ for the AMP model. As mentioned in the introduction, the evolution time needed to find the ground state increases as Δ_{min}^{-2}. To explore the performance of the standard uniform sweep method under different

problem models, we choose four sets of parameters: $\{A = 0.2, x_p = 0.8\}$; $\{A = 0.28, x_p = 0.7\}$; $\{A = 0.3, x_p = 0.64\}$; $\{A = 0.34, x_p = 0.59\}$ forming an ensemble of problem models with descending difficulty level. These parameters are chosen to approximately set $\Delta_{min} \propto \{2^{-N}, 2^{-3N/4}, 2^{-N/2}, 2^{-N/4}\}$, respectively. As mentioned previously, increasing A or decreasing x_p toward $1/2$ both decrease the difficulty exponent, and moving either parameter in the opposite direction makes the problem harder.

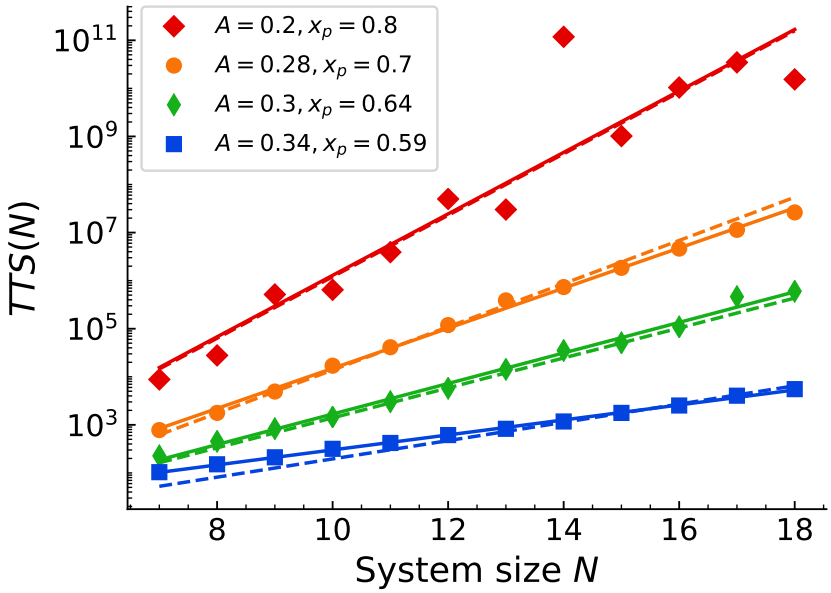

Figure 3.3 Time to solution to find the true ground state in four problem model sets using the standard uniform sweep method, computed from the final success probability for a runtime polynomially increasing with N. The difficulty level of the four models is arranged in descending order: $\{A = 0.2, x_p = 0.8\}$; $\{A = 0.28, x_p = 0.7\}$; $\{A = 0.3, x_p = 0.64\}$; $\{A = 0.34, x_p = 0.59\}$. Different markers are data with the standard uniform sweep method of four problem model sets, solid lines are best-fit curves of the numerical data and dashed lines are the inverse of the square of the numerically estimated minimum gap from Figure 3.9. The time to solution closely tracks the average minimum gap squared as expected. In all cases, the N-spin tunneling bottleneck in this problem leads to an exponentially increasing time to solution.

As expected by an exponentially closing gap, the time needed to find the solution exponentially increases with system size. This is confirmed in Figure 3.3, where the corresponding time to solution exponentially increases with the system size in all problem sets, and the difficulties of the four sets are well separated from each other. With the minimum gap and performance of the standard uniform sweep method rigorously understood, we now apply other methods from the literature to compare their performance with it and investigate their abilities of providing a quantum speedup.

Table 3.1 Summary of scaling exponents for each method. Fitting the time to solution $TTS(N)$ of each method to $2^{\beta+\gamma N}$, the table lists the exponential scaling coefficient "γ" value for each method. "S" represents the standard uniform sweep method, "I" represents the Inhomogeneous driving method, "$C_{F,A,M}$" represents the transverse couplers method, in which "F,A,M" corresponds to ferromagnetic, anti-ferromagnetic, mixed couplers, respectively. "M" represents the RFQA-M method, "CM", RFQA-M with couplers method, "$SyncM$", synchronized RFQA-M method, "$SyncMC$", synchronized RFQA-M with couplers method, and "D" represents the RQFA-D method.

	A=0.2,x_p=0.8	A=0.28,x_p=0.7	A=0.3,x_p=0.64	A=0.34,x_p=0.59
$1/\Delta^2_{min}$	2.25	1.48	1.04	0.61
S	2.12	1.39	1.06	0.52
I	0.79	0.70	0.69	0.69
$C_{F,A,M}$	1.77, 2.09, 2.50	1.25, 1.23, 1.67	0.87, 0.77, 1.12	0.48, 0.44, 0.54
M	1.48	0.89	0.62	0.45
CM	1.31	0.86	0.62	0.45
$SyncM$	1.28	0.84	0.64	0.45
$SyncMC$	0.86	0.64	0.62	0.51
D	1.56	1.05	0.50	0.40

3.5 Summary of results

Before we proceed to the detailed investigation of alternative QA methods, we compile a summary in Table 3.1, that lists the exponential fitting results of TTS for each method. We fit $TTS(N)$ to $2^{\beta+\gamma N}$ and extract the "γ" value to determine the difficulty scaling for each method. We find that in the harder problem sets where $x_p = 0.8, A = 0.2$ and $x_p = 0.7, A = 0.28$, synchronized RFQA-M (with transverse couplers) and Inhomogeneous driving show the best performance, but in the relatively easier problem sets where $x_p = 0.64, A = 0.3$ and $x_p = 0.59, A = 0.34$, the RFQA-D method shows the best scaling advantage. The details are illustrated and discussed in the following sections; we include this table as a central reference point for the results of all of our studies.

3.6 Modified Adiabatic annealing strategies: inhomogenous driving and transverse couplers

A wide range of modifications to quantum annealing have shown significant promise in theoretical studies [23, 26, 38, 134, 160, 170–173]. In this section, we begin applying methods from the literature to our AMP model and assess their performance by computing the TTS as in Eq. 3.9. We begin by considering inhomogeneous driving method and transverse couplers. Inhomogeneous driving and the

ferromagnetic transverse couplers belong to the class of stoquastic Hamiltonians, while the anti-ferromagnetic couplers and mixed-sign couplers have non-stoquastic Hamiltonians. A stoquastic Hamiltonian has real and non-positive off-diagonal matrix elements in the computational basis [174], and can often (but not always [140]) be efficiently simulated by sign-problem-free quantum Monte Carlo (QMC). Non-stoquastic Hamiltonians, on the other hand, suffer from a sign problem and thus cannot be efficiently simulated in QMC in general, though some particular non-stoquastic Hamiltonians can be simulated in QMC by clever schemes to avoid the sign problem [175]. Amenability (or not) to QMC is a critical issue in QA, as in recent studies, QMC displays comparable exponential scaling to the physical incoherent tunneling rate in quantum annealers [140, 176–179]. It's thus intuitive to infer that the efficiency of QMC and quantum annealers are similar in solving many problems, making it difficult to realize a genuine quantum speedup. Non-stoquastic Hamiltonians do not suffer from this issue, and have demonstrated significant benefits in some theoretical work [26–28, 134, 180].

3.6.1 Inhomogeneous driving

In inhomogeneous driving, the transverse fields are ramped down at different rates from one site to the next, as first described in [23, 162]. In the original proposal [162], the magnitude of the transverse field applied to the N spins is turned off sequentially with a set of time-dependent amplitudes $\Gamma_i(s)$. In that work, the inhomogeneous driving transverse field circumvents the first-order quantum phase transition and provides an exponential quantum speedup in a p-body interacting mean-field-type model. A more careful analysis [23] which included noise and disorder found the exponential speedup to be somewhat fragile, but showed that a consistent polynomial speedup persisted given these more realistic assumptions. Further, there is experimental evidence that inhomogenous driving is effective in real hardware [165].

Inspired by the performance improvements offered by inhomogeneous driving of the transverse field Hamiltonian, we apply it to the four AMP problem sets as follows

$$
\begin{aligned}
H(t) &= -\frac{1}{N}\sum_{i=1}^{N}\Gamma_i(s)\sigma_i^x + sH_p, \\
\Gamma_i(s) &= \begin{cases} 1 & \text{if } s < s_i \\ N(1-s^r) + (1-i) & \text{if } s_i \le s \le s_{i-1} \\ 0 & \text{if } s_{i-1} < s \end{cases}
\end{aligned}
\tag{3.10}
$$

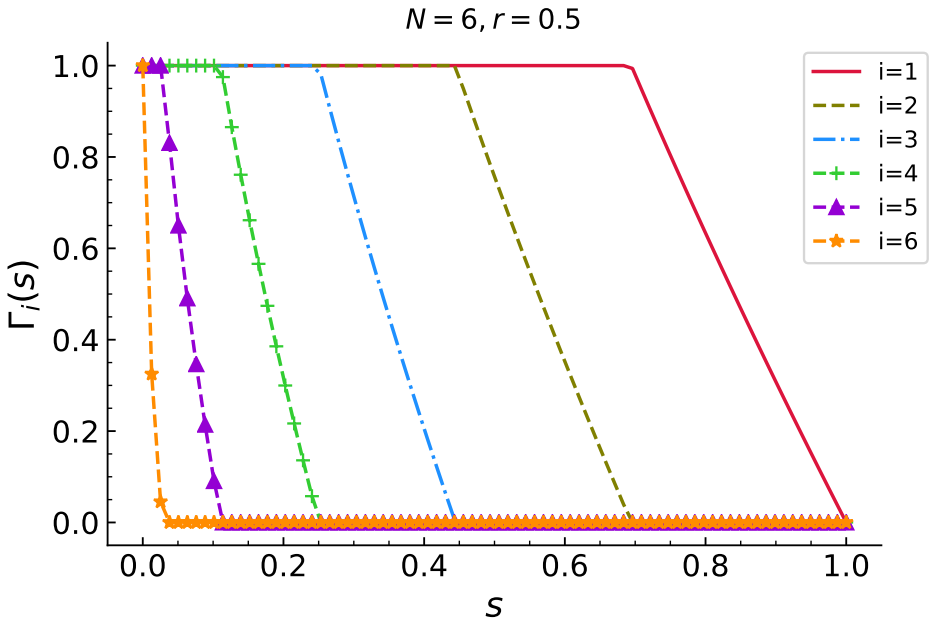

Figure 3.4 Transverse field strength $\Gamma_i(s)$ in the inhomogeneous driving method at each i, this scaling form is drawn from [162].

The scaling of $\Gamma_i(s)$ shown in Figure 3.4 is what suggested in [162]. Interestingly, the measurement of TTS in Figure 3.5 shows that the inhomogeneous driving method has a difficulty scaling which is very weakly dependent on the control parameters A and x_p, with the TTS scaling virtually identically in each case. It consequently outperforms the standard uniform sweep method for the harder problem regimes, but actually shows worse performance for the easiest parameter sets. While we cannot predict its performance analytically in this case (the perturbation theory we use to calculate Δ_{min} is not well defined for some of the transverse fields set equal to strictly zero), a clue to the origin of this behavior is found in a numerical analysis of the level structure, as we now describe.

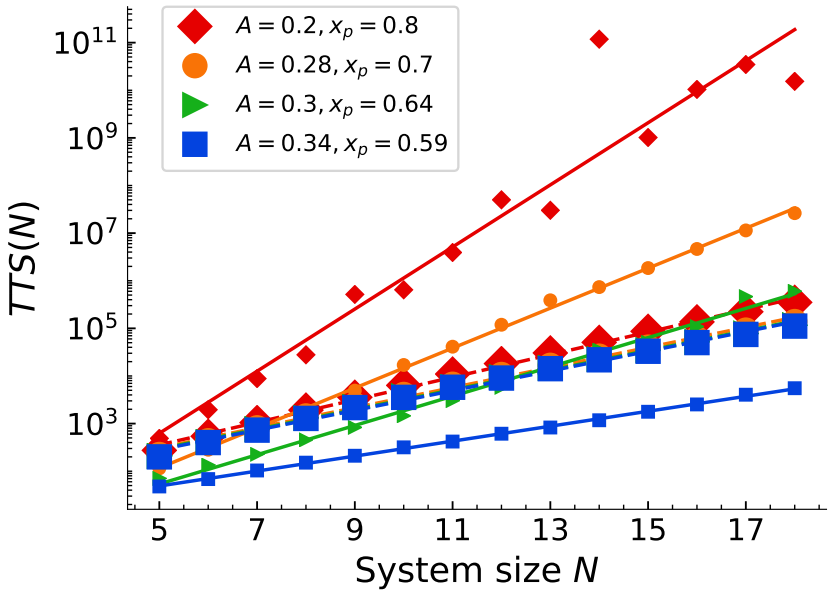

Figure 3.5 Time to find the true ground state in four problem model sets using the inhomogeneous driving method, computed from the final success probability for a runtime polynomially increasing with N. Larger markers are data with the inhomogeneous driving method, smaller markers are data with the standard uniform sweep method, dashed lines are best-fit curves of the inhomogeneous driving method, solid lines are best-fit curves of the standard uniform sweep method for comparison purpose. The inhomogeneous driving method helps in the harder cases but in the easier cases it is less efficient than the standard uniform sweep.

In Figure 3.6 we show the energy difference of the higher order excited states with the ground state in the hardest problem class with $N = 10$. In contrast to a uniform sweep, we find two avoided crossings in the annealing process, a generic feature of inhomogenous driving in this system that we observed for other parameter sets as well (data not shown). The presence of two crossings is likely what is responsible for the performance boost observed in the harder problems, and why it seems to have the same scaling for different parameters. A similar phenomenon is observed in the glued trees problem [148], where constructive interference of diabatically missing two avoided crossings leads to an exponential speedup. However, unlike the glued trees problem, there is no clear separation between the two competing minima and the higher excited states in the AMP model, that makes the performance hard to predict. It is clear from Figure 3.6 that there also exists an overlap region of the higher order excited states with the first excited state. As A and x_p are varied to make the difficulty scaling decrease, the two avoided crossings move closer together, and the distance from higher levels also shrinks and becomes exponentially small. Consequently, this effect does not result in an exponential speedup here, and shows worse performance than a uniform sweep in the easiest cases.

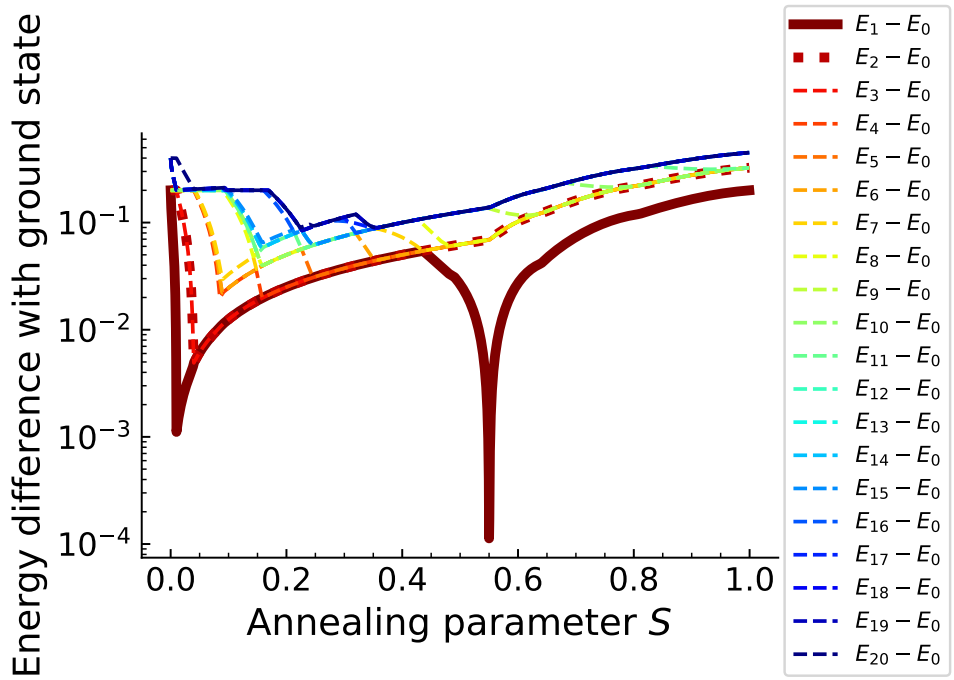

Figure 3.6 Energy difference of the higher order excited states with the ground state in the inhomogeneous driving method. This is the hardest problem where $\{A = 0.2, x_p = 0.8\}$, $N = 10$. We simulated the energy differences up to 20th excited state.

3.6.2 Transverse couplers

Adding two-body transverse coupling to QA [25–28, 134] is often considered to be a promising route to a quantum speedup. For instance, Hormozi *et al* [134], constructed a stoquastic Hamiltonian by inserting ferromagnetically coupled term H_I^F to the traditional Ising model, and a non-stoquastic Hamiltonian by inserting antiferromagnetically coupled term H_I^A or mixed coupled term H_I^M as listed in Eq.(1.6). In that work, they found that both stoquastic and non-stoquastic Hamiltonians showed an advantage over a uniform transverse field for a class of long-range Ising spin glass problems, with the non-stoquastic methods generally showing better performance. This motivated us to investigate the same method in our AMP model. We add transverse couplers into our model and choose a path of the form [134, 181]

$$H(s) = (1-s)\frac{1}{N}H_0 + s(1-s)\frac{1}{N}H_I + sH_p. \tag{3.11}$$

We apply the transverse coupler Hamiltonian to our four problem sets, plotting the results for the four scaling choices as in Figure 3.7.

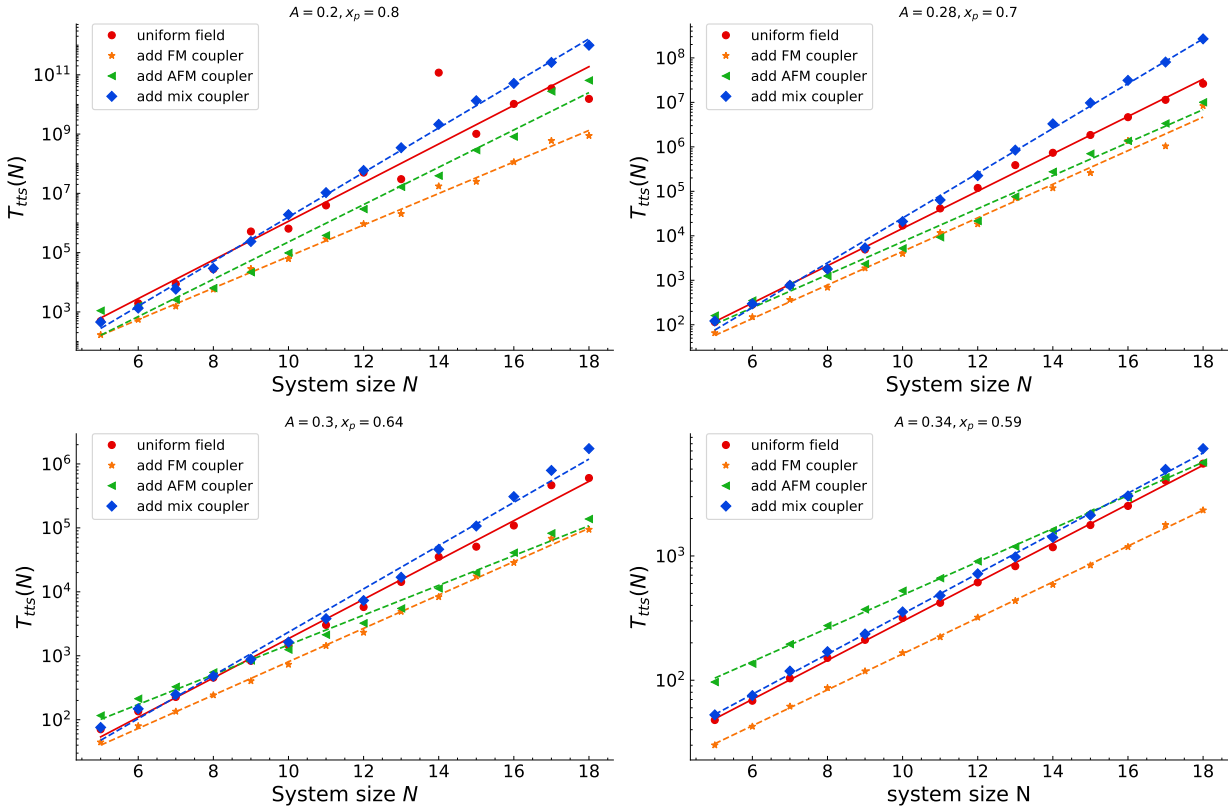

Figure 3.7 Time to find the true ground state in the 4 problem sets using the transverse coupler methods, computed from the final success probability for a run-time polynomially increasing with N. Data for adding a ferromagnetic coupler, an anti-ferromagnetic coupler, and mixed couplers are given by orange, green, blue markers, respectively. Red dots are data of the standard uniform sweep method for comparison purpose. The solid red line is the best-fit curve of the standard uniform sweep method for comparison. Other dashed lines are best-fit curves for the transverse couplers methods. Adding ferromagnetic and anti-ferromagnetic couplers to the conventional standard uniform sweep routine show obvious quantum speed up, although adding the mixed couplers reduces the advantage to some extent.

It is straightforward to see that adding ferromagnetic or anti-ferromagnetic coupler has a clear scaling advantage over a standard uniform sweep, but mixed couplers actually lead to decreased performance. The quantum speedup from coupler terms is probably because the couplers can flip two spins simultaneously, so the tunneling process from one configuration to the other can occur at lower order than with a uniform transverse field (where it occurs at Nth order in this model). The ferromagnetic coupler increases the minimum gap and thus provides a quantum speedup over the standard uniform sweep method, the same effect is observed in [134]. The antiferromagnetic couplers actually decreased the minimum gap but still show a scaling advantage, so the reason for the increased performance from the antiferromagnetic ones remains elusive. The behavior of the transverse coupler methods in other three problems sets are shown in TABLE I.

3.7 Reverse annealing and cold baths

Reverse annealing [39, 182–184], where the system is initialized in a local classical minimum and the transverse field is ramped up and down to search for other minima, unfortunately provides no benefit for the AMP. Reverse annealing was shown in [39] to provide benefit for the p-spin ferromagnet problem, if one is able to guess an initial state sufficiently close to the true ground state. However, in the AMP there are only two minima to choose from, separated by N spin flips. The only sensible choice (without dramatically modifying H_P) is thus to initialize the system in the false minimum. We simulated the reverse annealing protocol (data not shown) by initializing the system in the false minimum, ramping the transverse field up to a finite value guessed randomly from an $\mathcal{O}(1)$ range enclosing the phase transition point, evolving from that point for $\mathcal{O}(N^2)$ time, then ramping it back down to zero. With sufficient averaging over the location of the pause point (which is not knowable precisely in real problems), we found a time to solution which scaled nearly identically to the standard uniform sweep method for all parameters studied. Thus, we found no benefit in applying reverse annealing to this problem.

The influence of a cold bath on this system is more subtle. It is well known [38, 185–191] that coupling a quantum spin glass to a cold bath can improve the process of finding its low energy states. So let us consider coupling the AMP to a low temperature bath during annealing. Importantly, we here assume that T is small compared to the single qubit excitation energy, but it may still be large compared to the (exponentially small) minimum gap. How much can such a bath improve the time to solution?

Unfortunately, numerical simulation of such a system is prohibitively expensive [192] given the complexity of the Lindblad operators used to represent the finite temperature bath. We can however estimate the relaxation rate from the bath by appealing to the MSCALE conjecture [138]. This conjecture states that, for few-body operators, the scaling (with problem size N) of matrix elements of these operators between competing minima of quantum spin glasses near a phase transition is the same as the scaling of the minimum gap itself. This conjecture is true by inspection for the AMP, since the gap can be computed accurately using the modified forward approximation in the supplementary section. If we assume that each spin couples to a cold bath independently, then the rate of mixing near the phase transition scales as $N\Gamma_B^2/W$, where $\Gamma_B \propto \Delta_{\min}$ is the matrix element from a local spin operator and W is the energy range swept over. This produces a factor of N enhancement relative to the closed system, but does not change the scaling exponent as the other methods do. The cold bath may however improve performance in a real system by relaxing few-body excitations back toward the ground state, correcting "errors" induced by other channels.

3.8 RFQA

Stoquastic or not, the previous sections all explored "DC" schemes involving slow variations of transverse field and coupler terms. In this section, we consider an AC alternative, called RFQA [138]. In RFQA, the traditional transverse field driver Hamiltonian is modified by independently oscillating either the magnitude (RFQA-M) or direction (RFQA-D) of each transverse field term (M and D refer to magnitude and direction, respectively). As we will describe shortly, the qualitative explanation for a quantum speedup in RFQA is an exponential proliferation of weak many-spin processes, leading to accelerated mixing near first order quantum phase transitions. The total Hamiltonian in RFQA is given by

$$H(t) = (1-s)H_{M/D}(t) + sH_p, \tag{3.12}$$

where the driving fields in RFQA-M and RFQA-D are defined as follows

$$\begin{aligned} H_M(t) &= -\kappa \sum_{i=1}^{N} (1 + \bar{\alpha_i} \sin(2\pi f_i t))\sigma_i^x, \\ H_D(t) &= -\kappa \sum_{i=1}^{N} [\cos(\bar{\alpha_i} \sin(2\pi f_i t))\sigma_i^x + \\ &\quad \sin(\bar{\alpha_i} \sin(2\pi f_i t))\sigma_i^y]. \end{aligned} \tag{3.13}$$

Here, $\bar{\alpha_i}$ is the amplitude of each oscillation, the frequencies f_i of the field are randomly chosen between f_{min} and f_{max}, and κ is the magnitude of the transverse field. To avoid uncontrolled heating, both f_{min} and f_{max} have inverse polynomial scaling in N. To estimate the performance of RFQA, we average the success probability $p(t_f)$ over hundreds of random choices of the $\{f_i\}$ when computing time to solution. The RFQA methods all rely on finite frequency dynamics that are not captured by QMC, making them promising candidates for producing a quantum speedup. The two methods are straightforward to implement in flux qubit hardware, by applying oscillating magnetic fields as described in [138].

As described in the original work, the qualitative speedup mechanism from RFQA is complex and arises from an exponential proliferation of weak multi-photon transitions. As the system nears a phase transition point, whenever the energy of the two ground states crosses a combination of m oscillating frequencies there is an mth order driving process that (very weakly) mixes the two states. In general, the Rabi frequency of such a process decreases exponentially in m, but there are $2^m\binom{N}{m}$ such terms and the combination of all of them dramatically accelerates the phase transition. If the mth order resonance is smaller than the base tunneling rate $\Omega_0 = \Delta_{min}/2$ by a factor Λ^m, then the total transition rate is expected to scale exponentially with N as expressed in 2.23.

3.8.1 RFQA-M

In RFQA-M the magnitudes of the transverse field terms coherently oscillate with time as the global amplitude is ramped down toward 0, so that an individual transverse field term κ is replaced with $\kappa\left(1+\bar{\alpha}\sin 2\pi f_i t\right)$. In our simulations we used $\bar{\alpha}=0.9$, and magnitude of frequencies f_i is randomly chosen between $\{\frac{0.3}{N^{1.5}}, \frac{0.6}{N^{1.5}}\}$; the signs of the f_i are also randomly chosen. This is superficially similar to inhomogenous driving, but the coherent oscillations lead to non-monotonic changes of κ_i with time and very different scaling as a result. We also considered a few additional variations of RFQA-M. In one set of simulations, we explored a partially synchronized RFQA-M method, in which N spins are broken into k groups, instead of generating different random frequencies for each site, the transverse fields in each group are all oscillated in phase with the same frequencies. In this work, we only divided the N spins into two groups, but other arrangements are possible. We also explored adding ferromagnetic/antiferromagnetic couplers to the RFQA-M method, where all transverse couplers and fields are independently oscillated in magnitude. The total Hamiltonian in this method is defined as follows

$$\begin{aligned} H(s) &= (1-s)H_{M/D} + sH_p \\ &\quad + (1-s)\kappa_r \sum_{<i,j>} \sin(2\pi r_{ij} t)\sigma_i^x \sigma_j^x \end{aligned} \tag{3.14}$$

where κ_r is the magnitude of the coupler terms, r_{ij} are the oscillating frequencies of the coupler, randomly chosen between $\{r_{min}, r_{max}\}$. The magnitude r is defined to polynomially decrease with N, and the frequencies r_{ij} are also inverse polynomial in N. Finally, we looked at partially synchronized RFQA-M with transverse couplers, where the transverse couplers are also synchronized into groups.

We compare the TTS of the various implementations of RFQA-M with the standard uniform sweep method in Figure 3.8.

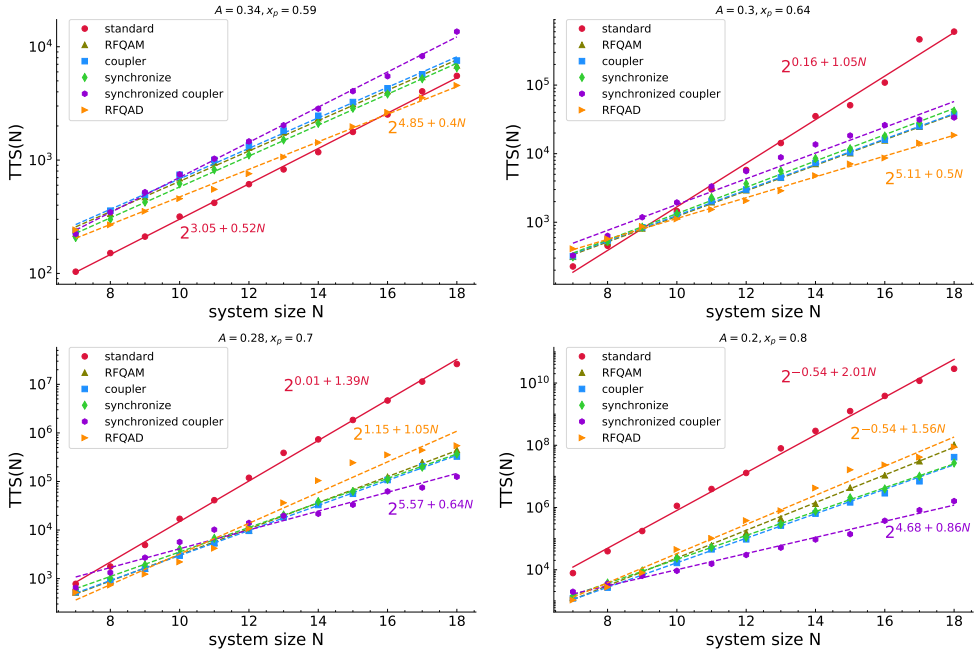

Figure 3.8 Time to find the true ground state in four problem model sets using the RFQA method, computed from the final success probability for a run-time polynomially increasing with N. Data of the RFQA methods are given by different markers. Red dots are data of the standard uniform sweep method, the solid red line is the best-fit curve of the standard uniform sweep method for comparison purpose. Other dashed lines are best-fit curves of the RFQA methods.

The results show that RFQA-M and its adaptions can provide quantum speed up over the standard uniform sweep routine, with a scaling advantage which is particularly obvious in harder problem sets.

3.8.2 RFQA-D

In RFQA-D the direction of each transverse field term oscillates in time, tipping back and forth in the $x - y$ plane. This can be engineered through oscillating z biases (which can be shown to be equivalent to a tipping transverse field through a time-dependent unitary transformation) and has the elegant property that the instantaneous spectrum of the system is preserved in the evolution, so the oscillations have no "steering" effect whatsoever (unlike RFQA-M, where changing transverse field magnitudes can change the relative energies of competing minima, in addition to any AC effects). Any performance advantage from RFQA thus comes directly from the proliferation of weak transitions described above.

As shown in Figure 3.8, we see that RFQA-D does provide an obvious quantum speed up over a uniform sweep. In all studied cases, RFQA-D reduced the exponent for $TTS(N)$ relative to the standard uniform sweep, and for the two easier difficulty regimes, it outperformed all other studied methods. We expect that these results will carry over to the larger class of optimization problems that experience

wrong-way steering towards false minima.

3.9 Conclusion

In this work, we defined a simple toy model– the asymmetric magnetization problem– with two competing minima separated by a global peak, and used it to benchmark a variety of modifications to quantum annealing in the literature. The problem is exponentially difficult to solve due to its exponentially closing gap, and the entropic steering toward a false minimum responsible for its difficulty is a generic bottleneck mechanism for a huge array of optimization problem classes. Thus, methods to accelerate finding the solution in it should prove beneficial in much broader contexts.

We studied an ensemble of problem model sets with descending difficulty:
$\{A = 0.2, x_p = 0.8\}; \{A = 0.28, x_p = 0.7\}; \{A = 0.3, x_p = 0.64\}; \{A = 0.34, x_p = 0.59\}$, and assessed a variety of new quantum methods by evaluating the scaling of the time to solution (TTS). To have a straightforward view of the performance of each method, we fit their TTS to exponential functions and extracted the exponential scaling value, summarized in TABLE I. The standard uniform sweep method shows inverse gap squared dependence as expected. In contrast, in the inhomogeneous driving approach, the TTS has a nearly constant difficulty scaling of $2^{\sim 7N/10}$, roughly independent of the tuning parameters. It likely means that the problem is steered less toward the false minimum in this case than it is for uniform driving, but that is not enough to avoid a first order transition and the resulting lack of guidance becomes counterproductive when the problem is easier.

While the problem we studied is homogeneous (in that energy is a function of total magnetization only), we don't expect disorder to significantly change the results for the standard uniform sweep, couplers and RFQA. If we modeled disorder as a simple random Z term with magnitude $1/N$ for each spin (recall that the problem energy is $O(1)$) added to H_p, it would change the relative energies of the ground states by $1/\sqrt{N}$ for the energy scale we have chosen. This will move the transition point s_c around from one instance to the next, but by an amount that vanishes as $N \to \infty$. Given that our modified forward approximation calculation predicts Δ_{min} fairly accurately, examination of those equations shows that this change should not effect the scaling exponent at large N. However, it might effect inhomogeneous driving more significantly, as has been seen in other problems [23, 148, 162, 193].

For the transverse coupler method, both ferromagnetic or anti-ferromagnetic coupler terms can provide obvious improvements, but adding a mixture of ferromagnetic and anti-ferromagnetic coupler terms proved counterproductive. We expect that the speedup from the coupler terms arises from creating more tunneling paths between the two competing minima, since each coupler flips two spins simultaneously. Interestingly, we saw very similar scaling benefits for both ferromagnetic (stoquastic) and anti-ferromagnetic

(non-stoquastic) coupler methods; there is no obvious connection between non-stoquasticity and increased performance in this problem.

Among the RFQA methods, synchronized RFQA-M with the added couplers provided the greatest quantum speedup in the two hardest problem sets, while RFQA-D showed the best scaling in the easier problem instances. The speedup mechanism for both couplers and RFQA methods is due to an amplification of the tunneling rate and has nothing to do with local energetic guidance.

We conclude that although we did not achieve an exponential speedup for this problem, all of the methods can provide a quantum speedup over the standard uniform sweep routine: inhomogeneous driving provides a significant boost in harder problem sets; transverse couplers added to the standard uniform sweep routine create more tunneling paths between two competing minima and help decrease the time needed to find the solution; and the introduction of oscillating fields in the RFQA methods can help to stimulate multi-tone transitions, providing more possibilities for the two competing minima to mix. Undoubtedly, the relative advantages of the methods will certainly depend on the problem class, but since our AMP model exhibits such a generic bottleneck mechanism, any methods to accelerate finding the solution in it should be very widely applicable. Given that all three of inhomogeneous driving, RFQA-M and RFQA-D only require modification to the control circuitry and not the qubit hardware itself, we see them as the most promising and cost-effective routes to a near-term benefit. It would be worthy to continue to study these methods on realistic problems at larger scales, and it requires minimal changes to existing hardware to verify their potential in experiment.

In the next chapter, we focus on the RFQA method and make a digitize version of RFQA based on the quantum circuit model, we believe the outstanding performance of the continuous time simulation of RFQA can be preserved in the digitized-RFQA. And a quantum gate model of RFQA also allows the possibility of error correction.

3.10 Supplementary material

We supply supplementary material in this section.

3.10.1 Analytical prediction of the minimum gap

The minimum gap Δ_{min} determines the worst case difficulty of a problem, so analytically predicting it can help us to better assess the behavior of the quantum annealing algorithm. To compute it, we use a modified form of the "forward approximation" Nth order perturbation theory employed in [194–198]. In this approximation, the minimum gap is predicted to be

$$\Delta_{min} = N! \frac{\prod_{i=1}^{N} \kappa_i}{\prod_{n=1}^{N-1} U_n} \tag{3.15}$$

where κ_i is the transverse field strength on each site i (evaluated at the critical point κ_c), and U_n^{-1} is the average of the inverse of the energy difference to flip n spins from either ground state

$$\frac{1}{U_n} = \left\langle \frac{1}{\epsilon_n + \delta_{\epsilon_n} - \epsilon_0 - \delta_{\epsilon_0}} \right\rangle. \tag{3.16}$$

Here, the ϵ terms are the classical energies defined in the problem Hamiltonian and the δ terms are their perturbative corrections from the transverse field, which act to increase the excitation energies in this case. For a problem Hamiltonian defined in Eq.3.7 as follow:

$$H_p = Nf(m), \tag{3.17}$$

which has a similar definition of the AMP problem model, where there are many tunneling path between the two competing ground states. In the conventional quantum annealing process where the Hamiltonian is expressed as

$$H(t) = H_p + \kappa(t)H_0, \tag{3.18}$$

we can take the driving field as a perturbation term with strength κ. Let us first consider the case of one spin flip from the all spin down state(false minimum), the unperturbed energy of two states will be lifted by the small perturbation from the uniform driving field H_0. Regarding the fact that the perturbation term H_0 only has nonzero off-diagonal matrix elements, and the absolute value of off-diagonal matrix elements are 1, the energy correction terms for the all spins down state and the one spin flip state are

$$\begin{aligned} \delta_{\epsilon_0} &\simeq -\kappa^2(\epsilon_1 - \epsilon_0) = -\kappa^2 x_p; \\ \delta_{\epsilon_1} &\simeq -\kappa^2(\epsilon_0 - \epsilon_1) = \kappa^2 x_p, \end{aligned} \tag{3.19}$$

the corrected energy difference between the two states is

$$\begin{aligned} U_1 &= (\epsilon_1 + \delta_{\epsilon_1}) - (\epsilon_0 + \delta_{\epsilon_0}) \\ &= \frac{1}{x_p} + 2\kappa^2 x_p. \end{aligned} \tag{3.20}$$

Including these corrections in the energy denominators (which is effectively a resummation scheme) is vital to obtaining relatively accurate predictions; explicitly, for the AMP

$$U_n \simeq \begin{cases} n\left(\frac{1}{x_p} + 2\kappa_c^2 x_p\right) & n \leq x_p N, \\ \\ (N-n)\left(\frac{1+A}{1-x_p} + 2\kappa_c^2 \frac{1-x_p}{1+A}\right) & n > x_p N. \end{cases} \tag{3.21}$$

From this expression, it is straightforward to predict the minimum gap in our problem.

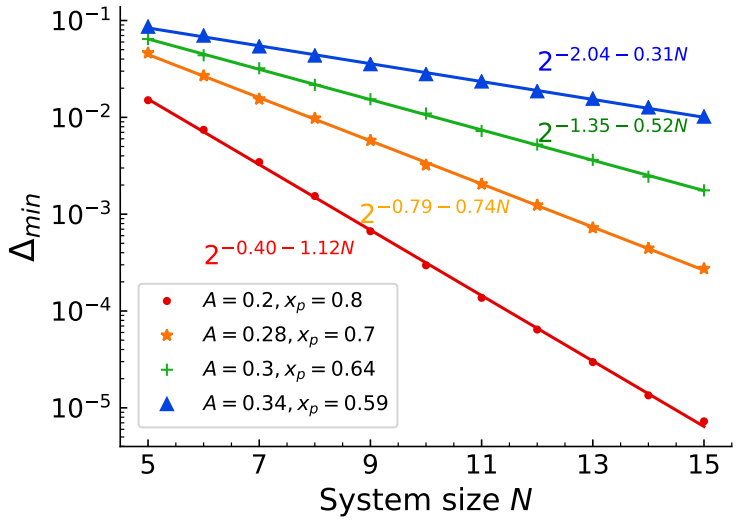

Figure 3.9 Numerical values of the minimum gap for four parameter sets in the standard uniform sweep method, with the system size N ranging from 5 to 12 spins. The markers are data of numerically estimated minimum gap energies, least squares fits of the minimum gap are red, orange, green and blue solid lines. The minimum gaps in the four problem sets all decrease exponentially with increasing system size.

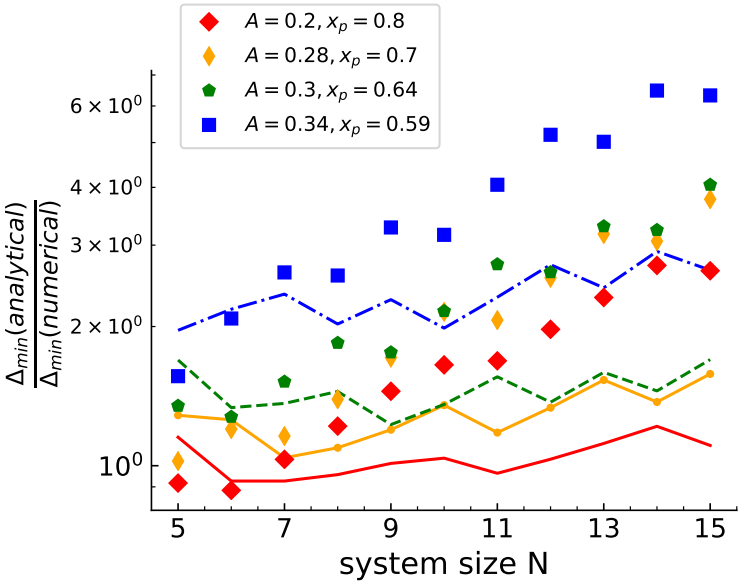

Figure 3.10 Ratio of analytical and numerical values of minimum gap for four problem sets in the standard uniform sweep method, system size N ranging from 5 to 12. The analytical values of Δ_{min} are from the modified forward approximation (Eqs.(3.15 – 3.21)). The markers represent the ratio of analytical and numerical values of minimum gap in four problem sets. dashdot line; dashed line; line with point marker and solid line represent the ratio of analytical and numerical values with a correction term $2\pi/N$ for problem set: $\{A = 0.34, x_p = 0.59\}$; $\{A = 0.3, x_p = 0.64\}$; $\{A = 0.28, x_p = 0.7\}$; $\{A = 0.2, x_p = 0.8\}$ separately. The corrected analytical predictions in the four sets match well with the numerical values.

As shown in Figure 3.9, the exponential fitting of numerical Δ_{min} as a function of N for descending difficulty problem sets are: $2^{-0.4-1.12N}$, $2^{-0.79-0.74N}$, $2^{-1.35-0.52N}$, $2^{-2.04-0.31N}$. Figure 3.10 indicates that the scaling of our theoretical prediction matches well with the numerical result by multiplying by a factor of $2\pi/N$. Eq.(3.15) appears to overestimate the true gap by a factor of $\sim N/2\pi$; the reason for this is unclear. Some level of disagreement is expected, however, particularly in the easiest of the four parameter sets. If the coefficient of the problem Hamiltonian is 1, the phase transition for those parameters occurs at $\kappa_c \simeq 1.73$. At such a large value of κ_c the ratio of κ to the single spin excitation energy approaches unity and thus a perturbative expansion may break down. As the log of the minimum gap is an integral of a function of total magnetization and the order in which spins are flipped doesn't matter, we expect that other Hamiltonians which are simple polynomials of total magnetization (such as p-spin models) would likely show similar physics to our AMP problem.

3.10.2 Survey on the inhomogeneous driving QA

The performance of the inhomogeneous driving method doesn't make much difference in different difficulty scaling problem sets. Quantum advantage from inhomgeneous driving QA is obvious in the harder problem sets:$\{A = 0.2, x_p = 0.8\}$; $\{A = 0.28, x_p = 0.7\}$; $\{A = 0.3, x_p = 0.64\}$, while in the easiest problem $\{A = 0.34, x_p = 0.59\}$, the inhomogeneous driving field performs even worse then the uniform transverse field. The worst behavior may result from the changing of the energy gap. Here we show how the energy gaps between ground state and higher order excited states are modified as we decrease the difficulty scaling in Figure 3.11. Besides the feature of the presence of two avoided crossings, the inhomogeneous driving field results in a much smaller minimum energy gap compared to the uniform driving field, especially in the easiest problem set. From the energy gap shown in Figure 3.11, as the difficulty level decreases, the two avoided crossing regions shrink and become flat, the overlap with higher levels shrinks as well. Taking the hardest problem set as an example, the overlap region is broad, so that even when the system jumps to the first excited state and other higher order excited states at the first avoided crossing, it still has chance to cool down to the ground state at the second avoided crossing. In the easier case, the overlap regions with higher order states shrink and even disappear in the easiest case. Once the system is excited to higher order excited state, it becomes more difficult to transition to the ground state. This could be one of the reason why the inhomogeneous driving method doesn't perform well in the easier problem models.

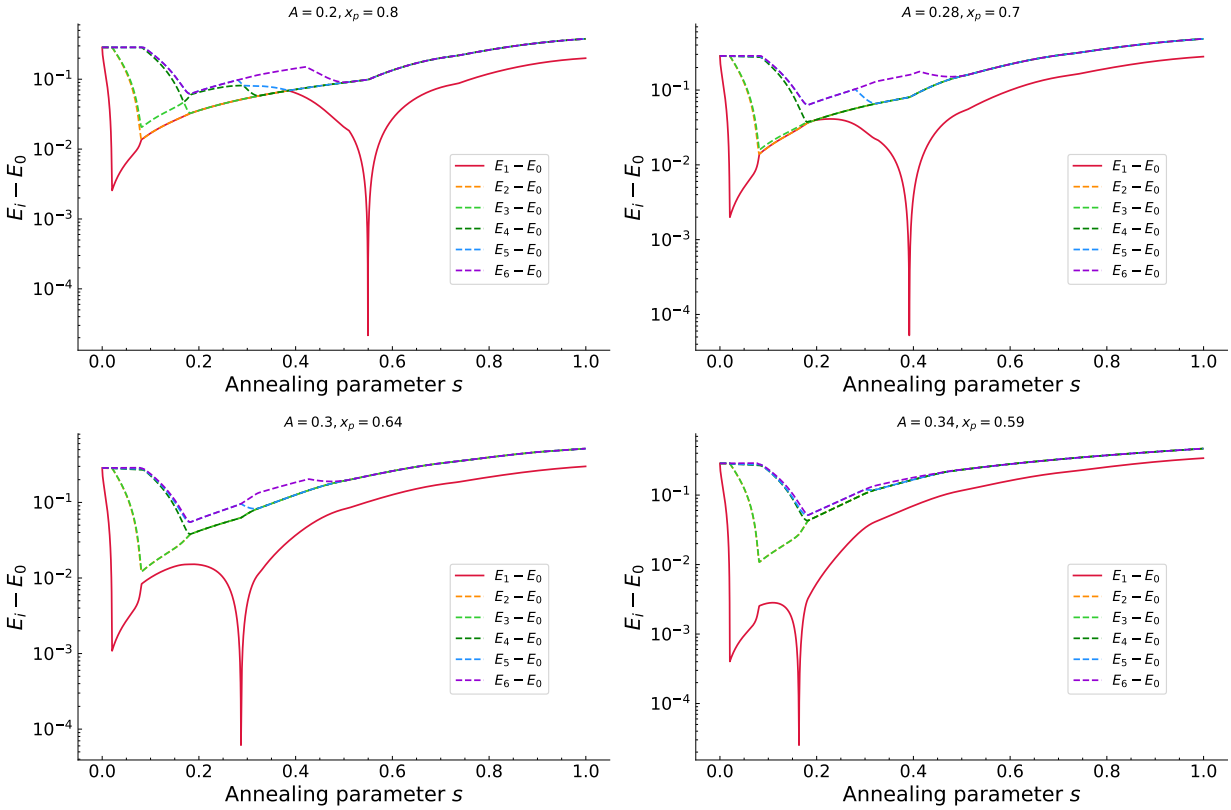

Figure 3.11 The energy gap between the ground state and other excited states in inhomogeneous driving method

3.10.3 Survey on the transverse coupler QA

In the investigation of adding a transverse coupler to the uniform field QA, we see both ferromagnetic and antiferromagnetic couplers provide a quantum advantage compared with uniform transverse field QA. The speedup of adding a ferromagnetic coupler is straightforward, since the ferromagnetic coupler increases the transverse field strength and thus increases the minimum energy gap between ground state and first excited state in the annealing process, which is confirmed in Figure 3.12.

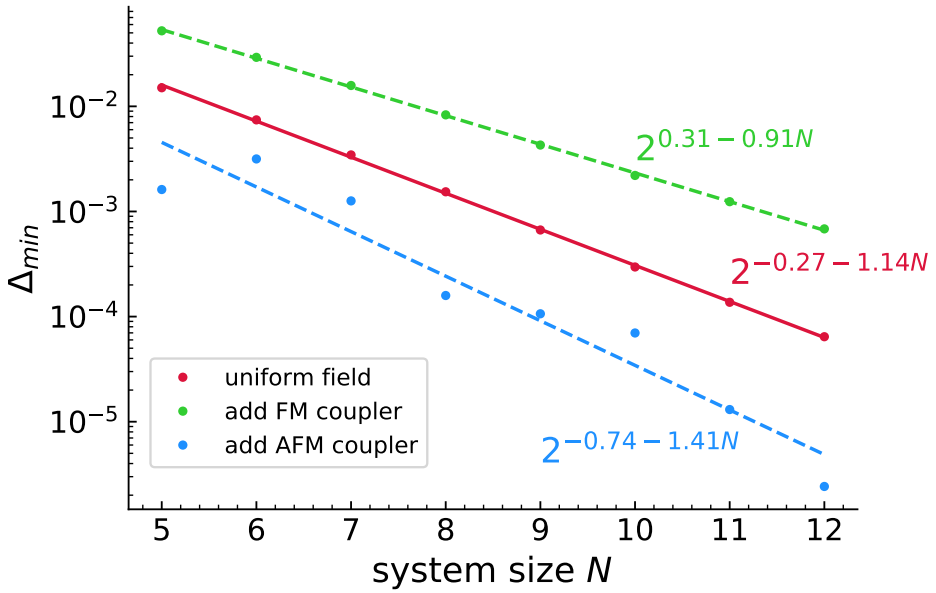

Figure 3.12 Numerical value of the minimum energy gap for standard uniform sweep method, add ferromagnetic and antiferromagnetic methods in the hardest problem set $\{A = 0.2, x_p = 0.8\}$. The dots are data of numerically estimated mininum gap energies, dashed lines are the least squares fits of the numerical data. Standard uniform field QA, QA with ferromagnetic coupler and QA with antiferromagnetic coupler are represented by red, green and blue lines(and dots). The ferromagnetic coupler increases the minimum gap compared with the conventional QA, while the antiferromagnetic coupler decreases the minimum gap.

However, the speedup mechanism of adding antiferromangetic coupler is still not clear and it's interesting that the antiferromagnetic coupler decreases the minimum gap but still outperforma the standard uniform sweep QA. In the study of a long-range Ising spin glass[134], the advantage of antiferromagnetic coupler is related to the increase of the number of anticrossings. We show in Figure 3.13 that for both ferromagnetic and antiferromagnetic couplers, there is only one avoided crossing between the ground state and the first excited state energies during the evolution. The avoided crossing in the antiferromagnetic coupler method is much smaller than in both the ferromagnetic coupler method and the standard uniform sweep method, which is consistent with Figure 3.12. Since the antiferromagnetic coupler comprises a non-stoquastic Hamiltonian and outperforms the conventional QA, we believe it's very promising tool even if the quantum advantage of it remains elusive.

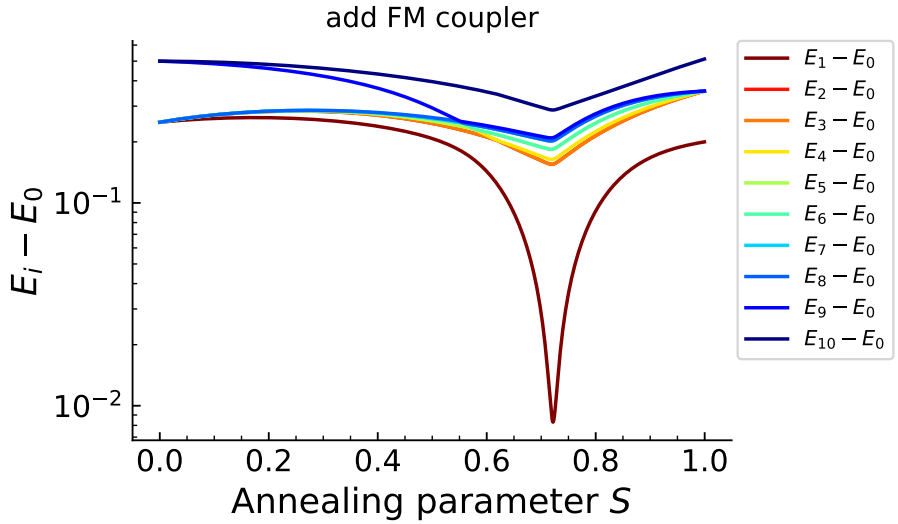

(a) Add ferromagnetic coupler

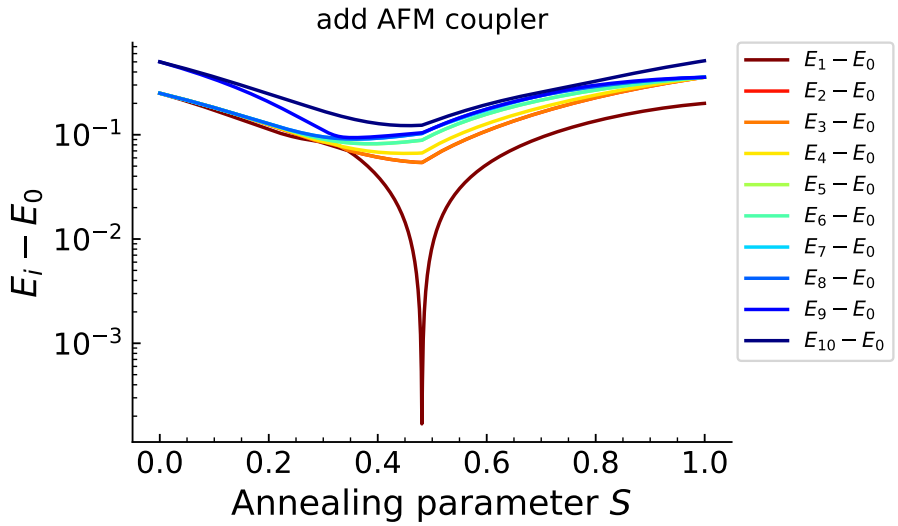

(b) Add antiferromagnetic coupler

Figure 3.13 The energy gap of adding ferromagnetic or antiferromangetic couplers in the hardest problem set $\{A = 0.2, x_p = 0.8\}$ with system size $N = 8$. The energy gap of both cases only exhibit one avoided crossing during the annealing, and adding an antiferromagnetic coupler decreases the minimum energy gap to a large extent.

CHAPTER 4

DIGITIZED QUANTUM ANNEALING WITH OSCILLATING AC TRANSVERSE FIELDS IN SOLVING OPTIMIZATION PROBLEMS

We study the behavior of digitized quantum annealing in this chapter, but the behavior of the digitized QA with noise added is unknown.

4.1 Abstract

Many realistic hard problems can be encoded into combinatorial optimization problems [119]. As two promising candidates in the Noisy Intermediate-Scale Quantum (NISQ) regime for solving optimization problems, the universal computations Quantum Annealing(QA) and Quantum Approximate Optimization Algorithm(QAOA) can be combined to contribute to a new algorithm: digitized-QA [101], which not only can include nonstoquastic terms but also can be a fault-tolerant scalable quantum algorithm. Inspired by the outperformance of RFQA(abbreviation of random field quantum annealing and radio frequency quantum annealing) in quantum annealing [138, 199], we infer that by making the time step dt sufficiently small, we can simulate the continuous evolution of RFQA in quantum annealing with many discrete quantum gates. It's intuitive to predict that RFQA in quantum gate model can also provide a quantum speedup against standard quantum annealing in solving some hard optimization problems. We come up with exponentially difficult problems that requires exponential runtime to solve with conventional uniform transverse field quantum annealing. We show RFQA is able to provide obvious quantum speedup compared to the standard quantum annealing in the quantum gate model version.

4.2 Introduction

Quantum computing technology has been developed fast in the past decades [200], however, the realization of a fault-tolerant quantum computer is still out of reach due to noise and decoherence. John Preskill proposed the NISQ regime [61], which takes advantage of existing imperfect quantum computers of relatively small qubit numbers. This has lead to growing interest in the study of near-term quantum computation. It's important to find quantum algorithms that run on NISQ technologies that can demonstrate quantum supremacy [201] or quantum speedup, that will be important in building useful quantum computer as a proof-of principle demonstration. There are some promising candidates such as Quantum Annealing(QA) [18, 126, 130, 146–149], quantum approximate optimization algorithm (QAOA) [109, 110, 202–204] ,variational quantum eigensolver (VQE) [205–207] and other hybrid quantum classical algorithms [208, 209].

Quantum Annealing (QA) is an important tool in solving combinatorial optimization problems in some artificial intelligence and machine learning tasks [150–155]. Different from its classical counterpart Simulated Annealing(SA) [47, 210], QA takes advantage of quantum fluctuation instead of thermal fluctuation to tunnel through the barriers in the energy landscape. By allowing a continuous time adiabatic evolution of a Hamiltonian that is a combination of two non-commuting Hamiltonians, $H(t) = (1 - s(t))H_0 + s(t)H_p$. QA tracks the instantaneous ground state of the system as the initial instantaneous ground state is the ground state of H_0, which is easy to prepare, and the final instantaneous ground state is the ground state of H_P, which encodes the solution of the optimization problems. The bottleneck [211] of QA lies in the regions of vanishing spectral gaps, especially when a first-order transition [121] happens which comes with an exponentially decreasing spectral gap, as the annealing time t_f has an inverse minimum gap squared dependence as demonstrated in Eq.(3.5). To address this severe issue, many strategies have been proposed, such as circumventing the first-order quantum phase transition with inhomogeneous transverse field [23, 162], increasing the minimum gap with ferromagnetic coupler [29], and the use of oscillating transverse fields(RFQA) [138, 199]to accelerate the mixing of two competing states near the first-order transition.

Quantum Annealing delivers continuous time evolution on an analog quantum device, the continuous time evolution of QA will suffer from non-adiabatic errors due to a finite runtime T, and since the fine tuning of the tunneling schedule to overcome the first-order transition always requires the knowledge of the energy landscape. This is hard to access in most realistic problems. An alternative way to realize quantum-enhanced information processing is a gate-model hybrid quantum-classical variational algorithm: The Quantum Approximate Optimization Algorithm (QAOA). The procedure of QAOA is similar to VQE as shown in Figure 1.6: first preparing an initial state $|\psi_0\rangle$(*ansatz state*), then repeatedly applying unitary operators $e^{-i\beta_i H_M}$ and $e^{-i\gamma_i H_C}$, followed by a classical algorithm to minimize the expectation value of H_C on the state $|\psi(\beta, \gamma)\rangle$, and updating the parameters sent to the QPU. This procedures repeats until a suitable convergence criteria is met.

Both QA and QAOA are computationally universal [212–215]. This work in [101] combines the advantages of them and comes up with the idea of "digitized-QA", which can be run on future error-corrected machines. The digitized-QA can be a scalable general-purpose algorithm and is very promising in the regime of NISQ. The digitized-QA, different from QAOA, doesn't need to optimize over the parameters $(\vec{\gamma}, \vec{\beta})$ since these parameters are determined once we decide the depth p of the circuit. This algorithm applied in gate model quantum circuits can be compatible with error correction.

We have explored the behavior of the oscillatory AC transverse fields method [138], aka RFQA, where local, low-frequency oscillations are added to transverse field terms in adiabatic quantum computing or

quantum annealing. RFQA takes advantage of the mutli-tone resonance from random driving frequencies and can generate polynomial quantum speedups in solving hard optimization problems. In the work [138, 199], we show RFQA method is able to provide polynomial quantum speedup over the standard uniform-sweep method in quantum annealing for a generic artificial problem, where the problem is entropically steering toward the local minimum, and the system has to traverse all possible states to reach the global minimum, and we expect to see RFQA outperform standard uniform-sweep method in the quantum gate model. Inspired by the performance of RFQA in continuous time evolution in quantum annealing, and the work in [101], which paved the way for us to investigate more complex problems with digitized-QA, we propose to digitize the RFQA method and investigate with similar generic problems that have exponential difficulty in reaching the global minimum. We explore a digitized version of RFQA that could be simulated on universal gate model machines. We apply the digitized version of RFQA to various trial problems using classical numerical simulation and show that RFQA is a potentially promising tool for solving hard problems in optimization and machine learning. We can find the answer to the optimization problem as long as the depth p is high enough, but noise will ultimately inhibit a long circuit depth with limited error correction in existing quantum computers. Thus finding a trade-off between the gate error induced by too many gates and algorithmic error(or digital error) when there are too few gates, is necessary in digitized-QA when implementing the algorithm on a real quantum device, and this will be discussed later in our paper. In the digitization process, if the time step dt is chosen to decay as $\frac{1}{N}$, the consequential increasing circuit depth hinders the performance without error correction. We find a constant dt works fine in giving decent results in our simulations, this indicates the polynomial speedup we achieved in our work is valuable and can be useful for optimizations[216]. The hard problem models we considered in our work steers toward the false minimum easily and requires N-spin tunneling through a small gap form the false minimum to the true minimum. The difficulty of the problem comes from the exponentially small tunneling rate through the energy barrier between the local minimum and global minimum. Another mechanism that gets the system stuck in the equilibrium high energy state induced by the entropic barriers [217] can also result in exponentially long runtime, but this is out of the scope of our work as it's not as easy as preparing such a scheme in small system size with few-body interactions.

In the work of digitized QA, we first introduce the RFQA method and its outperformance in the continuous simulation of Quantum Annealing. Secondly, we talk about the steps in digitizing RFQA method and the reverse annealing schedule applied to the problems. Then we introduce a series of benchmark problems to show that digitizing RFQA is a promising digital quantum optimization algorithm either for noisy machines or ultimately error corrected ones. Finally, we summarize our results and provides comments on the promises of digitzed RFQA.

4.3 The RFQA method in the continuous simulation of Quantum Annealing

Although there are extensive studies of QA in solving combinatorial optimization problems, it still lacks conclusive evidence to show quantum speedup. To date, many methods have been proposed to improve the performance of the conventional uniform transverse field QA, within them, we find RFQA is a very promising and easy to implement method as a variation of conventional QA.

In the conventional QA, the driving Hamiltonian is chosen as a uniform transverse field, the ground state of which is easy to prepare and is a uniform superposition of all possible solutions. The overlap between the instantaneous state and the ground state of the problem Hamiltonian will be maximized at the end of the annealing. In RFQA, we modify the uniform transverse field $-\sum_i \sigma_i^x$ to an oscillating time-dependent transverse field such that it is a uniform transverse field at the beginning of the annealing and starts to oscillate during the annealing process.

In the continuous time-evolution results from last Chapter, we see that RFQA provides a stark scaling advantage to the conventional quantum annealing method. The time to solution is polynomially reduced as shown in Figure 3.8. The RFQA methods are also implementable in analog quantum hardware, thus we regard it as a very promising variation of quantum annealing.

4.4 Digitization of RFQA method

From the original work of RFQA [138] and our investigation of RFQA in the artificial AMP problem [199], we see the potential of RFQA in providing a quantum speedup for solving hard optimization problems. The analog quantum annealing is promising in near-term quantum computation because it is resilient to decoherence to some extent. However, no evidence of a conclusive, broadly applicable quantum speedup has been shown in real experiments. Therefore the success of analog quantum annealer is not promised as the problem size increases. Another promising quantum computation technique, quantum circuit model, is compatible with error correction and can make fault-tolerant quantum computers possible. Thus, we propose to digitize the continuous time evolution of RFQA and investigate a series of benchmark problems with digitized-RFQA. We hope to see that the digitized version of RFQA provides a quantum advantage in solving hard optimization problems under a low error rate.

In the digitized-QA, we build a quantum circuit with a sequence of discrete unitary transformations. The basic form of the total Hamiltonian in Quantum Annealing is a combination of a driving Hamiltonian H_0 and a problem Hamiltonian H_p as shown in Eq.(1.2). To simulate the continuous time evolution $e^{iH(t)dt}\left|\psi\right\rangle$, we can decompose the exponentiation into two parts with small dt by using the first order Trotterization approximation as shown in Eq.(2.30). For a H_p that is diagonal in the Z basis, such as the Ising formulation, we can further split the exponentiation of H_p into $\prod_{j=1}^{N} e^{i(B(t)dt)h_j\sigma_j^z}$ and

$\prod_{j<k} e^{i(B(t)dt)J_{jk}\sigma_j^z\sigma_k^z}$. For large dt, a loose sense of the digitized version of AQC/QA with discrete time evolution is similar to the quantum approximate optimization algorithm (QAOA). Thus digitized-QA can combine the advantages of QAOA and AQC. Due to the errors in quantum computing, quantum computers cannot execute arbitrarily long sequences of logic gates for now. However, it's still possible to take advantage of existing quantum computers of relatively small qubit numbers in the NISQ regime.

The digitization of RFQA is straightforward. In RFQA-M, the H_0 in the conventional quantum annealing method will be simply replaced with a magnitude oscillating transverse field H_M. The gate sequence of problem Hamiltonian can be further split into separate Z and ZZ rotation gates. The exponentiation of time-evolution operator is

$$e^{-iH(t)dt} \simeq \Big(\prod_{j=1}^{N} e^{i[A(t)dt(1+\alpha sin(2\pi f_j t+\varphi_j)]\sigma_j^x}\Big)\Big(\prod_{j=1}^{N} e^{i[B(t)dth_j]\sigma_j^z}\Big)\Big(\prod_{j<k}^{N} e^{i[B(t)dtJ_{jk}]\sigma_j^z\sigma_k^z}\Big). \tag{4.1}$$

In RFQA-D, the drive Hamiltonian H_D is a direction oscillating transverse field, which is the summation of $cos\theta(t)\sigma_j^x + sin\theta(t)\sigma_j^y$. In quantum hardware, it's hard to adjust the directions of field in the x-y plane. So we need to take advantage of the conversion of H_D in Eq.(2.25), and decompose the H_D into 3 parts. The decomposition of H_p remains the same. The digitization of RFQA-D can be implemented by using additional Z rotations in the evolution:

$$\begin{aligned} e^{-iH(t)dt} \simeq & \Big(\prod_{j=1}^{N} e^{i[-\frac{\theta_j(t)}{2}]\sigma_j^z}\Big)\Big(\prod_{j=1}^{N} e^{i[A(t)dt]\sigma_j^x}\Big) \\ & \Big(\prod_{j=1}^{N} e^{i[B(t)dth_j+\frac{\theta_j(t)}{2}]\sigma_j^z}\Big)\Big(\prod_{j<k}^{N} e^{i[B(t)dtJ_{jk}]\sigma_j^z\sigma_k^z}\Big). \end{aligned} \tag{4.2}$$

where $\theta_j(t) = \bar{\alpha_i} \sin(2\pi f_i t)$. The time unitary operator during the evolution in 2.33 can be represented as

$$
\begin{aligned}
|\psi(t)\rangle &= e^{-iH(t)dt} e^{-iH(t-dt)dt} \cdots e^{-iH(dt)dt} |\psi(0)\rangle \\
&= e^{-\frac{i}{2}\sum_j \theta_j(t)\sigma_j^z} \left(1 - idt(-\sum_j \sigma_j^x + H_p)\right) e^{\frac{i}{2}\sum_j \theta_j(t)\sigma_j^z} \\
&\quad e^{-\frac{i}{2}\sum_j \theta_j(t-dt)\sigma_j^z} \left(1 - idt(-\sum_j \sigma_j^x + H_p)\right) e^{\frac{i}{2}\sum_j \theta_j(t-dt)\sigma_j^z} \\
&\quad \cdots \\
&\quad e^{-\frac{i}{2}\sum_j \theta_j(dt)\sigma_j^z} \left(1 - idt(-\sum_j \sigma_j^x + H_p)\right) e^{\frac{i}{2}\sum_j \theta_j(dt)\sigma_j^z} |\psi(0)\rangle \\
&= e^{-\frac{i}{2}\sum_j \theta_j(t)\sigma_j^z} \left(1 - idt(-\sum_j \sigma_j^x + H_p)\right) \left(1 + idt\frac{1}{2}\sum_j \partial_t \theta_j(t)\sigma_j^z\right) \\
&\quad \left(1 - idt(-\sum_j \sigma_j^x + H_p)\right) \left(1 + idt\frac{1}{2}\sum_j \partial_t \theta_j(t-dt)\sigma_j^z\right) \cdots |\psi(0)\rangle \\
&\simeq \left(1 - idt(-\sum_j \sigma_j^x + H_p - \frac{1}{2}\sum_j \partial_t \theta_j(t)\sigma_j^z)\right) \\
&\quad \left(1 - idt(-\sum_j \sigma_j^x + H_p - \frac{1}{2}\sum_j \partial_t \theta_j(t-dt)\sigma_j^z)\right) \cdots |\psi(0)\rangle \,.
\end{aligned}
\tag{4.3}
$$

It is clear from the Equation 4.3 that the layers in RFQA-D can be combined by merging the extra Z rotation angle $-\frac{1}{2}\sum_j \partial_t \theta_j(t)$ into any single qubit rotations.

Below is an example of one time sequence evolution for RFQA-D in Figure 4.1, which begins with a two-qubit ZZ rotation, then a single Z rotation, then a single X rotation. The realistic implementation is comparable with a uniform field QA since RFQA-D does not increase the gate depth. The exact application of the gates, of course, depends on the problem model. We repeat such a sequence many times until reach the total evolution time.

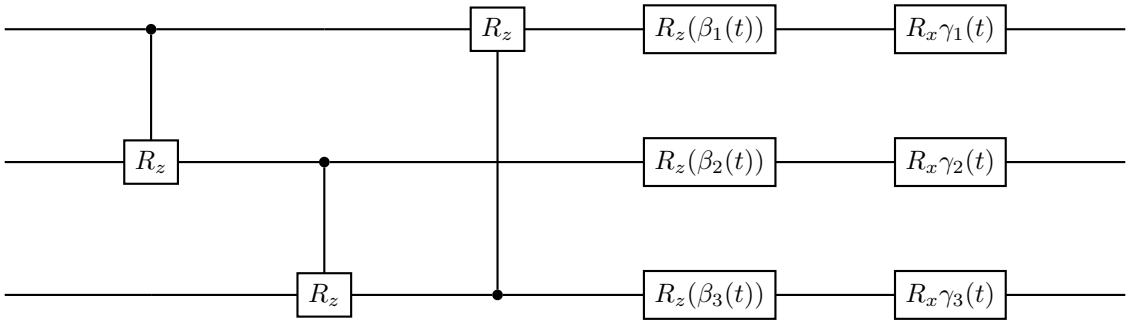

Figure 4.1 Gate sequence in evolution time t of RFQA-D. The final layer of Z rotations in this sequence is merged into the first layer of Z rotation in the next sequence.

In the iterating evolution of RFQA-D, we can merge the final layer of Z rotations at the left side of Eqs.4.2 for time t into the first layer of Z rotations for time $t + dt$ in the next step. So that incorporating

RFQA-D only needs one layer of Z terms. The gate model version of the promising RFQA method can be implemented on any digital quantum computer.

The choice of time step dt in the digitization process is important. As we increase the time step dt to a critical value, the success probability will start to drop off quickly as a result of the increasing trotter error. The errors in the quantum circuit model involves not only non-adiabatic errors, but also trotterization errors and gate errors. A larger dt leads to larger trotterization errors but can decrease the gate numbers and thus the gate errors. In near term quantum computers, error correction will introduce abundant ancilla qubits. However, the quantum computation power is still circumvented by gate errors. To simulate as large system as possible, we need to circumvent the time step dt and find a balance between the trotterization error and gate error. In the simulation, we use the largest dt that gives decent result to investigate the TTS scaling, the largest dt can ensure the trotterization error is not crucial in the simulation. For example, in the modified shamrock model that we will introduce in the following sections, we make a scrutiny of the success probability over a range of time step dt. As shown in Figure 4.2, in the problem set $\{h_0 = 0.25, A = 0.35\}$, the largest dt that gives quantitatively accurate results is 0.08. A time step beyond 0.08 could provide a qualitatively correct scaling of the problem, however, a quantitative prediction is more desirable to provide better guidance in the experimental implementation.

We notice that a fixed and reasonably large timestep dt that doesn't decrease with system size is able to give reliable results in RFQA methods, which suggests that RFQA could be a viable digital quantum algorithm as well.

4.5 Reverse annealing

In the implementation of digitized-QA, we not only evolved the system with forward annealing, but also investigated the behavior in reverse annealing to prove the speedup of RFQA is from the acceleration of multi-qubit tunneling. The quantum speedup from RFQA in forward annealing in some cases might be a result of circumventing the first order transition of the hard problem, where the system doesn't get trapped by the local minimum and thus doesn't have to flip many spins to reach a global minimum. If that were a generic thing it would actually be very powerful. In reverse annealing, we intentionally prepare the system in the local minimum state, which has a large hamming distance with the global minimum state, to make the problem hard. Although the hardness in reverse annealing does not necessarily generalize to more complex, real-world problems, the scaling advantage of RFQA reveals the quantum speedup comes from the multi-qubit tunneling acceleration.

As the pausing during annealling provides more powerful QA[38], we implement a reverse annealing schedule as shown in Figure 4.3. The annealing parameter $s(t)$ starts from 1 and decrease to a critical

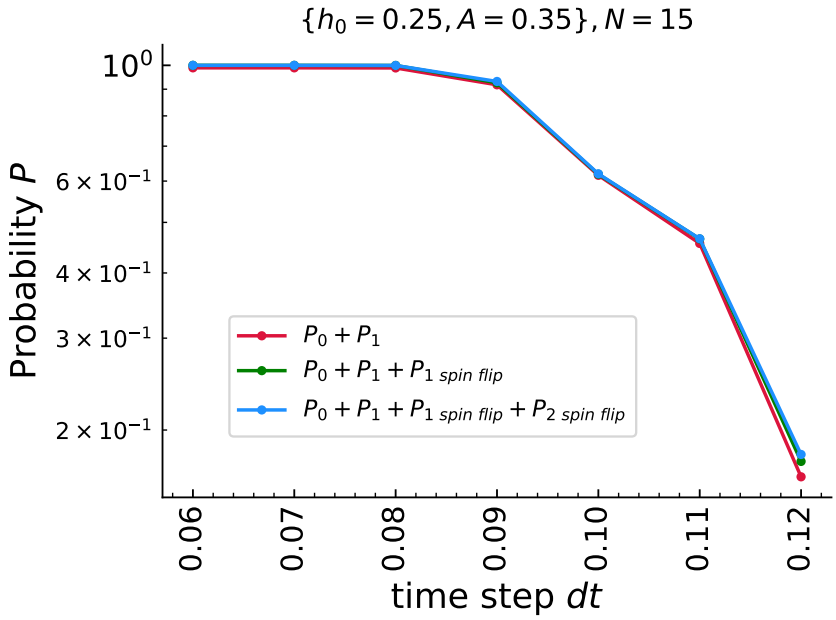

Figure 4.2 The probability P is the probability of remaining in the ground state manifold of the modified shamrock model, the probability is numerically simulated with the standard uniform field QA. The problem set here is $\{h_0 = 0.25, A = 0.35\}$ with the system size $N = 15$. The red circle line represents the success probability of finding the two competing ferromagnetic ground states, the green one represents the two ferromagnetic ground states and states that are one flip away from the two competing ground states, the blue one represents the two ferromagnetic ground states and states that are one and two spin flips away from them. The largest dt that gives descent result in this model is 0.08, dt that are larger than 0.08 can give a similar qualitative results but not quantitatively accurate.

value s^*, which is the adjacency of the transition. We then pause the annealing schedule for a relatively long time and then apply forward annealing to increase $s(t)$ to 1.

4.6 Problem models

In a combinatorial optimization problem where the local minimum and global minimum are separated by small Hamming distance, a few spin flips can steer the system to the global minimum easily. However, in a problem with entropic barrier[121, 138, 217], the false ground state and true ground state are separated by many metastable higher order excited states, which leads to the system always getting stuck in the metastable states. In the case of an energetic barrier[199], two competing ground states are separated by large Hamming distance that requires extensive energy to overcome. Both the entropic barrier and energetic barrier can lead to first order transitions, which is the bottleneck of quantum annealing and QAOA, that comes with exponentially small gaps.

We believe RFQA is capable of accelerating multiqubit tunneling in both cases, but it is hard to design hard problems with entropic barriers in small-N problems with few-body interactions. Thus, we propose a

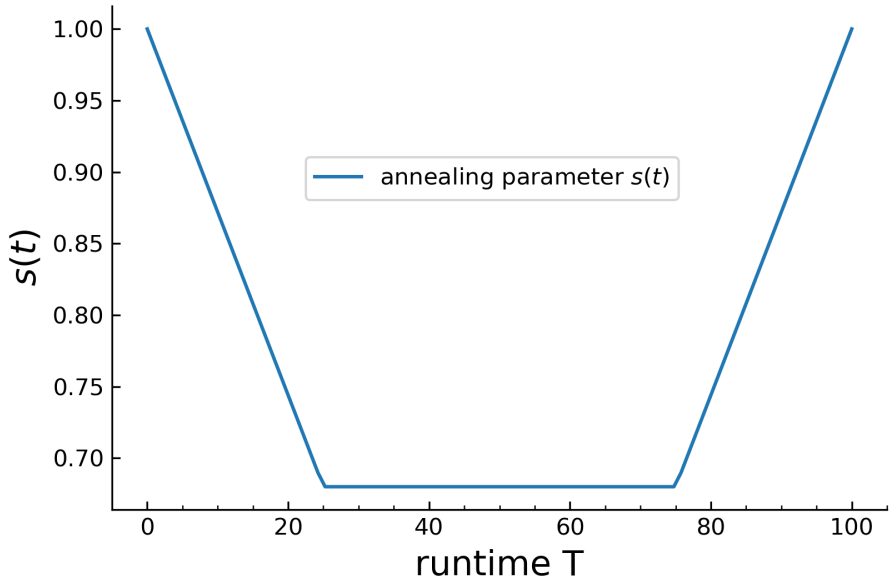

Figure 4.3 reverse annealing schedule, an example of the reverse annealing schedule we apply into the problem models, the annealing schedule reversely anneal to a critical value s^* at $\frac{T}{4}$ runtime. Then pause the annealing process from $\frac{T}{4}$ to $\frac{3T}{4}$. After the pausing, apply the forward annealing schedule to final time T.

series of benchmark problems that steer the system toward a false minimum, and require $\mathcal{O}(N)$-spin tunneling to reach the true minimum.

4.6.1 Modified shamrock model

In the original work of the shamrock model[140], used to compare the quantum scaling of QA and QMC, there are two competing ferromagnetic ground states. One "center" spin ferromagnetically is coupled to many frustrated 2-spin "petals". The couplings between each pair of petal spins are anti-ferromagnetic couplings. The topological frustration in this model generates exponential tunneling paths between two ground states, and thus the incoherent tunneling in QA shows exponential advantage over QMC.

Since there is only one central spin ferromagnetically connected to the petal spins, the energy to flip that central spin from either two competing ground states will be $\sim 2(N-1)$. This extensive energy cost will cause larger trotter error. To avoid this problem, we came up with a modified shamrock model.

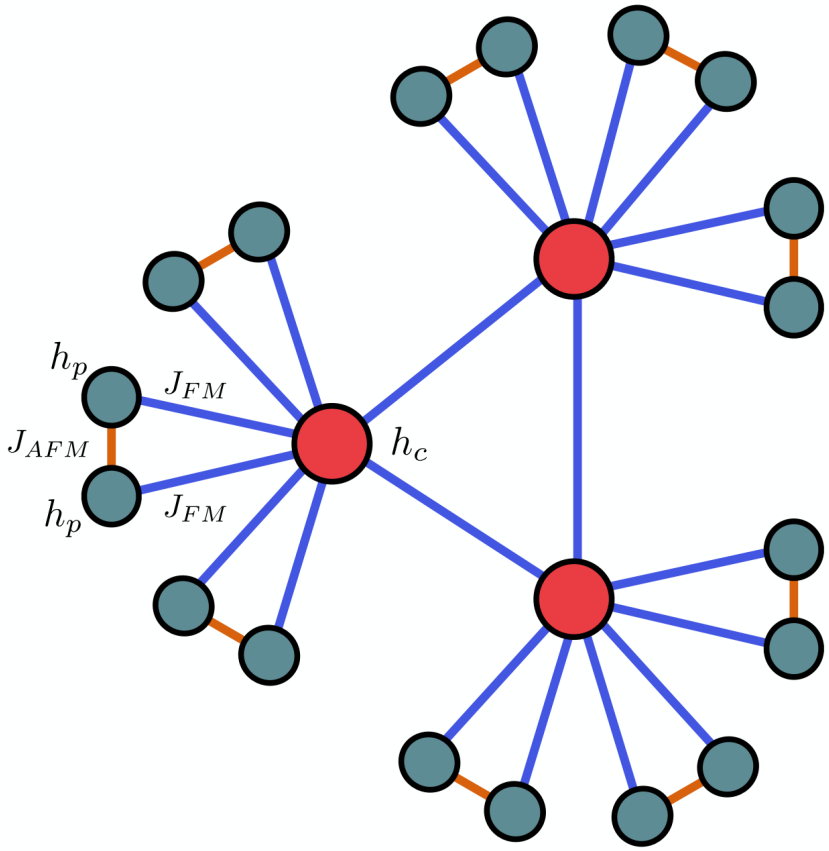

Figure 4.4 In the variation of the shamrock model [140], we extend one central spin to many ferromagnetically connected central spins(marked with red circles) to avoid an extensive energy cost caused by a single error in that central qubit. The modified shamrock model is composed of K central spins, and each central spin is ferromagnetically coupled to the M petals (petal spins are marked with green circles). The ferromagnetic coupling is defined as $J_{FM} = -1$, the antiferromagnetic coupling is defined as $J_{AFM} = 0.8$. We make the original shamrock problem hard by adding local z bias fields $h_p = -h_0/M$ to petal spins, and opposite stronger fields $h_c = h_0(1 - A)$ on the central spins which steer the system to the false minimum.

As shown in Figure 4.4, in the modified shamrock model, there are K central spins that are ferromagnetically coupled to each other, and they ferromagnetically coupled to M petals, where the petal spins are antiferromagnetically coupled. We make this problem hard by adding a local z bias field $h_0(1 - A)$ (for $0 < A < 1$) to each center spin, and an opposite local field $-\frac{h_0}{2M}$to the M petal spins. This leads to an energy difference between the two competing ferromagnetic ground states. The true minimum (all spins up state) aligns along the direction of the local fields in the petal, but much stronger local fields on the center spins steer the system toward the false minimum (all spins down state), making problem exponentially difficult to solve for both classical and quantum algorithms. The energy difference of the two competing ground states in the new model is $2KAh_0$, which indicates we can generate tunable hard

problems with the parameters A and h_0. The new formulation of the modified shamrock model preserves the basic hardness mechanism of the original shamrock model,

$$H_p = J_{FM} \sum_{<C,j>} \sigma_C^z \sigma_j^z + J_{AFM} \sum_{<j,k>} \sigma_j^z \sigma_k^z - \frac{h_0}{2M} \sum_j \sigma_j^z + h_0(1-A) \sum_C \sigma_C^z, \tag{4.4}$$

where σ_C is the C-th Central spin, the σ_j represents petal spins. The number of petals connected with each central spin M is set to 1 throughout. We study the modified shamrock model with RFQA methods to show that an oscillating transverse field can outperform the uniform transverse field in the quantum gate model.

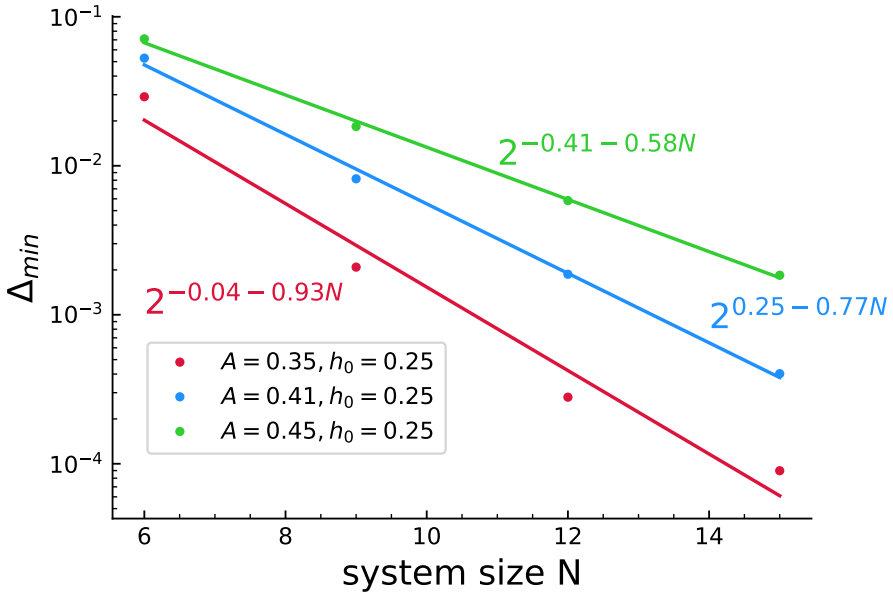

Figure 4.5 Numerical values of the minimum gap for 3 problem sets: $\{h_0 = 0.25, A = 0.35, 0.41, 0.45\}$ in the standard quantum annealing method, with the system size N ranging from 6 to 15 spins. The markers are data of numerically estimated minimum gap energies, least squares fits of the minimum gap are red, blue and green solid lines. The minimum gaps in the 3 problem sets all decrease exponentially with increasing system size.

In the case of standard QA/AQC, all N spins must simultaneously flip to reach the true ground state after the system freezes in the false minimum. By tuning the values of A, we make 3 problem sets with different exponential difficulty scaling levels, with fixed $h_0 = 0.25$, the sets $\{A = 0.35, 41, 45\}$ generate a problem set with descending hardness. As shown in Figure 4.5, the minimum gap in the 3 problems are decreasing exponentially with the system size, the runtime therefore increases exponentially with N. We also explore the behavior of standard uniform field QA and RFQA with several different frequency scaling choices such that high frequency set $\{0.1/\sqrt{N}, 0.2/\sqrt{N}\}$; lower frequency set $\{0.3/N, 0.6/N\}$ and lowest

frequency set $\{0.5/N^{1.5}, 1/N^{1.5}\}$. In both forward and reverse annealing, the time-to-solution (TTS) for finding true ground state with RFQA and standard quantum annealing for the low frequency set are shown in Figure 4.6. The runtime T is polynomially increasing with the system size N. RFQA shows stark scaling advantage (maybe exponential speedup) over standard uniform field QA. Other frequency sets show similar behavior to this. We list the data of other frequency sets in Appendix.

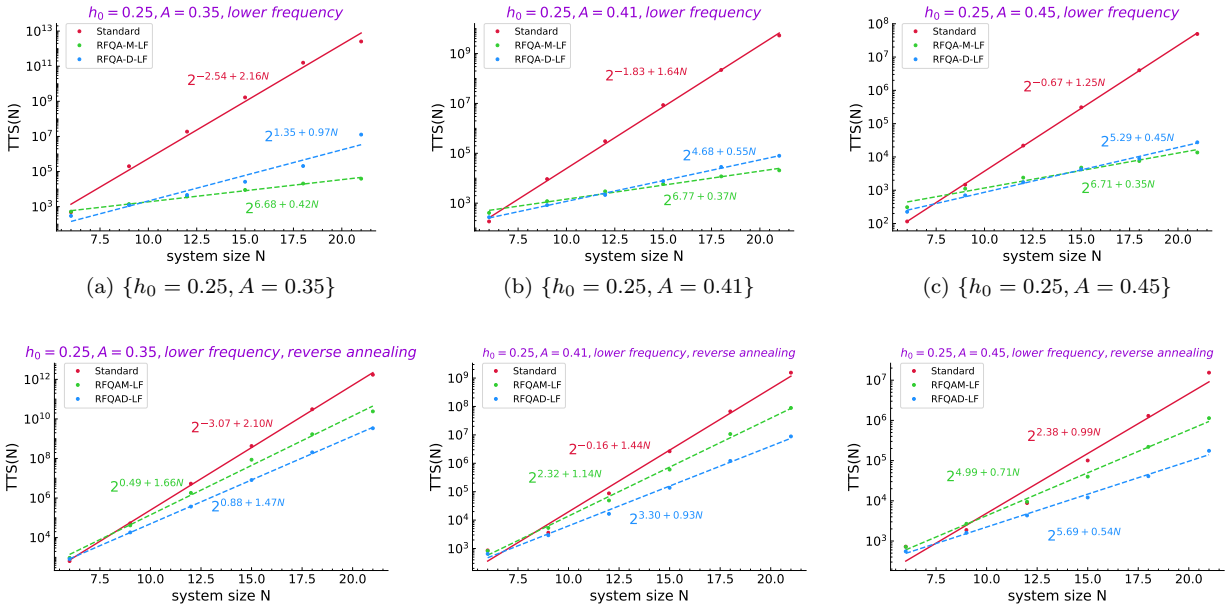

(a) $\{h_0 = 0.25, A = 0.35\}$ (b) $\{h_0 = 0.25, A = 0.41\}$ (c) $\{h_0 = 0.25, A = 0.45\}$

(d) $\{h_0 = 0.25, A = 0.35\}$ (e) $\{h_0 = 0.25, A = 0.41\}$ (f) $\{h_0 = 0.25, A = 0.45\}$

Figure 4.6 Forward and reverse annealing results: (a)(b)(c) are forward annealing results, (d)(e)(f) are reverse annealing results. Time to find the true ground state in 3 different difficulty problem sets: $\{h_0 = 0.25, A = 0.35, 0.41, 0.45\}$ with lower frequencies f_i chosen from $\{0.3/N, 0.6/N\}$ using RFQA, computed from the final success probability for a run-time polynomially increasing with N. Data for RFQA-M and RFQA-D are given by green, blue markers, respectively. Red dots are data of the standard quantum annealing method for comparison purpose. The solid red line is the best-fit curve of the standard quantum annealing method for comparison. Other dashed lines are best-fit curves for RFQA. Both RFQA-M and RFQA-D in forward and reverse annealing show obvious quantum speed up against the standard quantum annealing method. The problem sets with different frequency ranges show similar behavior.

We list the simulation results with different frequencies range in both forward annealing and reverse annealing in Table 4.1,Table 4.2 and Table 4.3. From high frequency to low frequency, the scaling of RFQA beats the standard uniform field QA in all cases.

4.6.2 Square grid model

In the "tile-planting" square grid model outlined in [218, 219], different frustrated subproblem types and rotations to each plaque can result in frustrated problems with many local minima. The model

Table 4.1 Summary of the scaling exponents for different frequencies range. Fitting the time to solution $TTS(N)$ of each method to $2^{\beta+\gamma N}$, the table lists the exponential scaling coefficient "γ" value for forward annealing in the modified shamrock problem, with high frequencies f_i chosen from $\{0.1/\sqrt{N}, 0.2/\sqrt{N}\}$. "*standard*" represents the uniform field QA. The subscript "f" and "r" represents forward and reverse annealing. The "S", "M", "D" represents the digitized standard uniform QA, digitized RFQA-M and digitized RFQA-D respectively.

Problem set	$1/\Delta^2_{min}$	S_r	M_r	D_r	S_f	M_f	D_f
A=0.35,h_0=0.25	1.86	2.10	1.67	1.46	2.16	0.50	0.55
A=0.41,h_0=0.25	1.54	1.44	1.14	0.93	1.64	0.49	0.40
A=0.45,h_0=0.25	1.16	0.99	0.77	0.57	1.25	0.48	0.33

Table 4.2 Summary of the scaling exponents for different frequencies range. Fitting the time to solution $TTS(N)$ of each method to $2^{\beta+\gamma N}$, the table lists the exponential scaling coefficient "γ" value for forward annealing in the modified shamrock problem, with low frequencies f_i chosen from $\{0.3/N, 0.6/N\}$.The subscript "f" and "r" represents forward and reverse annealing. The "S", "M", "D" represents the digitized standard uniform QA, digitized RFQA-M and digitized RFQA-D respectively.

Problem set	$1/\Delta^2_{min}$	S_r	M_r	D_r	S_f	M_f	D_f
A=0.35,h_0=0.25	1.86	2.10	1.66	1.47	2.16	0.42	0.97
A=0.41,h_0=0.25	1.54	1.44	1.14	0.93	1.64	0.37	0.55
A=0.45,h_0=0.25	1.16	0.99	0.71	0.54	1.25	0.35	0.45

Table 4.3 Summary of the scaling exponents for different frequencies range. Fitting the time to solution $TTS(N)$ of each method to $2^{\beta+\gamma N}$, the table lists the exponential scaling coefficient "γ" value for forward annealing in the modified shamrock problem, with lowest frequencies f_i chosen from $\{0.5/N^{1.5}, 1/N^{1.5}\}$. The subscript "$f$" and "$r$" represents forward and reverse annealing. The "S", "M", "D" represents the digitized standard uniform QA, digitized RFQA-M and digitized RFQA-D respectively.

Problem set	$1/\Delta^2_{min}$	S_r	M_r	D_r	S_f	M_f	D_f
A=0.35,h_0=0.25	1.86	2.10	1.94	1.95	2.16	0.58	1.37
A=0.41,h_0=0.25	1.54	1.44	1.13	1.29	1.64	0.46	1.32
A=0.45,h_0=0.25	1.16	0.99	0.70	0.78	1.25	0.37	1.02

provides a way to generate tunable hard optimization problems for benchmarking purposes. A square grid is composed of many edge-disjoint vertex-sharing subgraphs, where the subproblems share a common ground state, and this ground state is known a priori. We explored the "tile-planting" square grid problems with many local minima, however, these studies produced problems that are not exponentially hard to solve, so we did not consider them for benchmarking.

To make problems that are native to near term quantum computers, we reformulate the modified shamrock model for the square lattice, with the layout of the problem shown in Figure 4.7. The embedding of a square lattice is easier to study on near term quantum computers, and the asymmetric bias fields applied in the modified shamrock problem generates exponentially difficulty problems that are intractable for both classical and quantum algorithms.

The integration of the exponentially difficulty modified shamrock problem and "tile planting" methods compose hard optimization problems that are implemented in the square-grid chip. In this square-lattice modified shamrock problem, central spins are ferromagnetically coupled to each other, 3 ferromagnetically or antiferromagnetically coupled spins form one petal that connect with one central spin, the 3 petal spins and 1 central spin compose a subproblem in a square grid. Numerical simulations in the hard problem set $\{h_0 = 0.25, A = 0.25\}$ with random frequencies chosen from $\{\frac{0.1}{\sqrt{N}}, \frac{0.2}{\sqrt{N}}\}$, shown in Figure 4.8, demonstrate the exponential difficulty of the problem for standard QA, and a clear advantage for RFQA methods in Figure 4.9. In both forward and reverse annealing, RFQA is able to provide enhanced performance over standard uniform field QA. We have simulated up to a 4*4 square grid, in our future work, we will extend variants of this problem to a 5*5 square-lattice, that can maximally make use of the testbed chip (see chapter 5).

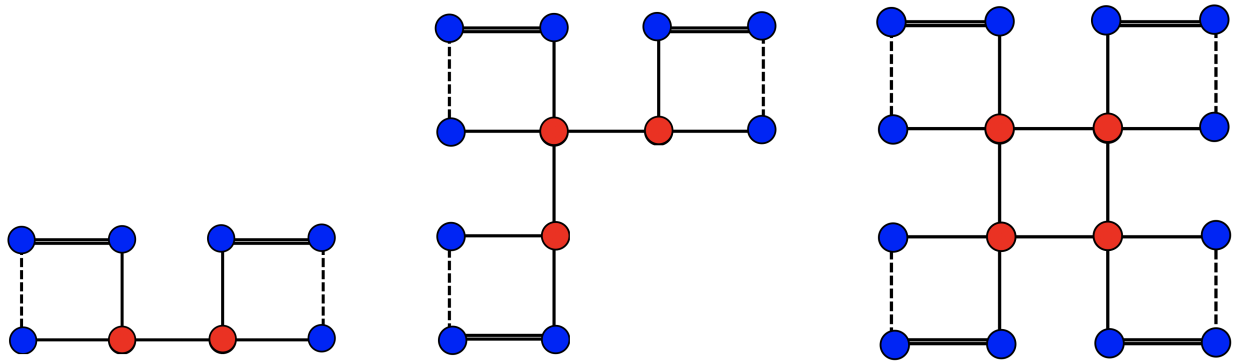

(a) $N = 8$ (b) $N = 12$ (c) $N = 16$

Figure 4.7 The three plots shows the layout of 8, 12 and 16 spin square-lattice shamrock problem. In each plot, central spins(marked with red circles) are ferromagnetically coupled, and connected with other 3 petal spins(marked with blue circles). 3 petal spins and one central spin form a subproblem, in each subproblem, one coupling is FM coupling (thin lines), one is a weaker AFM coupling (dashed lines) and one is a stronger FM coupling (thick lines). This variation of the modified shamrock model not only preserves the hardness of the modified shamrock model, but also can be mapped into a square lattices.

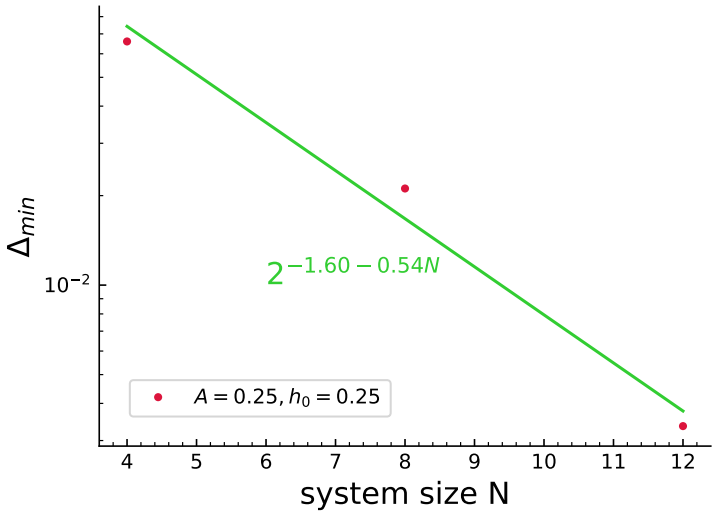

Figure 4.8 Numerical values of the minimum gap for a problem set: $\{h_0 = 0.25, A = 0.25\}$ in the standard quantum annealing method, with the system size N ranging from 4 to 12 spins. The red markers are data of numerically estimated minimum gap energies, least squares fit of the minimum gap is green solid line. The minimum gap in this problem set decreases exponentially with increasing system size.

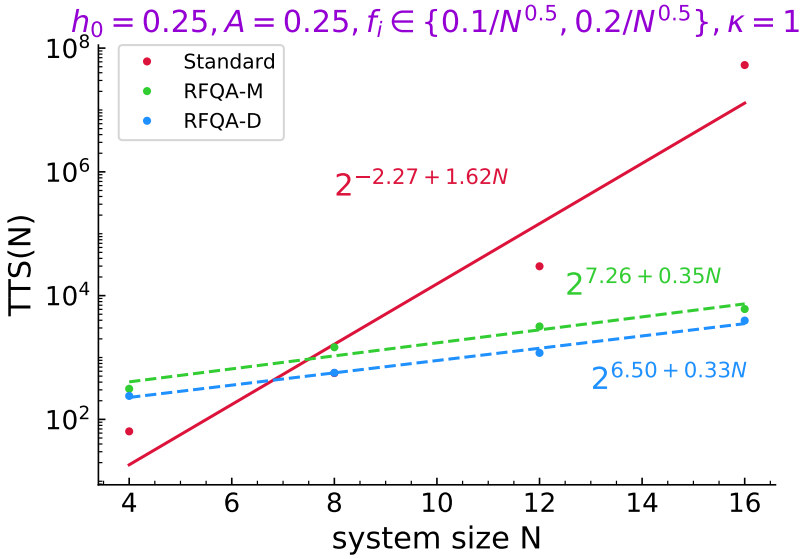

(a) TTS in forward annealing

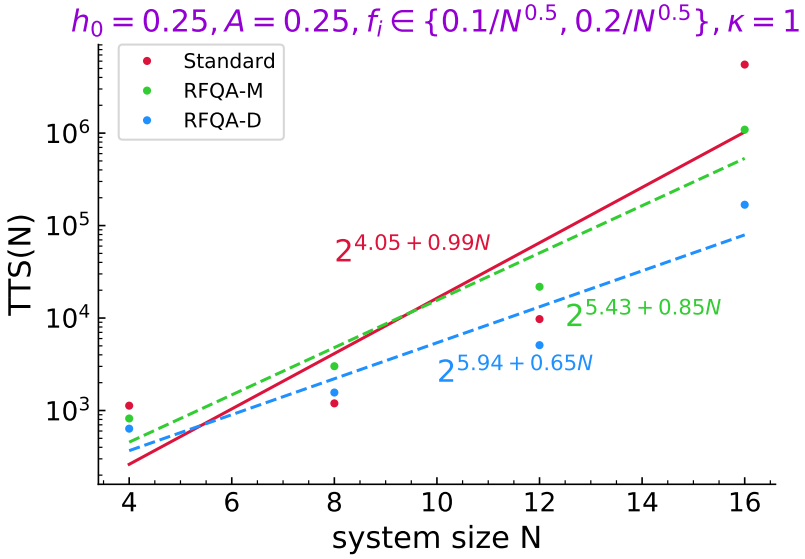

(b) TTS in reverse annealing

Figure 4.9 Time to find the true ground state in the problem set: $\{h_0 = 0.25, A = 0.25\}$ using the RFQA method with forward annealing and reverse annealing, computed from the final success probability for a run-time polynomially increasing with N. Data of the RFQA-M RFQA-D methods are given green and blue markers separately. Red dots are data of the standard quantum annealing method, the solid red line is the best-fit curve of the standard quantum annealing method for comparison purpose. Other dashed lines are best-fit curves of the RFQA methods. RFQA methods reduces the TTS in standard uniform field QA in both forward and reverse annealing.

CHAPTER 5

TFIM AND EXPERIMENTAL REALIZATION

The work in this chapter is in preparation for an experiment.

Most realistic problems are not native to a real quantum annealer, some logical problems can have arbitrary connectivity but the quantum quantum annealer does not. Generally, it's not possible to have a quantum device with native all to all connectivity at arbitrarily large N. Minor embedding is therefore needed to map a combinatorial optimization problem to the QPU hardware topology. However, minor embedding is often a challenge in experimental implementations [220–227]. There are no odd loops in the Chimera architecture and single logical variables have to be represented by many qubits. For example, in the D-Wave quantum annealer, a single variable is often encoded as a ferromagnetic chain of physical qubits because the Chimera topology is not fully connected. The algorithm to implement minor embedding in D-Wave QPUs is the known as the Cai-Macready-Roy or heuristic minor-embedding algorithm [228]. To ensure a chain of qubits returns the same value in the annealing process, the coupling between all qubits in the chain is set to be stronger than the coupling with other qubits. However, the strongly coupled chains are likely to freeze in the ferromagnetic states during the annealing, which requires a K-spin tunneling event to reach the global minimum, K here is the length of the chain. The K-spin tunneling rate exponentially decreases with chain length. Thus, the freezing of the chains slows down the tunneling rate to a great extend, especially in highly connected problems. Weaker couplings can mitigate the freezing problem, but it is easily broken by noise and control errors. The two coupled qubits might not return identical values due to a broken link in the chain, which scrambles the logical representation of the true ground state.

The process of solving a QUBO with QA is shown in Figure 5.1 and the minor embedding on a Chimera graph and a Pegasus graph is shown in Figure 5.2. Figures are reproduced from Zbinden et.al. [224]. Besides the heuristic minor-embedding algorithm, other advanced embedding algorithms such as clique minor embedding achieve success by providing smarter ways of embedding [221, 229–231]. Furthermore, due to the much higher connectivity in the Pegasus topology (the degree or number of qubits connected to any one qubit, in the Pegasus graph is 15), the chain length in minor embedding can be reduced and provides more stable dynamic behavior in the simulation. However, it may take $\mathcal{O}(N^2)$ qubits to embed an N variable problem for an arbitrarily connected graph. This can result in severe penalties, such as exponentially reducing the success probability.

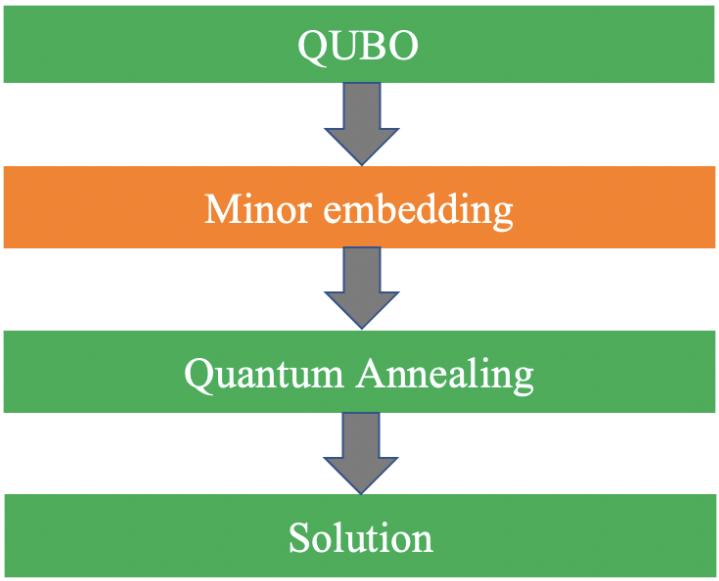

Figure 5.1 Solving an arbitrary QUBO with real QA hardware requires minor embedding to map the problem to the QPU.

The well studied 1D chain Transnsverse Field Ising Model(1D TFIM) is of great interest to us, not only because our simulations of RFQA in TFIM suggest that the impact of minor embedding problems can be reduced to some degree, but also because the simplicity of this model makes it easy to implement on existing QA hardware. The other aforementioned models require AFM coupling that is nearly equal in strength to the FM coupling, which has not yet been realized (but the AFM coupling calibration is now under construction; once the AFM coupling is viable, we can explore variations of the shamrock model on these devices). The TFIM model only requires FM couplings between qubits, we investigate whether RFQA can accelerate the tunneling between the two ferromagnetic state in TFIM. In this chapter, we show that RFQA does exhibit stark scaling advantage in TFIM, and we expect the experimental implementation of RFQA in TFIM to be carried out soon.

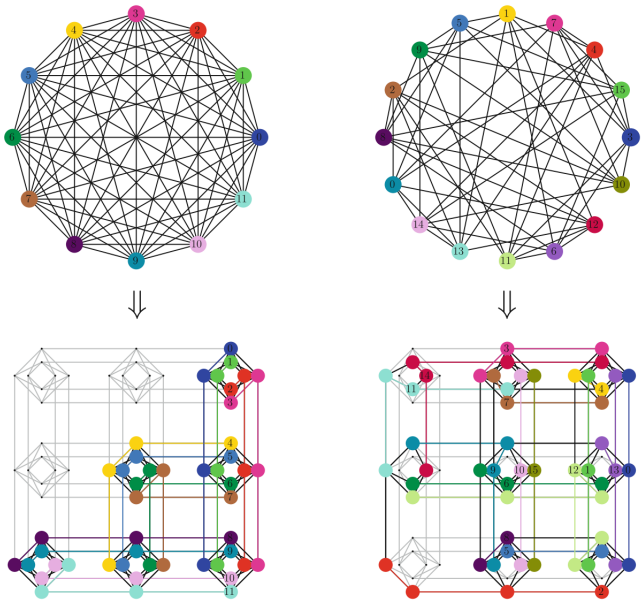

(a) (left) Mapping a clique K_{12} onto the Chimera graph C_3 with Clique minor embedding. (right) Embedding a 16-node, 7-regular graph to C_3 with heuristic minor embedding.

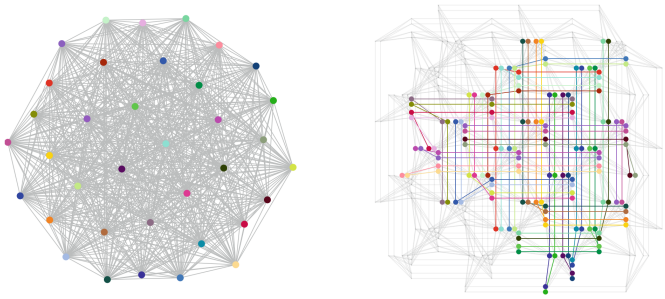

(b) Minor embedding of a K_{36} on a Pegasus $P4$ graph.

Figure 5.2 Figures from [224].

To support these future experiments on TFIM, we explore this problem with RFQA and use a small enough time step dt that could provide a credible prediction of the continuous time behavior in the gate model based simulation. We prepare the initial state as one ferromagnetic state and measure the success probability of reaching the other ferromagnetic state. The reverse annealing schedule is applied in this model, and we pause the anneal between times $\frac{T}{6}$ and $\frac{5T}{6}$.

In the formulation of TFIM, $H_p = -J\left(\sum_i \sigma_i^z \sigma_{i+1}^z + \kappa \sum_i \sigma_i^x\right)$, we use κ to denote the transverse field strength. A phase transition to the paramagnetic state happens at $\kappa = 1$. In our simulation, the overall transverse field strength is controlled by the reverse annealing parameter $s(t)$ and a prefactor "δ." In the reverse annealing, the overall transverse field will be ramped up to a critical value κ from time $\frac{T}{6}$ to $\frac{5T}{6}$, then ramped down to 0. The total runtime increases polynomially with system size. The annealing

parameter $s(t)$ ramps the transverse field with the prefactor "δ" that determines the overall transverse field in the anneal process, while the strength of the problem Hamiltonian is 1 throughout the anneal. The prefactor "δ" is only applied to one spin to reduce the strength of the transverse field on that spin. "δ" reduces the minimum gap without changing scaling, it helps to make small N scaling easier to estimate. The standard uniform field QA with reverse annealing in the TFIM can be formulated as

$$H = -\sum_{<i,j>} \sigma_i^z \sigma_j^z - s(t)\delta \sum_i \sigma_i^x. \tag{5.1}$$

We apply random, static disorder and sweep over a uniform Z bias during the anneal. The disorder can avoid the unwanted constructive interference effects in problems with exponentially small tunneling rates. Also, it resembles some type of noise and control errors in real world settings, giving us a reliable prediction of the experimental behavior. Nevertheless, the disorder is not able to simulate the interaction with cold bath, which is too hard to simulate so we ignore it here. The random static Z bias disorder splits the ground state energies in TFIM and leads to an energy difference between the two ferromagnetic ground states. We average over different fixed energy differences between the ferromagnetic states over 3000 trials. We tune the strength of the transverse field κ value (below 1) to form a problem set with different difficulty scaling. The parameters involved in this problem will be optimized to produce a significant quantum speedup from RFQA. The magnitude of the disorder is $\frac{1}{2\sqrt{N}}$, with the overall fixed energy difference between the two ferromagnetic ground states as 0.25, and a small dt that matches the continuous time simulation here is 0.02. The prefactor "δ" that controls the transverse field strength is chosen as 0.2, which gives a reliable behavior of uniform field QA that tracks the scaling of the inverse square gap.

In the standard application of RFQA that applies random frequencies to each site, we show that RFQA significantly enhances the tunneling rate between two ferromagnetic ground states in Figure 5.3. The TTS scaling advantage in RFQA for a small transverse field in the four problem sets is

$$\gamma_{QA} - \gamma_{RFQA} \simeq 0.4, \tag{5.2}$$

where γ is the scaling exponent. With even higher transverse field $\kappa = 0.85, 0.875, 0.9$, as shown in Figure 5.4, whether the scaling advantage of RFQA is exponential or polynomial is difficult to determine. This suggests that RFQA can dramatically outperform the uniform transverse field QA, and even has the possibility to provide an exponential speedup!

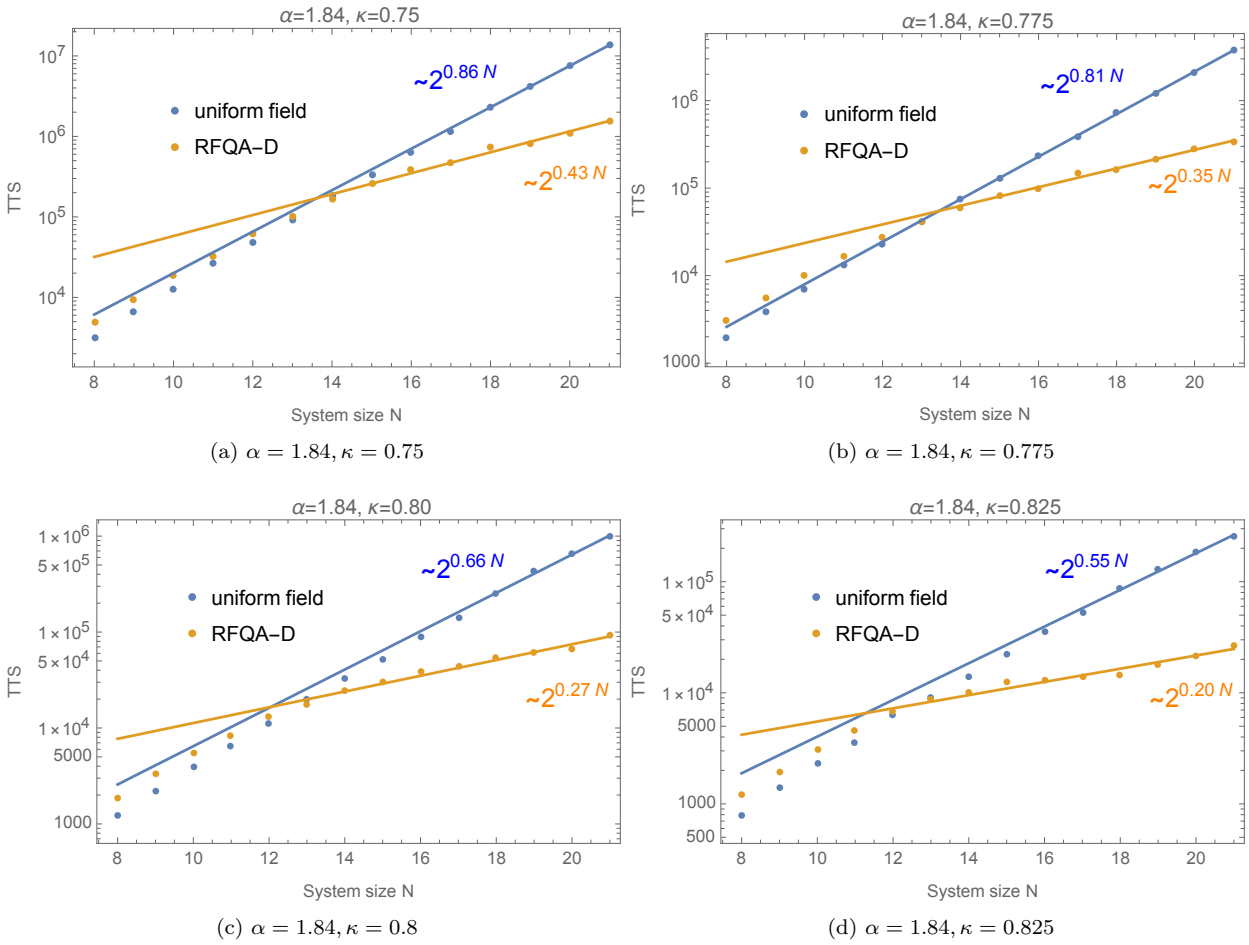

(a) $\alpha = 1.84, \kappa = 0.75$

(b) $\alpha = 1.84, \kappa = 0.775$

(c) $\alpha = 1.84, \kappa = 0.8$

(d) $\alpha = 1.84, \kappa = 0.825$

Figure 5.3 Time to find the true ground state in four different difficulty problems of TFIM:$\{\alpha = 1.84, \kappa = 0.75, 0.775, 0.8, 0.825\}$ with frequencies f_i chosen from $\{\frac{1}{3\sqrt{N}}, \frac{2}{3\sqrt{N}}\}$ using RFQA and reverse annealing, computed from the final success probability for a run-time that polynomially increases with N. The system size N ranges from 8 to 21. Data for RFQA-D is given by orange markers. Blue dots are data for the standard quantum annealing method for comparison purposes. The solid blue and orange lines are the best-fit curves of the standard quantum annealing method and RFQA-D, respectively. RFQA-D shows obvious quantum speed up against the standard quantum annealing method in the reverse annealing case.

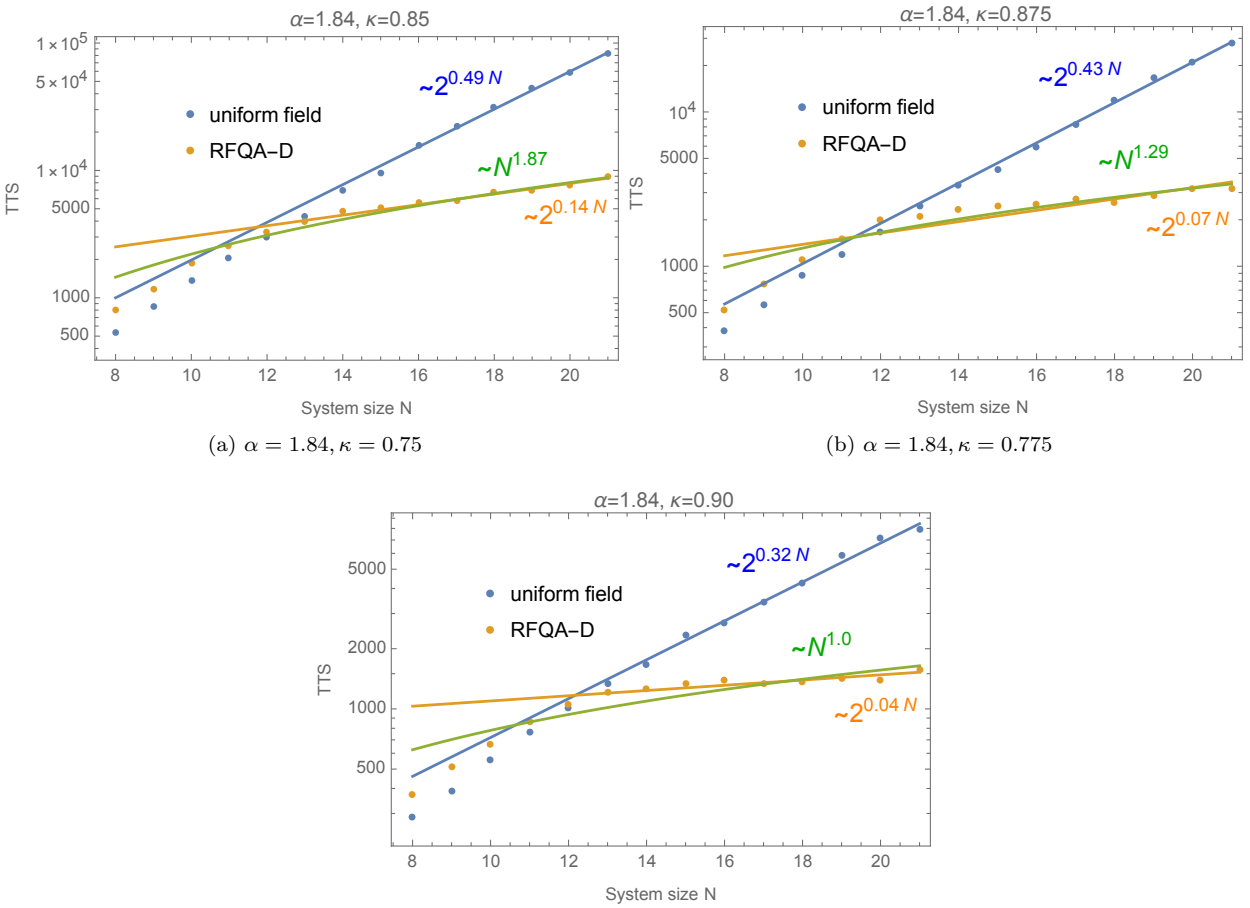

(a) $\alpha = 1.84, \kappa = 0.75$

(b) $\alpha = 1.84, \kappa = 0.775$

(c) $\alpha = 1.84, \kappa = 0.825$

Figure 5.4 Time to find the true ground state of TFIM with a larger transverse field:$\{\alpha = 1.84, \kappa = 0.85, 0.875, 0.9\}$ with frequencies f_i chosen from $\{\frac{1}{3\sqrt{N}}, \frac{2}{3\sqrt{N}}\}$ using RFQA and reverse annealing, computed from the final success probability for a run-time polynomially increasing with N. The system size N ranges from 8 to 21. Data for RFQA-D is given by orange markers. Blue dots are data for the standard quantum annealing method for comparison purposes. The solid blue and orange lines are the best-fit curves of the standard quantum annealing method and RFQA-D, respectively. RFQA-D shows an obvious quantum speed up over the standard quantum annealing method in the reverse annealing case.

To further enhance the performance of RFQA, we pair the frequencies of the system to "$AABBCC\cdots$" type rather than apply frequencies to each site randomly, and we investigated different values of the magnitude of the oscillating field α in RFQA. The performance of RFQA-D with pair frequencies and a larger oscillating magnitude $\alpha = 2.6$ is largely improved, as shown in Figure 5.5 and Figure 5.6. With the same magnitude of the oscillating field, pair frequencies in RFQA improves the behavior to a large extent, which suggests that tuning the oscillating fields of RFQA based on knowledge of the problem graph can be very helpful. Based on the pairing frequencies, a stronger oscillating field further improves the performance of RFQA.

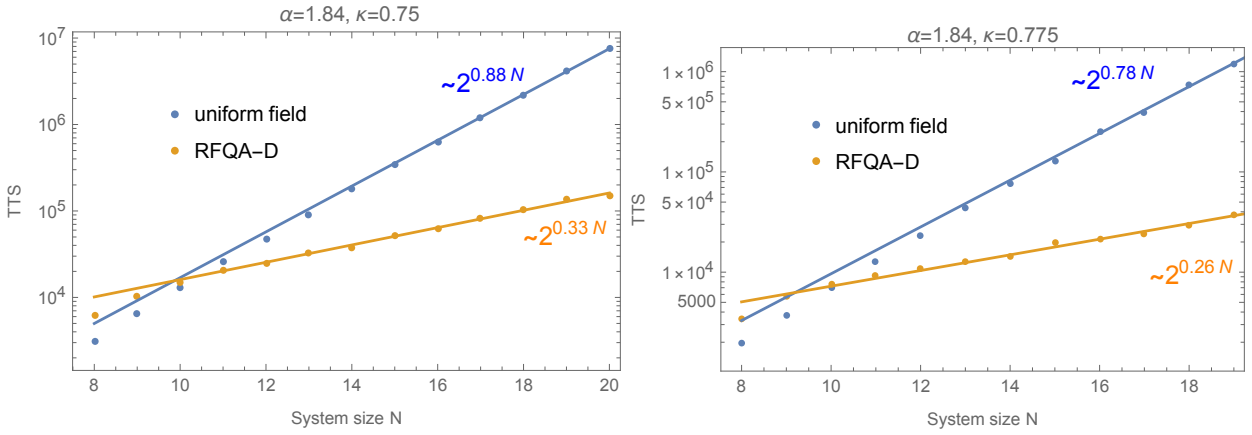

(a) $\alpha = 1.84, \kappa = 0.75$

(b) $\alpha = 1.84, \kappa = 0.775$

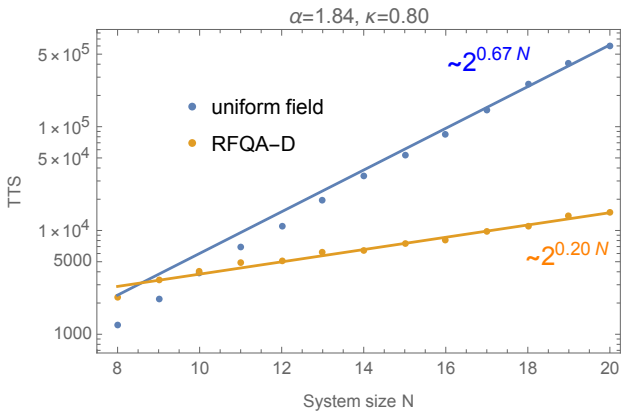

(c) $\alpha = 1.84, \kappa = 0.8$

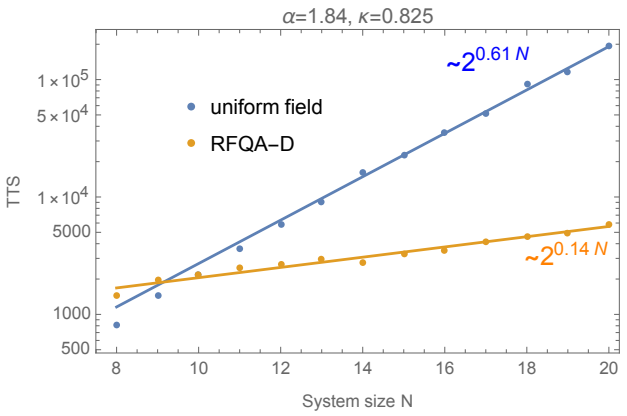

(d) $\alpha = 1.84, \kappa = 0.825$

Figure 5.5 The TTS in the Transverse Field Ising Model, the performance of RFQA-D over the uniform field QA is stark. Time to find the true ground state in four different difficulty problems of TFIM:$\{\alpha = 2.6, \kappa = 0.75, 0.775, 0.8, 0.825\}$ with frequencies f_i chosen from $\{\frac{1}{3\sqrt{N}}, \frac{2}{3\sqrt{N}}\}$ using RFQA and reverse annealing, computed from the final success probability for a run-time polynomially increasing with N. The frequencies are paired as "$AABBCC\cdots$" type instead of random frequencies on each site. Data for RFQA-D is given by orange markers. Blue dots are data for the standard quantum annealing method for comparison purposes. The solid blue and orange lines are the best-fit curves of the standard quantum annealing method and RFQA-D, respectively. RFQA-D shows an obvious quantum speed up over the standard quantum annealing method in the reverse annealing case.

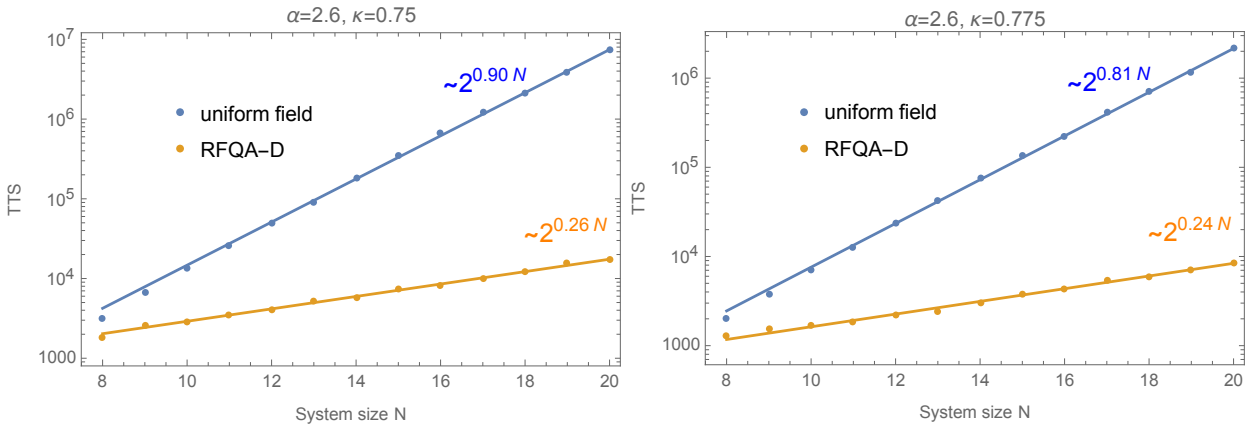

(a) $\alpha = 2.6, \kappa = 0.75$

(b) $\alpha = 2.6, \kappa = 0.775$

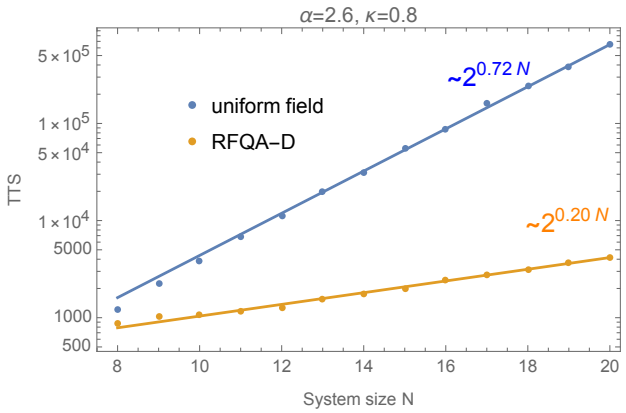

(c) $\alpha = 2.6, \kappa = 0.8$

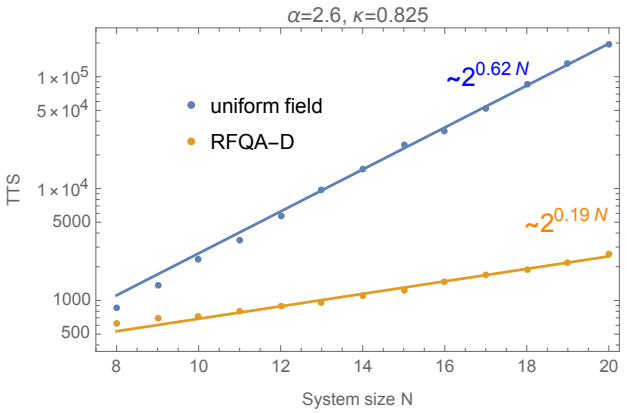

(d) $\alpha = 2.6, \kappa = 0.825$

Figure 5.6 The TTS in the Transverse Field Ising Model, performance of RFQA-D over uniform field QA is stark. Time to find the true ground state in four different difficulty problem set of TFIM:$\{\alpha = 2.6, \kappa = 0.75, 0.775, 0.8, 0.825\}$ with frequencies f_i chosen from $\{\frac{1}{3\sqrt{N}}, \frac{2}{3\sqrt{N}}\}$ using RFQA and reverse annealing, computed from the final success probability for a run-time polynomially increasing with N. The system size N ranges from 8 to 20. The frequencies are paired as "$AABBCC\cdots$" type instead of random frequencies on each site. Data for RFQA-D is given by orange markers. Blue dots are data for the standard quantum annealing method for comparison purposes. The solid blue and orange lines are the best-fit curves of the standard quantum annealing method and RFQA-D, respectively. RFQA-D shows an obvious quantum speed up over the standard quantum annealing method in the reverse annealing case.

We list all the results in the Table 5.1 and Table 5.3 to give a straightforward demonstration of the scaling advantage in RFQA.

Table 5.1 Summary of scaling exponents for different frequency ranges with a small transverse field. Fitting the time to solution $TTS(N)$ of each method to $2^{\beta+\gamma N}$, the table lists the exponential scaling coefficient γ values for reverse annealing in TFIM, with random frequencies f_i chosen from $\{\frac{1}{3\sqrt{N}}, \frac{2}{3\sqrt{N}}\}$ and apply random frequencies to each site. "$Standard''$ represents the digitized uniform field QA. The magnitude of oscillating field is 1.84.

Problem set	$Standard$	$RFQA-D$
$\alpha = 1.84, \kappa = 0.75$	0.86	0.43
$\alpha = 1.84, \kappa = 0.775$	0.81	0.35
$\alpha = 1.84, \kappa = 0.80$	0.66	0.27
$\alpha = 1.84, \kappa = 0.825$	0.55	0.20

Table 5.2 Summary of scaling exponents for different frequency ranges with a higher transverse field. Fitting the time to solution $TTS(N)$ of each method to an exponential function $2^{\beta+\gamma N}$ and polynomial function βN^{γ}, the table lists the exponential and polynomial scaling coefficient "γ" values for reverse annealing in TFIM, with random frequencies f_i chosen from $\{\frac{1}{3\sqrt{N}}, \frac{2}{3\sqrt{N}}\}$ and apply random frequencies to each site. "$Standard$" represents the digitized uniform field QA. The subscript "exp" represents the exponential scaling coefficient and "$poly$" represents the polynomial scaling coefficient. The magnitude of oscillating field is 1.84.

Problem set	$Standard_{exp}$	$RFQA-D_{exp}$	$RFQA-D_{poly}$
$\alpha = 1.84, \kappa = 0.85$	0.49	0.14	1.87
$\alpha = 1.84, \kappa = 0.875$	0.43	0.07	1.29
$\alpha = 1.84, \kappa = 0.90$	0.32	0.04	1.0

Table 5.3 Summary of scaling exponents for different frequency ranges. Fitting the time to solution $TTS(N)$ of each method to $2^{\beta+\gamma N}$, the table lists the exponential scaling coefficient "γ" values for reverse annealing in TFIM, with random frequencies f_i chosen from $\{\frac{1}{3\sqrt{N}}, \frac{2}{3\sqrt{N}}\}$ and pair the frequencies set to the "$AABBCC\cdots$" type rather than random frequencies on each site. "S" and "D" represent the digitized uniform field QA and digitized RFQA-D methods, respectively, the subscript 1.84 and 2.6 represents different oscillating field strengths.

Problem set	$S_{1.84}$	$D_{1.84}$	$S_{2.6}$	$D_{2.6}$
$\kappa = 0.75$	0.88	0.33	0.90	0.26
$\kappa = 0.775$	0.78	0.26	0.81	0.24
$\kappa = 0.80$	0.67	0.20	0.72	0.20
$\kappa = 0.825$	0.61	0.14	0.62	0.19

RFQA provides a polynomially (or even exponentially in some cases) quantum speedup in N-spin tunneling, the bottleneck of embedding. And in Table 5.2 are the exponential and polynomial scaling coefficients with higher transverse field. The results indicate RFQA is promising in providing even exponential speedup over transverse field QA. Fast tunneling in the frozen phase with RFQA suggests that a strong chain in the embedding will not lead to very long annealing time. The potential of mitigating the

cost of minor embedding overhead is a strong motivation for us to implement RFQA in the testbed(collaborate with MIT Lincoln Lab)[34, 232–234]. We believe the simulation results can offer guidance to the experimental implementation.

The work in this chapter is in collaboration with Eliot Kapit and Gianni Mossi.

CHAPTER 6

CONCLUSION

Many realistic hard problems can be encoded into combinatorial optimization problems, in which we need to find a global minimum of a system.

In the analog QA, adiabatic theorem states that if we prepare a time-dependent system in its ground state, it will stay in its ground state if a given perturbation is acting on it slowly enough and if there is a gap between the eigenvalue and the rest of the Hamiltonian's spectrum. QA makes an easily prepared initial ground state for the system, the final ground state of the system after a slowly evolution encodes the solution. The conventional initial Hamiltonian is a uniform transverse field, the ground state of which is a superposition of all possible states.

We proposed a new variation of Quantum Annealing that modifies the conventional uniform transverse field to an oscillating one, we name the method as RFQA, which stands for Random Field Quantum Annealing. There are two ways to make an oscillating field. One is independently oscillating the magnitudes, we refer to as RFQA-M, another is independently oscillating directions in the x-y plane, we refer to as RFQA-D. The frequencies for each spin in RFQA is randomly chosen from a scale set. In a system that has an exponentially closing gap, the random frequencies provides external energies to mix the ground state and first excited state. We predict that RFQA can provide a quantum speedup over standard uniform field QA with the acceleration of multi-qubit tunneling.

In the simulations on analog QA, we define a toy problem model(AMP model) that exhibits a generic bottleneck mechanism to benchmark some variations of traditional QA. The ferromagnetic states are the two competing ground states in this problem. The system is entropically steered to a false minimum, which is a generic bottleneck for many optimization problems. We studied the performance of inhomogeneous driving method, transverse couplers method and RFQA, as well as the variations of RFQA. All the methods can provide some quantum speedup over the traditional QA. They should be capable of providing beneficial in many optimization problems that share the similar bottleneck with AMP. Between the methods, inhomogeneous driving and RFQA only require some modification to the control circuitry in a quantum hardware, the two methods are promising in near-term quantum computing.

However, the scalability of analog QA with noise and decoherence is not clear. Also, the tunneling rate from a uniform field in the traditional QA is empirically not fast enough to beat the best classical algorithms in most cases, and the traditional QA can usually be simulated with QMC. Thus, we need RFQA, which forms a non-stoquastic Hamiltonian that cannot be efficiently simulated by QMC and can

provides possible quantum speedup. The quantum circuit model, as an alternative approach, is more flexible and is compatible with error correction. It's worth exploring gate model versions of RFQA as they may lead to better algorithms for future error corrected machines.

In the simulations on digitized QA, we investigate a series of benchmark problems to show that digitizing RFQA could be a good basis for a digital quantum optimization algorithm either for noisy machines or ultimately error corrected ones, as a new tool to complement QAOA and traditional digitized QA. The original shamrock model simulates a generic N-spin tunneling bottleneck in both quantum and classical simulations. However, it requires extensive cost for an error in one central qubit. We make a modified shamrock model to overcome this issue. We studied an ensemble of problem model sets with descending difficulty:$\{A = 0.35, h_0 = 0.25\}; \{A = 0.41, h_0 = 0.25\}; \{A = 0.45, h_0 = 0.25\}$. We also make three frequencies range sets: $\{0.1/\sqrt{N}, 0.2/\sqrt{N}\}; \{0.3/N, 0.6/N\}; \{0.5/N^{1.5}, 1/N^{1.5}\}$. We compared the scaling of the time to solution (TTS) of digitized RFQA with the scaling of digitized QA. The digitized QA shows inverse gap squared dependence as expected. Digitized RFQA provides a polynomial scaling advantage over digitized QA in forward annealing, with the scaling exponent $\gamma_{QA} - \gamma_{RFQA} \simeq 1$. And in the reverse annealing where the initial state is prepared as the ferromagnetic false minimum, digitized RFQA still provides some quantum advantage over digitized QA. The advantage of RFQA in reverse annealing indicates that RFQA is able to provide quantum speedup in N-spin tunneling between two competing ground state. We further map the modified shamrock model to the square grid to make it easier to implement on near term quantum computers. In both models, we show the digitized RFQA provides obvious quantum speedup over the digitized uniform field QA. We also investigated the behavior of RFQA in helping finding many target ground states in the many fold degenerate problem, however, digitized RFQA couldn't exhibit a scaling advantage in it.

To prepare for an experiment, we also investigated the 1D ferromagnetic chain with a transverse field(1D TFIM). The model is easier to implement on the government's testbed, and an advantage of RFQA in this model can help to mitigate the minor embedding overhead. In the 1D Transverse Field Ising Model, we prepare the initial state as one ferromagnetic state and measure the success probability of reaching the other ferromagnetic state with reverse annealing. For oscillating magnitude $\alpha = 1.86$, we studied an ensemble of problem model sets: $\{\kappa = 0.75, 0.775, 0.8, 0.825, 0.85, 0.857, 0.9\}$, the difficulty level decreases with increasing κ value. The random frequencies is chosen from $\{\frac{1}{3\sqrt{N}}, \frac{2}{3\sqrt{N}}\}$. RFQA provides performance enhancement over the uniform field QA, with the scaling exponent $\gamma_{QA} - \gamma_{RFQA} \simeq 0.4$. The advantage of RFQA indicates that the embedding problems can be mitigated. Since the acceleration of K-spin tunneling event with RFQA can help to prevent the freezing of strong chains in minor embedding. We show that a larger oscillating magnitude can provide more quantum speedup, and pairing the random

frequencies in RFQA provides can further improve the performance.

Nowadays, it's not clear if a Grover-like square root speedup is sufficient to be useful given the overhead of error correction, so it's meaningful to explore optimization algorithms that provides speedups go beyond it. Any kind of broadly applicable speedup beyond quadratic is very useful for a huge range of real-world problems, we don't know if that's the case for RFQA yet, but our simulation results indicate that some variations on traditional QA(such as RFQA and inhomogenous driving) are potentially quite powerful!

REFERENCES

[1] YaoChong Li, Ri-Gui Zhou, RuQing Xu, Jia Luo, and WenWen Hu. A quantum deep convolutional neural network for image recognition. *Quantum Science and Technology*, 5(4):044003, 2020.

[2] Kalyanmoy Deb. *Optimization for engineering design: Algorithms and examples*. PHI Learning Pvt. Ltd., 2012.

[3] Alejandro Perdomo-Ortiz, Neil Dickson, Marshall Drew-Brook, Geordie Rose, and Alán Aspuru-Guzik. Finding low-energy conformations of lattice protein models by quantum annealing. *Scientific reports*, 2(1):1–7, 2012.

[4] Simon C Benjamin, Liming Zhao, and Joseph F Fitzsimons. Measurement-driven quantum computing: Performance of a 3-sat solver. *arXiv preprint arXiv:1711.02687*, 2017.

[5] Suman Dutta. *Formulation of Optimization Problems in Chemical and Biochemical Engineering*, page 12–39. Cambridge University Press, 2016. doi: 10.1017/CBO9781316134504.003.

[6] Adam Callison, Nicholas Chancellor, Florian Mintert, and Viv Kendon. Finding spin glass ground states using quantum walks. *New Journal of Physics*, 21(12):123022, 2019.

[7] John Watrous. Quantum computational complexity. *arXiv preprint arXiv:0804.3401*, 2008.

[8] Bill Waggener, William N Waggener, and William M Waggener. *Pulse code modulation techniques*. Springer Science & Business Media, 1995.

[9] Matthias Troyer and Uwe-Jens Wiese. Computational complexity and fundamental limitations to fermionic quantum monte carlo simulations. *Physical review letters*, 94(17):170201, 2005.

[10] Scott Kirkpatrick, C Daniel Gelatt Jr, and Mario P Vecchi. Optimization by simulated annealing. In *Readings in Computer Vision*, pages 606–615. Elsevier, 1987.

[11] Robert H Swendsen and Jian-Sheng Wang. Replica monte carlo simulation of spin-glasses. *Physical review letters*, 57(21):2607, 1986.

[12] Koji Hukushima and Koji Nemoto. Exchange monte carlo method and application to spin glass simulations. *Journal of the Physical Society of Japan*, 65(6):1604–1608, 1996.

[13] Marco Falcioni and Michael W Deem. A biased monte carlo scheme for zeolite structure solution. *The Journal of chemical physics*, 110(3):1754–1766, 1999.

[14] Yuji Sugita and Yuko Okamoto. Replica-exchange molecular dynamics method for protein folding. *Chemical physics letters*, 314(1-2):141–151, 1999.

[15] David J Earl and Michael W Deem. Parallel tempering: Theory, applications, and new perspectives. *Physical Chemistry Chemical Physics*, 7(23):3910–3916, 2005.

[16] Arnab Das and Bikas K Chakrabarti. *Quantum annealing and related optimization methods*, volume 679. Springer Science & Business Media, 2005.

[17] Giuseppe E Santoro and Erio Tosatti. Optimization using quantum mechanics: quantum annealing through adiabatic evolution. *Journal of Physics A: Mathematical and General*, 39(36):R393, 2006.

[18] Arnab Das and Bikas K Chakrabarti. Colloquium: Quantum annealing and analog quantum computation. *Reviews of Modern Physics*, 80(3):1061, 2008.

[19] Sei Suzuki, Hidetoshi Nishimori, and Masuo Suzuki. Quantum annealing of the random-field ising model by transverse ferromagnetic interactions. *Physical Review E*, 75(5):051112, 2007.

[20] Marek M Rams, Masoud Mohseni, and Adolfo del Campo. Inhomogeneous quasi-adiabatic driving of quantum critical dynamics in weakly disordered spin chains. *New Journal of Physics*, 18(12):123034, 2016.

[21] Trevor Lanting, Andrew D King, Bram Evert, and Emile Hoskinson. Experimental demonstration of perturbative anticrossing mitigation using nonuniform driver hamiltonians. *Physical Review A*, 96(4): 042322, 2017.

[22] Yuki Susa, Yu Yamashiro, Masayuki Yamamoto, and Hidetoshi Nishimori. Exponential speedup of quantum annealing by inhomogeneous driving of the transverse field. *Journal of the Physical Society of Japan*, 87(2):023002, 2018.

[23] Yuki Susa, Yu Yamashiro, Masayuki Yamamoto, Itay Hen, Daniel A Lidar, and Hidetoshi Nishimori. Quantum annealing of the p-spin model under inhomogeneous transverse field driving. *Physical Review A*, 98(4):042326, 2018.

[24] Juan I Adame and Peter L McMahon. Inhomogeneous driving in quantum annealers can result in orders-of-magnitude improvements in performance. *Quantum Science and Technology*, 5(3):035011, 2020.

[25] Yoshiki Matsuda, Hidetoshi Nishimori, and Helmut G Katzgraber. Ground-state statistics from annealing algorithms: quantum versus classical approaches. *New Journal of Physics*, 11(7):073021, 2009.

[26] Yuya Seki and Hidetoshi Nishimori. Quantum annealing with antiferromagnetic fluctuations. *Physical Review E*, 85(5):051112, 2012.

[27] Yuya Seki and Hidetoshi Nishimori. Quantum annealing with antiferromagnetic transverse interactions for the hopfield model. *Journal of Physics A: Mathematical and Theoretical*, 48(33): 335301, jul 2015. doi: 10.1088/1751-8113/48/33/335301. URL https://doi.org/10.1088%2F1751-8113%2F48%2F33%2F335301.

[28] Yuki Susa, Johann F Jadebeck, and Hidetoshi Nishimori. Relation between quantum fluctuations and the performance enhancement of quantum annealing in a nonstoquastic hamiltonian. *Physical Review A*, 95(4):042321, 2017.

[29] Layla Hormozi, Ethan W Brown, Giuseppe Carleo, and Matthias Troyer. Nonstoquastic hamiltonians and quantum annealing of an ising spin glass. *Physical review B*, 95(18):184416, 2017.

[30] David Ceperley and Berni Alder. Quantum monte carlo. *Science*, 231(4738):555–560, 1986.

[31] Elijah Pelofske, Georg Hahn, and Hristo N Djidjev. Advanced anneal paths for improved quantum annealing. In *2020 IEEE International Conference on Quantum Computing and Engineering (QCE)*, pages 256–266. IEEE, 2020.

[32] Shunji Matsuura, Samantha Buck, Valentin Senicourt, and Arman Zaribafiyan. Variationally scheduled quantum simulation. *arXiv preprint arXiv:2003.09913*, 2020.

[33] Yuki Susa and Hidetoshi Nishimori. Variational optimization of the quantum annealing schedule for the lechner-hauke-zoller scheme. *Physical Review A*, 103(2):022619, 2021.

[34] Mostafa Khezri, Xi Dai, Rui Yang, Tameem Albash, Adrian Lupascu, and Daniel A Lidar. Customized quantum annealing schedules. *arXiv preprint arXiv:2103.06461*, 2021.

[35] Seung Woo Shin, Graeme Smith, John A Smolin, and Umesh Vazirani. How" quantum" is the d-wave machine? *arXiv preprint arXiv:1401.7087*, 2014.

[36] Tameem Albash, Troels F Rønnow, Matthias Troyer, and Daniel A Lidar. Reexamining classical and quantum models for the d-wave one processor. *The European Physical Journal Special Topics*, 224(1): 111–129, 2015.

[37] Kohji Nishimura, Hidetoshi Nishimori, Andrew J Ochoa, and Helmut G Katzgraber. Retrieving the ground state of spin glasses using thermal noise: Performance of quantum annealing at finite temperatures. *Physical Review E*, 94(3):032105, 2016.

[38] Jeffrey Marshall, Davide Venturelli, Itay Hen, and Eleanor G Rieffel. Power of pausing: Advancing understanding of thermalization in experimental quantum annealers. *Physical Review Applied*, 11(4): 044083, 2019.

[39] Masaki Ohkuwa, Hidetoshi Nishimori, and Daniel A Lidar. Reverse annealing for the fully connected p-spin model. *Physical Review A*, 98(2):022314, 2018.

[40] Davide Venturelli and Alexei Kondratyev. Reverse quantum annealing approach to portfolio optimization problems. *Quantum Machine Intelligence*, 1(1):17–30, 2019.

[41] Gianluca Passarelli, Ka-Wa Yip, Daniel A Lidar, Hidetoshi Nishimori, and Procolo Lucignano. Reverse quantum annealing of the p-spin model with relaxation. *Physical Review A*, 101(2):022331, 2020.

[42] John Golden and Daniel O'Malley. Reverse annealing for nonnegative/binary matrix factorization. *Plos one*, 16(1):e0244026, 2021.

[43] Jeffrey Marshall, Davide Venturelli, Itay Hen, and Eleanor G. Rieffel. Power of pausing: Advancing understanding of thermalization in experimental quantum annealers. *Phys. Rev. Applied*, 11:044083, Apr 2019. doi: 10.1103/PhysRevApplied.11.044083. URL https://link.aps.org/doi/10.1103/PhysRevApplied.11.044083.

[44] Kohji Nishimura and Hidetoshi Nishimori. Quantum annealing with a nonvanishing final value of the transverse field. *Physical Review A*, 96(4):042310, 2017.

[45] Elizabeth Crosson, Edward Farhi, Cedric Yen-Yu Lin, Han-Hsuan Lin, and Peter Shor. Different strategies for optimization using the quantum adiabatic algorithm. *arXiv preprint arXiv:1401.7320*, 2014.

[46] Hayato Goto and Taro Kanao. Quantum annealing using vacuum states as effective excited states of driven systems. *Communications Physics*, 3(1):1–9, 2020.

[47] Edward Farhi, Jeffrey Goldstone, and Sam Gutmann. Quantum adiabatic evolution algorithms versus simulated annealing, 2002.

[48] Linghang Kong and Elizabeth Crosson. The performance of the quantum adiabatic algorithm on spike hamiltonians. *International Journal of Quantum Information*, 15(02):1750011, 2017.

[49] Richard P Feynman. Simulating physics with computers. In *Feynman and computation*, pages 133–153. CRC Press, 2018.

[50] Peter W Shor. Polynomial-time algorithms for prime factorization and discrete logarithms on a quantum computer. *SIAM review*, 41(2):303–332, 1999.

[51] Peter W Shor. Scheme for reducing decoherence in quantum computer memory. *Physical review A*, 52(4):R2493, 1995.

[52] Andrew M Steane. Error correcting codes in quantum theory. *Physical Review Letters*, 77(5):793, 1996.

[53] Michael Calderbank. The rsa cryptosystem: History, algorithm, primes. *Fundamental Concepts of Encryption*, 2007.

[54] Lov K Grover. Quantum mechanics helps in searching for a needle in a haystack. *Physical review letters*, 79(2):325, 1997.

[55] Olawale Titiloye and Alan Crispin. Quantum annealing of the graph coloring problem. *Discrete Optimization*, 8(2):376–384, 2011.

[56] Steven H Adachi and Maxwell P Henderson. Application of quantum annealing to training of deep neural networks. *arXiv preprint arXiv:1510.06356*, 2015.

[57] Davide Venturelli, Dominic JJ Marchand, and Galo Rojo. Quantum annealing implementation of job-shop scheduling. *arXiv preprint arXiv:1506.08479*, 2015.

[58] Kazuki Ikeda, Yuma Nakamura, and Travis S Humble. Application of quantum annealing to nurse scheduling problem. *Scientific reports*, 9(1):1–10, 2019.

[59] Daniel Gottesman. An introduction to quantum error correction and fault-tolerant quantum computation. In *Quantum information science and its contributions to mathematics, Proceedings of Symposia in Applied Mathematics*, volume 68, pages 13–58, 2010.

[60] Earl T Campbell, Barbara M Terhal, and Christophe Vuillot. Roads towards fault-tolerant universal quantum computation. *Nature*, 549(7671):172–179, 2017.

[61] John Preskill. Quantum computing in the nisq era and beyond. *Quantum*, 2:79, 2018.

[62] John Preskill. Quantum computing 40 years later. *arXiv preprint arXiv:2106.10522*, 2021.

[63] David Deutsch. Quantum theory, the church–turing principle and the universal quantum computer. *Proceedings of the Royal Society of London. A. Mathematical and Physical Sciences*, 400(1818): 97–117, 1985.

[64] Abel Molina and John Watrous. Revisiting the simulation of quantum turing machines by quantum circuits. *Proceedings of the Royal Society A*, 475(2226):20180767, 2019.

[65] Christopher M Dawson and Michael A Nielsen. The solovay-kitaev algorithm. *arXiv preprint quant-ph/0505030*, 2005.

[66] Michael A Nielsen and Isaac L Chuang. Quantum computation and quantum information. *Phys. Today*, 54(2):60, 2001.

[67] Aaron Somoroff, Ray Mencia, and Ron Belyansky. Quantum error correction. 2018.

[68] James L Park. The concept of transition in quantum mechanics. *Foundations of Physics*, 1(1):23–33, 1970.

[69] William K Wootters and Wojciech H Zurek. A single quantum cannot be cloned. *Nature*, 299(5886): 802–803, 1982.

[70] DGBJ Dieks. Communication by epr devices. *Physics Letters A*, 92(6):271–272, 1982.

[71] Emanuel Knill, Raymond Laflamme, and Wojciech H Zurek. Resilient quantum computation. *Science*, 279(5349):342–345, 1998.

[72] Dorit Aharonov and Michael Ben-Or. Fault-tolerant quantum computation with constant error rate. *SIAM Journal on Computing*, 2008.

[73] Asher Peres. Reversible logic and quantum computers. *Physical review A*, 32(6):3266, 1985.

[74] Simon J Devitt, William J Munro, and Kae Nemoto. Quantum error correction for beginners. *Reports on Progress in Physics*, 76(7):076001, 2013.

[75] Andrew Steane. Multiple-particle interference and quantum error correction. *Proceedings of the Royal Society of London. Series A: Mathematical, Physical and Engineering Sciences*, 452(1954): 2551–2577, 1996.

[76] A Yu Kitaev. Quantum communication, computing, and measurement. In *Proceedings of the 3rd International Conference of Quantum Communication and Measurement, New York: Plenum*, 1997.

[77] Todd Brun, Igor Devetak, and Min-Hsiu Hsieh. Correcting quantum errors with entanglement. *science*, 314(5798):436–439, 2006.

[78] Min-Hsiu Hsieh. *Entanglement-assisted coding theory*. University of Southern California, 2008.

[79] Michel H Devoret, Andreas Wallraff, and John M Martinis. Superconducting qubits: A short review. *arXiv preprint cond-mat/0411174*, 2004.

[80] Philip Krantz, Morten Kjaergaard, Fei Yan, Terry P Orlando, Simon Gustavsson, and William D Oliver. A quantum engineer's guide to superconducting qubits. *Applied Physics Reviews*, 6(2): 021318, 2019.

[81] He-Liang Huang, Dachao Wu, Daojin Fan, and Xiaobo Zhu. Superconducting quantum computing: a review. *Science China Information Sciences*, 63(8):1–32, 2020.

[82] Dietrich Leibfried, Rainer Blatt, Christopher Monroe, and David Wineland. Quantum dynamics of single trapped ions. *Reviews of Modern Physics*, 75(1):281, 2003.

[83] Rainer Blatt and Christian F Roos. Quantum simulations with trapped ions. *Nature Physics*, 8(4): 277–284, 2012.

[84] Colin D Bruzewicz, John Chiaverini, Robert McConnell, and Jeremy M Sage. Trapped-ion quantum computing: Progress and challenges. *Applied Physics Reviews*, 6(2):021314, 2019.

[85] Daniel Loss and David P DiVincenzo. Quantum computation with quantum dots. *Physical Review A*, 57(1):120, 1998.

[86] David G Cory, Mark D Price, and Timothy F Havel. Nuclear magnetic resonance spectroscopy: An experimentally accessible paradigm for quantum computing. *Physica D: Nonlinear Phenomena*, 120 (1-2):82–101, 1998.

[87] Tao Xin, Bi-Xue Wang, Ke-Ren Li, Xiang-Yu Kong, Shi-Jie Wei, Tao Wang, Dong Ruan, and Gui-Lu Long. Nuclear magnetic resonance for quantum computing: Techniques and recent achievements. *Chinese Physics B*, 27(2):020308, 2018.

[88] I Chiorescu, Y Nakamura, CJP Ma Harmans, and JE Mooij. Coherent quantum dynamics of a superconducting flux qubit. *Science*, 299(5614):1869–1871, 2003.

[89] M Grajcar, A Izmalkov, and E Il'ichev. Possible implementation of adiabatic quantum algorithm with superconducting flux qubits. *Physical Review B*, 71(14):144501, 2005.

[90] Yuriy Makhlin, Gerd Schön, and Alexander Shnirman. Quantum-state engineering with josephson-junction devices. *Reviews of modern physics*, 73(2):357, 2001.

[91] Andrew A Houck, Jens Koch, Michel H Devoret, Steven M Girvin, and Robert J Schoelkopf. Life after charge noise: recent results with transmon qubits. *Quantum Information Processing*, 8(2): 105–115, 2009.

[92] F Hassler, AR Akhmerov, and CWJ Beenakker. The top-transmon: a hybrid superconducting qubit for parity-protected quantum computation. *New Journal of Physics*, 13(9):095004, 2011.

[93] KB Cooper, Matthias Steffen, Robert McDermott, Raymond W Simmonds, Seongshik Oh, Dustin A Hite, David P Pappas, and John M Martinis. Observation of quantum oscillations between a josephson phase qubit and a microscopic resonator using fast readout. *Physical Review Letters*, 93 (18):180401, 2004.

[94] Erik Lucero, Rami Barends, Yu Chen, Julian Kelly, Matteo Mariantoni, Anthony Megrant, Peter O'Malley, Daniel Sank, Amit Vainsencher, James Wenner, et al. Computing prime factors with a josephson phase qubit quantum processor. *Nature Physics*, 8(10):719–723, 2012.

[95] Alexandre Avraamovitch Golubov, Evert Pieter Houwman, JG Gijsbertsen, VM Krasnov, Jakob Flokstra, Horst Rogalla, and M Yu Kupriyanov. Proximity effect in superconductor-insulator-superconductor josephson tunnel junctions: Theory and experiment. *Physical Review B*, 51(2):1073, 1995.

[96] L Fritzsch, M Schubert, G Wende, and H-G Meyer. Superconductor-normal metal-superconductor josephson junctions with ti interlayer. *Applied physics letters*, 73(11):1583–1585, 1998.

[97] Ady Stern and Erez Berg. Fractional josephson vortices and braiding of majorana zero modes in planar superconductor-semiconductor heterostructures. *Physical review letters*, 122(10):107701, 2019.

[98] VI Shnyrkov, AA Soroka, AM Korolev, and OG Turutanov. Superposition of states in flux qubits with a josephson junction of the scs type. *Low Temperature Physics*, 38(4):301–310, 2012.

[99] Brian David Josephson. Possible new effects in superconductive tunnelling. *Physics letters*, 1(7): 251–253, 1962.

[100] BRIAN D Josephson. The discovery of tunnelling supercurrents. *Reviews of Modern Physics*, 46(2): 251, 1974.

[101] Rami Barends, Alireza Shabani, Lucas Lamata, Julian Kelly, Antonio Mezzacapo, Urtzi Las Heras, Ryan Babbush, Austin G Fowler, Brooks Campbell, Yu Chen, et al. Digitized adiabatic quantum computing with a superconducting circuit. *Nature*, 534(7606):222–226, 2016.

[102] Glen Bigan Mbeng, Luca Arceci, and Giuseppe E Santoro. Optimal working point in digitized quantum annealing. *Physical Review B*, 100(22):224201, 2019.

[103] Glen Bigan Mbeng, Rosario Fazio, and Giuseppe Santoro. Quantum annealing: A journey through digitalization, control, and hybrid quantum variational schemes. *arXiv preprint arXiv:1906.08948*, 2019.

[104] Narendra N Hegade, Koushik Paul, Yongcheng Ding, Mikel Sanz, Francisco Albarrán-Arriagada, Enrique Solano, and Xi Chen. Shortcuts to adiabaticity in digitized adiabatic quantum computing. *Physical Review Applied*, 15(2):024038, 2021.

[105] Naomichi Hatano and Masuo Suzuki. Finding exponential product formulas of higher orders. In *Quantum annealing and other optimization methods*, pages 37–68. Springer, 2005.

[106] A Peruzzo et al. A variational eigenvalue solver on a quantum processor. eprint. *arXiv preprint arXiv:1304.3061*, 2013.

[107] Nikolaj Moll, Panagiotis Barkoutsos, Lev S Bishop, Jerry M Chow, Andrew Cross, Daniel J Egger, Stefan Filipp, Andreas Fuhrer, Jay M Gambetta, Marc Ganzhorn, et al. Quantum optimization using variational algorithms on near-term quantum devices. *Quantum Science and Technology*, 3(3):030503, 2018.

[108] Yifan Li, Jiaqi Hu, Xiao-Ming Zhang, Zhigang Song, and Man-Hong Yung. Variational quantum simulation for quantum chemistry. *Advanced Theory and Simulations*, 2(4):1800182, 2019.

[109] Edward Farhi, Jeffrey Goldstone, and Sam Gutmann. A quantum approximate optimization algorithm. *arXiv preprint arXiv:1411.4028*, 2014.

[110] JS Otterbach, R Manenti, N Alidoust, A Bestwick, M Block, B Bloom, S Caldwell, N Didier, E Schuyler Fried, S Hong, et al. Unsupervised machine learning on a hybrid quantum computer. *arXiv preprint arXiv:1712.05771*, 2017.

[111] Zhihui Wang, Stuart Hadfield, Zhang Jiang, and Eleanor G Rieffel. Quantum approximate optimization algorithm for maxcut: A fermionic view. *Physical Review A*, 97(2):022304, 2018.

[112] G Pagano, A Bapat, P Becker, KS Collins, A De, PW Hess, HB Kaplan, A Kyprianidis, WL Tan, C Baldwin, et al. Quantum approximate optimization with a trapped-ion quantum simulator. *arXiv preprint arXiv:1906.02700*, 6, 2019.

[113] Edward Farhi and Aram W Harrow. Quantum supremacy through the quantum approximate optimization algorithm. *arXiv preprint arXiv:1602.07674*, 2016.

[114] Zhang Jiang, Eleanor G Rieffel, and Zhihui Wang. Near-optimal quantum circuit for grover's unstructured search using a transverse field. *Physical Review A*, 95(6):062317, 2017.

[115] Murphy Yuezhen Niu, Sirui Lu, and Isaac L Chuang. Optimizing qaoa: Success probability and runtime dependence on circuit depth. *arXiv preprint arXiv:1905.12134*, 2019.

[116] Gian Giacomo Guerreschi and Anne Y Matsuura. Qaoa for max-cut requires hundreds of qubits for quantum speed-up. *Scientific reports*, 9(1):1–7, 2019.

[117] Panagiotis Kl Barkoutsos, Giacomo Nannicini, Anton Robert, Ivano Tavernelli, and Stefan Woerner. Improving variational quantum optimization using cvar. *Quantum*, 4:256, 2020.

[118] Joao Basso, Edward Farhi, Kunal Marwaha, Benjamin Villalonga, and Leo Zhou. The quantum approximate optimization algorithm at high depth for maxcut on large-girth regular graphs and the sherrington-kirkpatrick model. *arXiv preprint arXiv:2110.14206*, 2021.

[119] Christos H Papadimitriou and Kenneth Steiglitz. *Combinatorial optimization: algorithms and complexity*. Courier Corporation, 1998.

[120] M Born and V Fock. Proof of the adiabatic theorem. *Z. Phys*, 51:165–169, 1928.

[121] Thomas Jörg, Florent Krzakala, Jorge Kurchan, Anthony C Maggs, and Justine Pujos. Energy gaps in quantum first-order mean-field–like transitions: The problems that quantum annealing cannot solve. *EPL (Europhysics Letters)*, 89(4):40004, 2010.

[122] CR Laumann, R Moessner, A Scardicchio, and Shivaji Lal Sondhi. Quantum adiabatic algorithm and scaling of gaps at first-order quantum phase transitions. *Physical review letters*, 109(3):030502, 2012.

[123] Boris Altshuler, Hari Krovi, and Jérémie Roland. Anderson localization makes adiabatic quantum optimization fail. *Proceedings of the National Academy of Sciences*, 107(28):12446–12450, 2010.

[124] Curt Wittig. The landau- zener formula. *The Journal of Physical Chemistry B*, 109(17):8428–8430, 2005.

[125] Jingwei Zhou, Pu Huang, Qi Zhang, Zixiang Wang, Tian Tan, Xiangkun Xu, Fazhan Shi, Xing Rong, S Ashhab, and Jiangfeng Du. Observation of time-domain rabi oscillations in the landau-zener regime with a single electronic spin. *Physical review letters*, 112(1):010503, 2014.

[126] Tadashi Kadowaki and Hidetoshi Nishimori. Quantum annealing in the transverse ising model. *Physical Review E*, 58(5):5355, 1998.

[127] Edward Farhi, Jeffrey Goldstone, Sam Gutmann, and Michael Sipser. Quantum computation by adiabatic evolution. *arXiv preprint quant-ph/0001106*, 2000.

[128] Edward Farhi, Jeffrey Goldstone, Sam Gutmann, Joshua Lapan, Andrew Lundgren, and Daniel Preda. A quantum adiabatic evolution algorithm applied to random instances of an np-complete problem. *Science*, 292(5516):472–475, 2001.

[129] Dorit Aharonov, Wim Van Dam, Julia Kempe, Zeph Landau, Seth Lloyd, and Oded Regev. Adiabatic quantum computation is equivalent to standard quantum computation. *SIAM review*, 50 (4):755–787, 2008.

[130] Giuseppe E Santoro, Roman Martoňák, Erio Tosatti, and Roberto Car. Theory of quantum annealing of an ising spin glass. *Science*, 295(5564):2427–2430, 2002.

[131] Lorenzo Stella and Giuseppe E Santoro. Quantum annealing of an ising spin-glass by green's function monte carlo. *Physical Review E*, 75(3):036703, 2007.

[132] A Rajak and BK Chakrabarti. Quantum annealing search of ising spin glass ground state (s) with tunable transverse and longitudinal fields. *Indian Journal of Physics*, 88(9):951–955, 2014.

[133] Sergey Knysh. Zero-temperature quantum annealing bottlenecks in the spin-glass phase. *Nature communications*, 7(1):1–9, 2016.

[134] Layla Hormozi, Ethan W Brown, Giuseppe Carleo, and Matthias Troyer. Nonstoquastic hamiltonians and quantum annealing of an ising spin glass. *Physical review B*, 95(18):184416, 2017.

[135] Hidetoshi Nishimori. *Statistical physics of spin glasses and information processing: an introduction*. Number 111. Clarendon Press, 2001.

[136] David Sherrington. Spin glasses. *Physics Bulletin*, 30(11):477, 1979.

[137] Neil G Dickson, MW Johnson, MH Amin, R Harris, F Altomare, AJ Berkley, P Bunyk, J Cai, EM Chapple, P Chavez, et al. Thermally assisted quantum annealing of a 16-qubit problem. *Nature communications*, 4(1):1–6, 2013.

[138] Eliot Kapit and Vadim Oganesyan. Noise-tolerant quantum speedups in quantum annealing without fine tuning. *Quantum Science and Technology*, 6(2):025013, 2021.

[139] Ronald D Ruth et al. A canonical integration technique. *IEEE Trans. Nucl. Sci*, 30(4):2669–2671, 1983.

[140] Evgeny Andriyash and Mohammad H Amin. Can quantum monte carlo simulate quantum annealing? *arXiv preprint arXiv:1703.09277*, 2017.

[141] Itay Hen, Joshua Job, Tameem Albash, Troels F Rønnow, Matthias Troyer, and Daniel A Lidar. Probing for quantum speedup in spin-glass problems with planted solutions. *Physical Review A*, 92 (4):042325, 2015.

[142] Andrew D King, Trevor Lanting, and Richard Harris. Performance of a quantum annealer on range-limited constraint satisfaction problems. *arXiv preprint arXiv:1502.02098*, 2015.

[143] Jeffrey Marshall, Victor Martin-Mayor, and Itay Hen. Practical engineering of hard spin-glass instances. *Physical review A*, 94(1):012320, 2016.

[144] Wenlong Wang, Salvatore Mandrà, and Helmut G Katzgraber. Patch-planting spin-glass solution for benchmarking. *Physical Review E*, 96(2):023312, 2017.

[145] Firas Hamze, Darryl C Jacob, Andrew J Ochoa, Dilina Perera, Wenlong Wang, and Helmut G Katzgraber. From near to eternity: spin-glass planting, tiling puzzles, and constraint-satisfaction problems. *Physical Review E*, 97(4):043303, 2018.

[146] A.B. Finnila, M.A. Gomez, C. Sebenik, C. Stenson, and J.D. Doll. Quantum annealing: A new method for minimizing multidimensional functions. *Chemical Physics Letters*, 219(5):343 – 348, 1994. ISSN 0009-2614. doi: https://doi.org/10.1016/0009-2614(94)00117-0. URL http://www.sciencedirect.com/science/article/pii/0009261494001170.

[147] M. W. Johnson, M. H. S. Amin, S. Gildert, T. Lanting, F. Hamze, N. Dickson, R. Harris, A. J. Berkley, J. Johansson, P. Bunyk, E. M. Chapple, C. Enderud, J. P. Hilton, K. Karimi, E. Ladizinsky, N. Ladizinsky, T. Oh, I. Perminov, C. Rich, M. C. Thom, E. Tolkacheva, C. J. S. Truncik, S. Uchaikin, J. Wang, B. Wilson, and G. Rose. Quantum annealing with manufactured spins. *Nature*, 473(7346):194–198, May 2011. ISSN 1476-4687. doi: 10.1038/nature10012. URL https://doi.org/10.1038/nature10012.

[148] Rolando D Somma, Daniel Nagaj, and Mária Kieferová. Quantum speedup by quantum annealing. *Physical review letters*, 109(5):050501, 2012.

[149] Tameem Albash and Daniel A Lidar. Adiabatic quantum computation. *Reviews of Modern Physics*, 90(1):015002, 2018.

[150] Sergio Boixo, Troels F Rønnow, Sergei V Isakov, Zhihui Wang, David Wecker, Daniel A Lidar, John M Martinis, and Matthias Troyer. Evidence for quantum annealing with more than one hundred qubits. *Nature Physics*, 10(3):218–224, 2014. ISSN 1745-2481. doi: 10.1038/nphys2900. URL https://doi.org/10.1038/nphys2900.

[151] G. Rosenberg, P. Haghnegahdar, P. Goddard, P. Carr, K. Wu, and M. L. de Prado. Solving the optimal trading trajectory problem using a quantum annealer. *IEEE Journal of Selected Topics in Signal Processing*, 10(6):1053–1060, 2016.

[152] Florian Neukart, Gabriele Compostella, Christian Seidel, David von Dollen, Sheir Yarkoni, and Bob Parney. Traffic flow optimization using a quantum annealer. *Frontiers in ICT*, 4:29, 2017. ISSN 2297-198X. doi: 10.3389/fict.2017.00029. URL https://www.frontiersin.org/article/10.3389/fict.2017.00029.

[153] Davide Venturelli, Minh Do, Eleanor Rieffel, and Jeremy Frank. Compiling quantum circuits to realistic hardware architectures using temporal planners. *Quantum Science and Technology*, 3(2): 025004, feb 2018. doi: 10.1088/2058-9565/aaa331. URL https://doi.org/10.1088%2F2058-9565%2Faaa331.

[154] Andrew D King, Juan Carrasquilla, Jack Raymond, Isil Ozfidan, Evgeny Andriyash, Andrew Berkley, Mauricio Reis, Trevor Lanting, Richard Harris, Fabio Altomare, Kelly Boothby, Paul I Bunyk, Colin Enderud, Alexandre Fréchette, Emile Hoskinson, Nicolas Ladizinsky, Travis Oh, Gabriel Poulin-Lamarre, Christopher Rich, Yuki Sato, Anatoly Yu. Smirnov, Loren J Swenson, Mark H Volkmann, Jed Whittaker, Jason Yao, Eric Ladizinsky, Mark W Johnson, Jeremy Hilton, and Mohammad H Amin. Observation of topological phenomena in a programmable lattice of 1,800 qubits. *Nature*, 560(7719):456–460, 2018. ISSN 1476-4687. doi: 10.1038/s41586-018-0410-x. URL https://doi.org/10.1038/s41586-018-0410-x.

[155] Davide Venturelli and Alexei Kondratyev. Reverse quantum annealing approach to portfolio optimization problems. *Quantum Machine Intelligence*, 1(1):17–30, 2019. ISSN 2524-4914. doi: 10.1007/s42484-019-00001-w. URL https://doi.org/10.1007/s42484-019-00001-w.

[156] Andrew D. King, Jack Raymond, Trevor Lanting, Sergei V. Isakov, Masoud Mohseni, Gabriel Poulin-Lamarre, Sara Ejtemaee, William Bernoudy, Isil Ozfidan, Anatoly Yu. Smirnov, Mauricio Reis, Fabio Altomare, Michael Babcock, Catia Baron, Andrew J. Berkley, Kelly Boothby, Paul I. Bunyk, Holly Christiani, Colin Enderud, Bram Evert, Richard Harris, Emile Hoskinson, Shuiyuan Huang, Kais Jooya, Ali Khodabandelou, Nicolas Ladizinsky, Ryan Li, P. Aaron Lott, Allison J. R. MacDonald, Danica Marsden, Gaelen Marsden, Teresa Medina, Reza Molavi, Richard Neufeld, Mana Norouzpour, Travis Oh, Igor Pavlov, Ilya Perminov, Thomas Prescott, Chris Rich, Yuki Sato, Benjamin Sheldan, George Sterling, Loren J. Swenson, Nicholas Tsai, Mark H. Volkmann, Jed D. Whittaker, Warren Wilkinson, Jason Yao, Hartmut Neven, Jeremy P. Hilton, Eric Ladizinsky, Mark W. Johnson, and Mohammad H. Amin. Scaling advantage in quantum simulation of geometrically frustrated magnets, 2019.

[157] James King, Masoud Mohseni, William Bernoudy, Alexandre Fréchette, Hossein Sadeghi, Sergei V. Isakov, Hartmut Neven, and Mohammad H. Amin. Quantum-assisted genetic algorithm, 2019.

[158] Jérémie Roland and Nicolas J Cerf. Quantum search by local adiabatic evolution. *Physical Review A*, 65(4):042308, 2002.

[159] Andrew Lucas. Ising formulations of many np problems. *Frontiers in Physics*, 2:5, 2014. ISSN 2296-424X. doi: 10.3389/fphy.2014.00005. URL https://www.frontiersin.org/article/10.3389/fphy.2014.00005.

[160] Elizabeth Crosson, Edward Farhi, Cedric Yen-Yu Lin, Han-Hsuan Lin, and Peter Shor. Different strategies for optimization using the quantum adiabatic algorithm, 2014.

[161] Hidetoshi Nishimori and Kabuki Takada. Exponential enhancement of the efficiency of quantum annealing by non-stoquastic hamiltonians. *Frontiers in ICT*, 4:2, 2017.

[162] Yuki Susa, Yu Yamashiro, Masayuki Yamamoto, and Hidetoshi Nishimori. Exponential speedup of quantum annealing by inhomogeneous driving of the transverse field. *Journal of the Physical Society of Japan*, 87(2):023002, 2018. doi: 10.7566/JPSJ.87.023002. URL https://doi.org/10.7566/JPSJ.87.023002.

[163] Linghang Kong and Elizabeth Crosson. The performance of the quantum adiabatic algorithm on spike hamiltonians, 2015.

[164] M V Berry. Transitionless quantum driving. *Journal of Physics A: Mathematical and Theoretical*, 42 (36):365303, aug 2009. doi: 10.1088/1751-8113/42/36/365303. URL https://doi.org/10.1088%2F1751-8113%2F42%2F36%2F365303.

[165] Juan Ignacio Adame and Peter McMahon. Inhomogeneous driving in quantum annealers can result in orders-of-magnitude improvements in performance. *Quantum Science and Technology*, 2020.

[166] Tameem Albash and Daniel A Lidar. Demonstration of a scaling advantage for a quantum annealer over simulated annealing. *Physical Review X*, 8(3):031016, 2018.

[167] Sergey Knysh. Zero-temperature quantum annealing bottlenecks in the spin-glass phase. *Nature communications*, 7, 2016.

[168] Jacek Dziarmaga. Dynamics of a quantum phase transition and relaxation to a steady state. *Advances in Physics*, 59(6):1063–1189, 2010. doi: 10.1080/00018732.2010.514702. URL https://doi.org/10.1080/00018732.2010.514702.

[169] CR Laumann, R Moessner, A Scardicchio, and Shivaji Lal Sondhi. Quantum adiabatic algorithm and scaling of gaps at first-order quantum phase transitions. *Physical review letters*, 109(3):030502, 2012.

[170] Dries Sels and Anatoli Polkovnikov. Minimizing irreversible losses in quantum systems by local counterdiabatic driving. *Proceedings of the National Academy of Sciences*, 114(20):E3909–E3916, 2017. ISSN 0027-8424. doi: 10.1073/pnas.1619826114. URL https://www.pnas.org/content/114/20/E3909.

[171] Walter Vinci and Daniel A Lidar. Non-stoquastic hamiltonians in quantum annealing via geometric phases. *npj Quantum Information*, 3(1):1–6, 2017.

[172] Tobias Graß. Quantum annealing with longitudinal bias fields. *Physical review letters*, 123(12): 120501, 2019.

[173] Philipp Hauke, Helmut G Katzgraber, Wolfgang Lechner, Hidetoshi Nishimori, and William D Oliver. Perspectives of quantum annealing: methods and implementations. *Reports on Progress in Physics*, 83(5):054401, may 2020. doi: 10.1088/1361-6633/ab85b8. URL https://doi.org/10.1088%2F1361-6633%2Fab85b8.

[174] Sergey Bravyi, David P. DiVincenzo, Roberto I. Oliveira, and Barbara M. Terhal. The complexity of stoquastic local hamiltonian problems, 2006.

[175] Masayuki Ohzeki. Quantum Monte Carlo simulation of a particular class of non-stoquastic Hamiltonians in quantum annealing. *Scientific Reports*, 7(1):41186, 2017. ISSN 2045-2322. doi: 10.1038/srep41186. URL https://doi.org/10.1038/srep41186.

[176] Vasil S Denchev, Sergio Boixo, Sergei V Isakov, Nan Ding, Ryan Babbush, Vadim Smelyanskiy, John Martinis, and Hartmut Neven. What is the computational value of finite-range tunneling? *Physical Review X*, 6(3):031015, 2016.

[177] Sergei V Isakov, Guglielmo Mazzola, Vadim N Smelyanskiy, Zhang Jiang, Sergio Boixo, Hartmut Neven, and Matthias Troyer. Understanding quantum tunneling through quantum monte carlo simulations. *Physical review letters*, 117(18):180402, 2016.

[178] Zhang Jiang, Vadim N Smelyanskiy, Sergei V Isakov, Sergio Boixo, Guglielmo Mazzola, Matthias Troyer, and Hartmut Neven. Scaling analysis and instantons for thermally assisted tunneling and quantum monte carlo simulations. *Physical Review A*, 95(1):012322, 2017.

[179] Guglielmo Mazzola, Vadim N Smelyanskiy, and Matthias Troyer. Quantum monte carlo tunneling from quantum chemistry to quantum annealing. *Physical Review B*, 96(13):134305, 2017.

[180] Hidetoshi Nishimori and Kabuki Takada. Exponential enhancement of the efficiency of quantum annealing by non-stoquastic hamiltonians. *Frontiers in ICT*, 4:2, 2017. ISSN 2297-198X. doi: 10.3389/fict.2017.00002. URL https://www.frontiersin.org/article/10.3389/fict.2017.00002.

[181] Edward Farhi, Jeffrey Goldstone, and Sam Gutmann. Quantum adiabatic evolution algorithms with different paths. *arXiv preprint quant-ph/0208135*, 2002.

[182] Alejandro Perdomo-Ortiz, Salvador E Venegas-Andraca, and Alán Aspuru-Guzik. A study of heuristic guesses for adiabatic quantum computation. *Quantum Information Processing*, 10(1):33–52, 2011.

[183] Nicholas Chancellor. Modernizing quantum annealing using local searches. *New Journal of Physics*, 19(2):023024, 2017.

[184] Andrew D King, Juan Carrasquilla, Jack Raymond, Isil Ozfidan, Evgeny Andriyash, Andrew Berkley, Mauricio Reis, Trevor Lanting, Richard Harris, Fabio Altomare, et al. Observation of topological phenomena in a programmable lattice of 1,800 qubits. *Nature*, 560(7719):456–460, 2018.

[185] Maximilian Keck, Simone Montangero, Giuseppe E Santoro, Rosario Fazio, and Davide Rossini. Dissipation in adiabatic quantum computers: Lessons from an exactly solvable model. *New Journal of Physics*, 19(11):113029, 2017.

[186] Vadim N Smelyanskiy, Davide Venturelli, Alejandro Perdomo-Ortiz, Sergey Knysh, and Mark I Dykman. Quantum annealing via environment-mediated quantum diffusion. *Physical review letters*, 118(6):066802, 2017.

[187] Lorenzo Campos Venuti, Tameem Albash, Milad Marvian, Daniel Lidar, and Paolo Zanardi. Relaxation versus adiabatic quantum steady-state preparation. *Physical Review A*, 95(4):042302, 2017.

[188] Luca Arceci, Simone Barbarino, Davide Rossini, and Giuseppe E Santoro. Optimal working point in dissipative quantum annealing. *Physical Review B*, 98(6):064307, 2018.

[189] Tadashi Kadowaki and Masayuki Ohzeki. Experimental and theoretical study of thermodynamic effects in a quantum annealer. *Journal of the Physical Society of Japan*, 88(6):061008, 2019.

[190] Sei Suzuki, Hiroki Oshiyama, and Naokazu Shibata. Quantum annealing of pure and random ising chains coupled to a bosonic environment. *Journal of the Physical Society of Japan*, 88(6):061003, 2019.

[191] David Roberts, Lukasz Cincio, Avadh Saxena, Andre Petukhov, and Sergey Knysh. Noise amplification at spin-glass bottlenecks of quantum annealing: a solvable model. *arXiv preprint arXiv:1909.00322*, 2019.

[192] Daniel Jaschke, Lincoln D Carr, and Inés de Vega. Thermalization in the quantum ising model—approximations, limits, and beyond. *Quantum Science and Technology*, 4(3):034002, 2019.

[193] EJ Crosson and DA Lidar. Prospects for quantum enhancement with diabatic quantum annealing. *arXiv preprint arXiv:2008.09913*, 2020.

[194] Francesca Pietracaprina, Valentina Ros, and Antonello Scardicchio. Forward approximation as a mean-field approximation for the anderson and many-body localization transitions. *Physical Review B*, 93(5):054201, 2016.

[195] CL Baldwin, CR Laumann, A Pal, and A Scardicchio. The many-body localized phase of the quantum random energy model. *Physical Review B*, 93(2):024202, 2016.

[196] CL Baldwin, CR Laumann, A Pal, and A Scardicchio. Clustering of nonergodic eigenstates in quantum spin glasses. *Physical review letters*, 118(12):127201, 2017.

[197] Antonello Scardicchio and Thimothée Thiery. Perturbation theory approaches to anderson and many-body localization: some lecture notes. *arXiv preprint arXiv:1710.01234*, 2017.

[198] CL Baldwin and CR Laumann. Quantum algorithm for energy matching in hard optimization problems. *Physical Review B*, 97(22):224201, 2018.

[199] Zhijie Tang and Eliot Kapit. Unconventional quantum annealing methods for difficult trial problems. *Physical Review A*, 103(3):032612, 2021.

[200] Michael A Nielsen and Isaac Chuang. Quantum computation and quantum information, 2002.

[201] Sergio Boixo, Sergei V Isakov, Vadim N Smelyanskiy, Ryan Babbush, Nan Ding, Zhang Jiang, Michael J Bremner, John M Martinis, and Hartmut Neven. Characterizing quantum supremacy in near-term devices. *Nature Physics*, 14(6):595–600, 2018.

[202] Guido Pagano, Aniruddha Bapat, Patrick Becker, Katherine S Collins, Arinjoy De, Paul W Hess, Harvey B Kaplan, Antonis Kyprianidis, Wen Lin Tan, Christopher Baldwin, et al. Quantum approximate optimization of the long-range ising model with a trapped-ion quantum simulator. *Proceedings of the National Academy of Sciences*, 117(41):25396–25401, 2020.

[203] Leo Zhou, Sheng-Tao Wang, Soonwon Choi, Hannes Pichler, and Mikhail D Lukin. Quantum approximate optimization algorithm: Performance, mechanism, and implementation on near-term devices. *Physical Review X*, 10(2):021067, 2020.

[204] Linghua Zhu, Ho Lun Tang, George S Barron, FA Calderon-Vargas, Nicholas J Mayhall, Edwin Barnes, and Sophia E Economou. An adaptive quantum approximate optimization algorithm for solving combinatorial problems on a quantum computer. *arXiv preprint arXiv:2005.10258*, 2020.

[205] Alberto Peruzzo, Jarrod McClean, Peter Shadbolt, Man-Hong Yung, Xiao-Qi Zhou, Peter J Love, Alán Aspuru-Guzik, and Jeremy L O'brien. A variational eigenvalue solver on a photonic quantum processor. *Nature communications*, 5(1):1–7, 2014.

[206] Peter JJ O'Malley, Ryan Babbush, Ian D Kivlichan, Jonathan Romero, Jarrod R McClean, Rami Barends, Julian Kelly, Pedram Roushan, Andrew Tranter, Nan Ding, et al. Scalable quantum simulation of molecular energies. *Physical Review X*, 6(3):031007, 2016.

[207] Abhinav Kandala, Antonio Mezzacapo, Kristan Temme, Maika Takita, Markus Brink, Jerry M Chow, and Jay M Gambetta. Hardware-efficient variational quantum eigensolver for small molecules and quantum magnets. *Nature*, 549(7671):242–246, 2017.

[208] Edward Farhi and Hartmut Neven. Classification with quantum neural networks on near term processors. *arXiv preprint arXiv:1802.06002*, 2018.

[209] Edward Grant, Marcello Benedetti, Shuxiang Cao, Andrew Hallam, Joshua Lockhart, Vid Stojevic, Andrew G Green, and Simone Severini. Hierarchical quantum classifiers. *npj Quantum Information*, 4(1):1–8, 2018.

[210] Scott Kirkpatrick, C Daniel Gelatt, and Mario P Vecchi. Optimization by simulated annealing. *science*, 220(4598):671–680, 1983.

[211] Sergey Knysh. Computational bottlenecks of quantum annealing. *arXiv preprint arXiv:1506.08608*, 2015.

[212] D Aharonov, W van Dam, Z Landau, S Lloyd, J Kempe, and O Regev. Universality of adiabatic quantum computation. In *Proceedings of 45th FOCS*, 2004.

[213] Ari Mizel, Daniel A Lidar, and Morgan Mitchell. Simple proof of equivalence between adiabatic quantum computation and the circuit model. *Physical review letters*, 99(7):070502, 2007.

[214] Seth Lloyd. Quantum approximate optimization is computationally universal. *arXiv preprint arXiv:1812.11075*, 2018.

[215] Mauro ES Morales, Jacob D Biamonte, and Zoltán Zimborás. On the universality of the quantum approximate optimization algorithm. *Quantum Information Processing*, 19(9):1–26, 2020.

[216] Ryan Babbush, Jarrod R McClean, Michael Newman, Craig Gidney, Sergio Boixo, and Hartmut Neven. Focus beyond quadratic speedups for error-corrected quantum advantage. *PRX Quantum*, 2 (1):010103, 2021.

[217] Matteo Bellitti, Federico Ricci-Tersenghi, and Antonello Scardicchio. Entropic barriers as a reason for hardness in both classical and quantum algorithms. *arXiv preprint arXiv:2102.00182*, 2021.

[218] Dilina Perera, Inimfon Akpabio, Firas Hamze, Salvatore Mandra, Nathan Rose, Maliheh Aramon, and Helmut G Katzgraber. Chook–a comprehensive suite for generating binary optimization problems with planted solutions. *arXiv preprint arXiv:2005.14344*, 2020.

[219] Dilina Perera, Firas Hamze, Jack Raymond, Martin Weigel, and Helmut G Katzgraber. Computational hardness of spin-glass problems with tile-planted solutions. *Physical Review E*, 101 (2):023316, 2020.

[220] Vasil S Denchev, Sergio Boixo, Sergei V Isakov, Nan Ding, Ryan Babbush, Vadim Smelyanskiy, John Martinis, and Hartmut Neven. What is the computational value of finite-range tunneling? *Physical Review X*, 6(3):031015, 2016.

[221] Tomas Boothby, Andrew D King, and Aidan Roy. Fast clique minor generation in chimera qubit connectivity graphs. *Quantum Information Processing*, 15(1):495–508, 2016.

[222] Ryan Hamerly, Takahiro Inagaki, Peter L McMahon, Davide Venturelli, Alireza Marandi, Tatsuhiro Onodera, Edwin Ng, Carsten Langrock, Kensuke Inaba, Toshimori Honjo, et al. Experimental investigation of performance differences between coherent ising machines and a quantum annealer. *Science advances*, 5(5):eaau0823, 2019.

[223] Robert Patton, Catherine Schuman, Thomas Potok, et al. Efficiently embedding qubo problems on adiabatic quantum computers. *Quantum Information Processing*, 18(4), 2019.

[224] Stefanie Zbinden, Andreas Bärtschi, Hristo Djidjev, and Stephan Eidenbenz. Embedding algorithms for quantum annealers with chimera and pegasus connection topologies. In *International Conference on High Performance Computing*, pages 187–206. Springer, 2020.

[225] Tameem Albash and Matthew Kowalsky. Diagonal catalysts in quantum adiabatic optimization. *Physical Review A*, 103(2):022608, 2021.

[226] Mario S Könz, Wolfgang Lechner, Helmut G Katzgraber, and Matthias Troyer. Scaling overhead of embedding optimization problems in quantum annealing. *arXiv preprint arXiv:2103.15991*, 2021.

[227] Matthew Kowalsky, Tameem Albash, Itay Hen, and Daniel A Lidar. 3-regular 3-xorsat planted solutions benchmark of classical and quantum heuristic optimizers. *arXiv preprint arXiv:2103.08464*, 2021.

[228] Jun Cai, William G Macready, and Aidan Roy. A practical heuristic for finding graph minors. *arXiv preprint arXiv:1406.2741*, 2014.

[229] Shuntaro Okada, Masayuki Ohzeki, Masayoshi Terabe, and Shinichiro Taguchi. Improving solutions by embedding larger subproblems in a d-wave quantum annealer. *Scientific reports*, 9(1):1–10, 2019.

[230] David E Bernal, Kyle EC Booth, Raouf Dridi, Hedayat Alghassi, Sridhar Tayur, and Davide Venturelli. Integer programming techniques for minor-embedding in quantum annealers. In *International Conference on Integration of Constraint Programming, Artificial Intelligence, and Operations Research*, pages 112–129. Springer, 2020.

[231] Thiago Serra, Teng Huang, Arvind U Raghunathan, and David Bergman. Template-based minor embedding for adiabatic quantum optimization. *INFORMS Journal on Computing*, 2021.

[232] Sergey Novikov, Robert Hinkey, Steven Disseler, James I Basham, Tameem Albash, Andrew Risinger, David Ferguson, Daniel A Lidar, and Kenneth M Zick. Exploring more-coherent quantum annealing. In *2018 IEEE International Conference on Rebooting Computing (ICRC)*, pages 1–7. IEEE, 2018.

[233] Jeffrey A Grover, James I Basham, Alexander Marakov, Steven M Disseler, Robert T Hinkey, Moe Khalil, Zachary A Stegen, Thomas Chamberlin, Wade DeGottardi, David J Clarke, et al. Fast, lifetime-preserving readout for high-coherence quantum annealers. *PRX Quantum*, 1(2):020314, 2020.

[234] X Dai, DM Tennant, R Trappen, AJ Martinez, D Melanson, MA Yurtalan, Y Tang, S Novikov, JA Grover, SM Disseler, et al. Calibration of flux crosstalk in large-scale flux-tunable superconducting quantum circuits. *arXiv preprint arXiv:2105.14360*, 2021.

APPENDIX

MODIFIED SHAMROCK PROBLEM

For the time-to-solution (TTS) for finding true ground state of modified shamrock problems with RFQA and standard QA, we list the data of higher frequencies and lowest frequencies in this chapter.

A.1 The performance of RFQA in other frequency range in the modified shamrock model

We investigate the energy difference between the ground state and excitation states in the modified shamrock model, only one avoided crossing exists in this model as shown in Figure A.1.

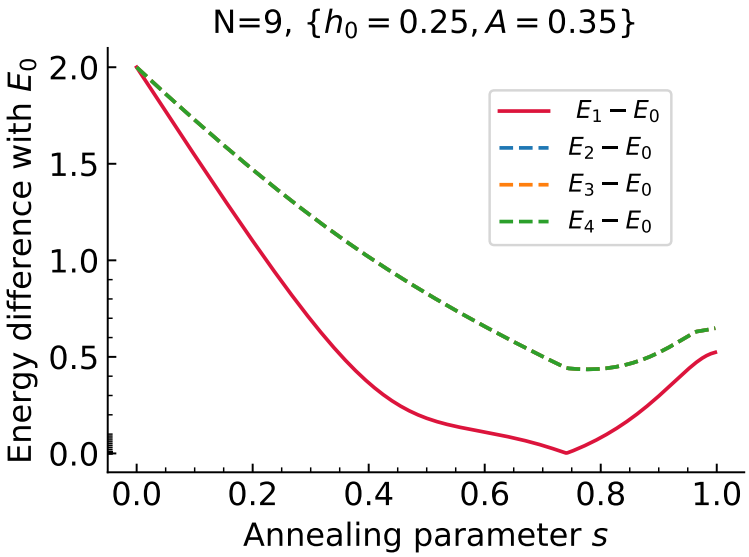

Figure A.1 The energy gap in the modified shamrock model

The performance of digitized-QA and digitized-RFQA in the other frequency scale sets in forward annealing and reverse annealing are shown in Figure A.2 and Figure A.3.

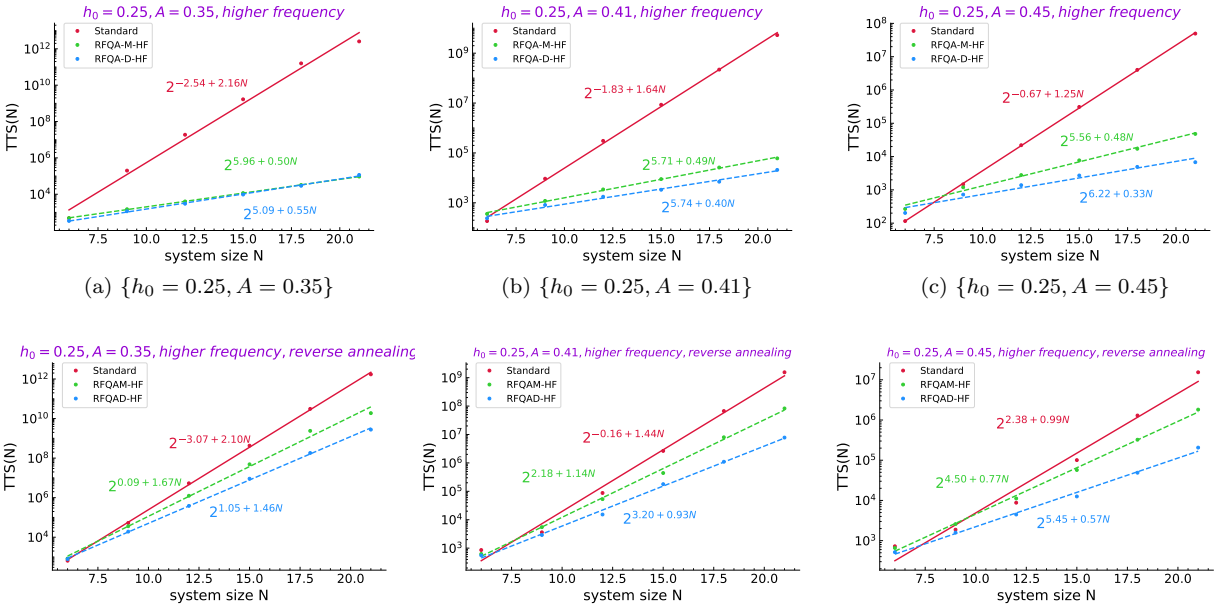

(a) $\{h_0 = 0.25, A = 0.35\}$ (b) $\{h_0 = 0.25, A = 0.41\}$ (c) $\{h_0 = 0.25, A = 0.45\}$

(d) $\{h_0 = 0.25, A = 0.35\}$ (e) $\{h_0 = 0.25, A = 0.41\}$ (f) $\{h_0 = 0.25, A = 0.45\}$

Figure A.2 Forward and reverse annealing results: (a)(b)(c) are forward annealing results, (d)(e)(f) are reverse annealing results. Time to find the true ground state in 3 different difficulty problem set:$\{h_0 = 0.25, A = 0.35, 0.41, 0.45\}$ with high frequencies f_i chosen from $\{0.1/\sqrt{N}, 0.2/\sqrt{N}\}$ using RFQA. Data for RFQA-M and RFQA-D are given by green, blue markers, respectively. Red dots are data of the standard quantum annealing method for comparison purpose. The solid red line is the best-fit curve of the standard quantum annealing method for comparison. Other dashed lines are best-fit curves for RFQA.

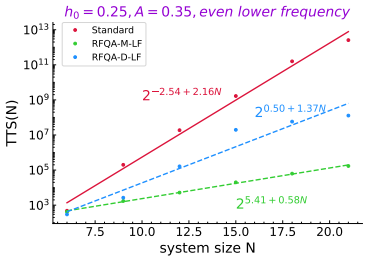

(a) $\{h_0 = 0.25, A = 0.35\}$

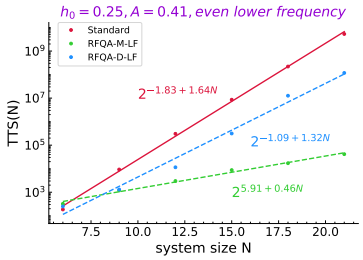

(b) $\{h_0 = 0.25, A = 0.41\}$

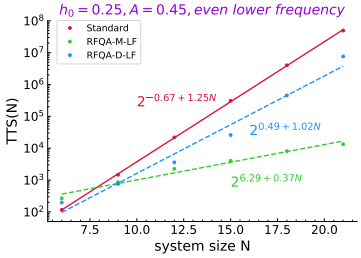

(c) $\{h_0 = 0.25, A = 0.45\}$

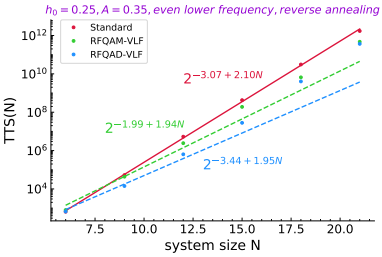

(d) $\{h_0 = 0.25, A = 0.35\}$

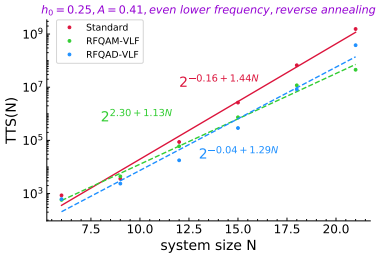

(e) $\{h_0 = 0.25, A = 0.41\}$

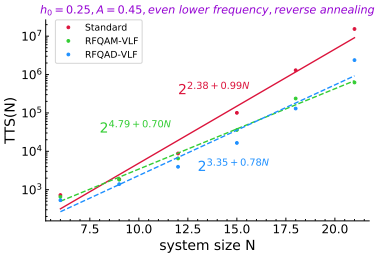

(f) $\{h_0 = 0.25, A = 0.45\}$

Figure A.3 Forward and reverse annealing results: (a)(b)(c) are forward annealing results, (d)(e)(f) are reverse annealing results. Time to find the true ground state in 3 different difficulty problem set:$\{h_0 = 0.25, A = 0.35, 0.41, 0.45\}$ with lowest frequencies f_i chosen from $\{0.5/N^{1.5}, 1/N^{1.5}\}$ using RFQA. Data for RFQA-M and RFQA-D are given by green, blue markers, respectively. Red dots are data of the standard quantum annealing method for comparison purpose. The solid red line is the best-fit curve of the standard quantum annealing method for comparison. Other dashed lines are best-fit curves for RFQA.